ENV Report 37

Interim Report For The Upper Mississippi River - Illinois Waterway System Navigation Study

Entrainment and Transport of Sediments by Towboats in the Upper Mississippi River and Illinois Waterway, Numerical Model Study

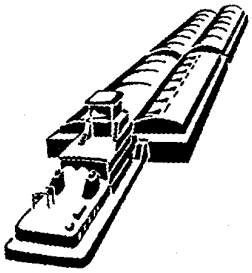

January 2001

Rock Island District
St. Louis District
St. Paul District

US Army Corps of Engineers

Upper Mississippi River - Illinois Waterway System Navigation Study

ENV Report 37
January 2001

Entrainment and Transport of Sediments by Towboats in the Upper Mississippi River and Illinois Waterway, Numerical Model Study

by Ronald R. Copeland, David D. Abraham, Gregory H. Nail, Rebecca Seal, Gary L. Brown

Coastal and Hydraulics Laboratory
U.S. Army Engineer Research and Development Center
3909 Halls Ferry Road
Vicksburg, MS 39180-6199

Interim report

Approved for public release; distribution is unlimited

Prepared for U.S. Army Engineer District, Rock Island
Rock Island, IL 61204-2004
U.S. Army Engineer District, St. Louis
St. Louis, MO 63103-2833
U.S. Army Engineer District, St. Paul
St. Paul, MN 55101-1638

Contents

Preface ix

1—Introduction 1

Background 1
Purpose 2
Scope 2

2—Numerical Models 4

Model Descriptions 4
Modifications to SED2D 6
Model Geometry 7
Hydrodynamic Boundary Conditions 8
Simulated Tow Characteristics 13
Tow-Induced Hydrodynamics 14
Sediment Transport Functions 15
Shear velocity calculations 15
Sediment entrainment function for sand 16
Cohesive sediment entrainment function 19
Bed Material Gradations 19
Sampling methods 20
Laboratory analysis and data 21
LaGrange Pool 26
Pool 8 30
Pool 26 34
Application to numerical models 37
Sediment Boundary Conditions 37

3—Model Adjustment 38

Hydrodynamic Model 38
Sedimentation Model 40

4—Model Results 43

Simulation Conditions 43

Pool 8 Sediment Modeling 44
Pool 26 Sediment Modeling 51
LaGrange Pool Sediment Modeling 56
Sand bed 56
Cohesive bed 62
Postprocessing of the SED2D Simulations 67
Design curves 67
NAVSED 72

5—Conclusions and Recommendations 76

Conclusions 76
Recommendations 77

References 79

SF 298

List of Figures

Figure 1. Typical tow shear-stress time series (prototype units) 7

Figure 2. Numerical grid for Pool 8 9

Figure 3. Numerical grid for Pool 26 10

Figure 4. Numerical grid for LaGrange Pool 11

Figure 5. Bed-material sample locations on LaGrange Pool 22

Figure 6. Bed-material sample locations on Pool 8 23

Figure 7. Bed-material sample locations on Pool 26 25

Figure 8. Numerical grid for Pool 8, enlarged section 46

Figure 9. Sediment concentration contours, Pool 8, low flow, boat-shear stresses 47

Figure 10. Sediment concentration time history at new Gauge 1, Pool 8, low flow, boat-shear stresses 47

Figure 11. Sediment concentration time history at new Gauge 2, Pool 8, low flow, boat-shear stresses 47

Figure 12. Sediment concentration time history at new Gauge 2, Pool 8, low flow, shear stress from return current 48

Figure 13. Sediment concentration contours, Pool 8, medium flow, boat-shear stresses 49

Figure 14. Sediment concentration time history at new Gauge 1, Pool 8, medium flow, boat-shear stresses 49

Figure 15. Sediment concentration time history at new Gauge 2, Pool 8, medium flow, boat-shear stresses 49

Figure 16. Sediment concentration contours, Pool 8, high flow, boat-shear stresses 50

Figure 17. Sediment concentration time history at new Gauge 1, Pool 8, high flow, boat-shear stresses 50

Figure 18. Sediment concentration time history at new Gauge 2, Pool 8, high flow, boat-shear stresses 50

Figure 19. Numerical grid for Pool 26, enlarged section 52

Figure 20. Sediment concentration contours, Pool 26, low flow, boat-shear stresses 52

Figure 21. Sediment concentration time history at new Gauge 1, Pool 26, low flow, boat-shear stresses 53

Figure 22. Sediment concentration time history at new Gauge 2, Pool 26, low flow, boat-shear stresses 53

Figure 23. Sediment concentration contours, Pool 26, medium flow, boat-shear stresses 54

Figure 24. Sediment concentration time history at new Gauge 1, Pool 26, medium flow, boat-shear stresses 54

Figure 25. Sediment concentration time history at new Gauge 2, Pool 26, medium flow, boat-shear stresses 55

Figure 26. Sediment concentration contours, Pool 26, high flow, boat-shear stresses 55

Figure 27. Sediment concentration time history at new Gauge 1, Pool 26, high flow, boat-shear stresses 55

Figure 28. Sediment concentration time history at new Gauge 2, Pool 26, high flow, boat-shear stresses 56

Figure 29. Numerical grid for LaGrange Pool, enlarged section 57

Figure 30. Sediment concentration contours, LaGrange Pool, sand, low flow, boat-shear stresses 58

Figure 31. Sediment concentration time history at new Gauge 1, LaGrange Pool, sand, low flow, boat-shear stresses 59

Figure 32. Sediment concentration time history at new Gauge 2, LaGrange Pool, sand, low flow, boat-shear stresses 59

Figure 33. Sediment concentration time history at new Gauge 2, LaGrange Pool, sand, low flow, shear stress from return current 59

Figure 34. Sediment concentration contours, LaGrange Pool, medium flow, boat-shear stresses 60

Figure 35. Sediment concentration time history at new Gauge 1, LaGrange Pool, sand, medium flow, boat-shear stresses 60

Figure 36. Sediment concentration time history at new Gauge 2, LaGrange Pool, sand, medium flow, boat-shear stresses 60

Figure 37. Sediment concentration time history at new Gauge 2, LaGrange Pool, sand, medium flow, shear stress from return current 61

Figure 38. Sediment concentration contours, LaGrange Pool, sand, high flow, boat-shear stresses 62

Figure 39. Sediment concentration time history at new Gauge 1, LaGrange Pool, sand, high flow, boat-shear stresses 62

Figure 40. Sediment concentration time history at new Gauge 2, LaGrange Pool, sand, high flow, boat-shear stresses 63

Figure 41. Sediment concentration time history at new Gauge 2, LaGrange Pool, sand, high flow, shear stress from return current 63

Figure 42. Sediment concentration contours, LaGrange Pool, fines, low flow, boat-shear stresses 64

Figure 43. Sediment concentration time history at new Gauge 1, LaGrange Pool, fines, low flow, boat-shear stresses 64

Figure 44. Sediment concentration time history at new Gauge 2, LaGrange Pool, fines, low flow, boat-shear stresses 65

Figure 45. Sediment concentration contours, LaGrange Pool, fines, low flow, shear stress from return current 65

Figure 46. Sediment concentration time history at new Gauge 1, LaGrange Pool, fines, low flow, shear stress from return current 65

Figure 47. Sediment concentration time history at new Gauge 2, LaGrange Pool, fines, low flow, shear stress from return current 66

Figure 48. Sediment concentration contours, LaGrange Pool, fines, medium flow, boat-shear stresses 66

Figure 49. Sediment concentration time history at new Gauge 1, LaGrange Pool, fines, medium flow, boat-shear stresses 66

Figure 50. Sediment concentration time history at new Gauge 2, LaGrange Pool, fines, medium flow, boat-shear stresses 68

Figure 51. Sediment concentration contours, LaGrange Pool, fines, medium flow, shear stress from return current 68

Figure 52. Sediment concentration time history at new Gauge 1, LaGrange Pool, fines, medium flow, shear stress from return current 68

Figure 53. Sediment concentration time history at new Gauge 2, LaGrange Pool, fines, medium flow, shear stress from return current 69

Figure 54. Sediment concentration contours, LaGrange Pool, fines, high flow, boat-shear stresses 69

Figure 55. Sediment concentration time history at new Gauge 1, LaGrange Pool, fines, high flow, boat-shear stresses 69

Figure 56. Sediment concentration time history at new Gauge 2, LaGrange Pool, fines, high flow, boat-shear stresses 70

Figure 57. Sediment concentration contours, LaGrange Pool, fines, high flow, shear stress from return current 70

Figure 58. Sediment concentration time history at new Gauge 1, LaGrange Pool, fines, high flow, shear stress from return current 70

Figure 59. Sediment concentration time history at new Gauge 2, LaGrange Pool, fines, high flow, shear stress from return current 71

Figure 60. Typical set of design curves 71

List of Tables

Table 1. Hydrodynamic Boundary Conditions 12

Table 2. LaGrange Pool Bed Material Characteristics 27

Table 3. Laboratory Determined Cohesive Bed Characteristics, LaGrange Pool 30

Table 4. Pool 8 Bed Material Characteristics 32

Table 5. Pool 26 Bed Material Characteristics 35

Table 6. Model Adjustment Coefficients for RMA2 39

Table 7. Sediment Diffusion Coefficients, m^2/sec 41

Table 8. Typical Design Curve Tabulation 73

Preface

The work reported herein was conducted as part of the Upper Mississippi River - Illinois Waterway (UMR-IWW) System Navigation Study. The information generated for this report will be considered as part of the plan formulation process for the System Navigation Study.

The UMR-IWW System Navigation Study is being conducted by the U.S. Army Engineer Districts of Rock Island, St. Louis, and St. Paul under the authority of Section 216 of the Flood Control Act of 1970. Commercial navigation traffic is increasing and, in consideration of existing lock constraints, will result in traffic delays that will continue to grow in the future. The System Navigation Study scope is to examine the feasibility of navigation improvements to the Upper Mississippi River and Illinois Waterway to reduce delays to commercial navigation traffic. The study will determine the location and appropriate sequencing of potential navigation improvements on the system, prioritizing the improvements for the 50-year planning horizon from 2000 through 2050. The final product of the System Navigation Study will be a Feasibility Report, which will be the decision document for processing to Congress.

The work described in this report was sponsored by the U.S. Army Engineer District, Rock Island, as part of the Navigation Effects Study. Specifically, this work was identified as Sediment Transport Modeling.

The work was performed by personnel of the Coastal and Hydraulics Laboratory (CHL), U.S. Army Engineer Research and Development Center (ERDC), Vicksburg, MS. The study was conducted under the general supervision of Dr. J. R. Houston, former Director, CHL, and under the direct supervision of Mr. W. H. McAnally, Chief, Estuaries and Hydrosciences Division (EHD); Dr. Phil Combs, Chief, Rivers and Structures Division (RSD); and Mr. T. J. Pokrefke, Jr., Scientific Technical Director, EHD. The engineers in immediate charge of the study were Drs. G. E. Freeman and R. R. Copeland, RSD. Engineers with principal task assignments were Dr. R. Seal and Mr. D. D. Abraham, RSD. Assistance was also provided by Dr. G. H. Nail and Messrs. R. A. Evans and G. L. Brown, EHD.

During the course of the study, close working relationships were maintained with members of the Modeling Integration and Simulation Team at quarterly meetings.

Valuable technical review of this document was provided by Dr. F. M. Holly, Jr., University of Iowa; Mr. B. R. Hall, Northwest Hydraulic Consultants; and Mr. K. J. Landwehr, U.S. Army Engineer District, Rock Island.

At the time of publication of this report, Director of ERDC was Dr. James R. Houston, and COL James S. Weller, EN, was Commander.

1 Introduction

Background

Excessive concentrations of sediment in the Mississippi and Illinois Rivers may have detrimental effects on existing aquatic organisms including fish, mussels, and plants. It is known by observation that moving towboats, under certain conditions and at certain locations, cause an increase in sediment concentration as they pass. Once entrained from the riverbed, the sediment may be moved by both the river current and turbulent diffusion. This sediment may find its way into backwater areas. Eventually, however, most of the entrained sediment will fall back to the riverbed due to gravity, although some of the smallest clay size sediments may stay in suspension indefinitely. Thus, the increase in sediment concentration is temporary. In order to assess the effect of increases in sediment concentration on aquatic organisms due to tow passage, it is necessary to determine the conditions, locations, quantity, and timing of increases in sediment concentration by a variety of towboat passages.

It is important to note that towboats are not the only cause of resuspension of sediment in the river and that they supply no new sediment to the river system. Riverbed sediment resuspended by towboats may be redistributed into backwater areas, but this is not the only sediment source for backwater areas. Sediment sources include erosion off of the upstream watershed, erosion of upstream river banks, and tributaries. Backwater areas may naturally receive considerable sediment loads from the main river channel, especially during floods. The natural flow of the river continuously creates shear stresses that will entrain sediment from the riverbed. Higher flow intensity results in greater sediment entrainment. Typically, sediment entrained by the flow from the riverbed is replaced by sediment falling to the riverbed due to gravity. Wind can create waves which in turn may create shear stresses on the riverbed of sufficient strength to entrain sediment. The effects of wind are typically only important in shallow water where there is sufficient fetch length to allow for significant wave heights to develop.

Towboats are responsible for three processes that may entrain sediment and increase sediment concentrations. Towboats create waves that can produce bottom shear stresses sufficient to entrain sediment. This typically occurs in shallow water near the shoreline. Towboats also create a drawdown due to

displacement. This drawdown temporarily increases shear stresses, and its effect may extend all the way from the tow to the shoreline and typically is most significant in shallow water with heavily loaded barges. Finally, towboat propellers may create a dramatic increase in shear stress on the riverbed.

Three typical reaches of the Mississippi and Illinois Rivers were chosen for detailed study. This report describes the numerical modeling efforts on those three reaches. Numerical model simulations were conducted for reaches of Pool 8 and Pool 26 on the Mississippi River and for LaGrange Pool, upstream from Beardstown, Illinois, on the Illinois River. These three river reaches were selected as representative "trend" reaches for the study by the Modeling Integration and Simulation Team (MIST). Insight gained from these detailed studies was then used to help determine tow effects at other pools and under different conditions.

Purpose

The purpose of the numerical model study was to determine the extent to which sediments might be entrained (removed from the bed and thrust into the water column) and transported as a direct consequence of tow traffic in these three trend reaches and whether or not any such entrainment and transport would result in increased sedimentation in backwater areas.

The results of these numerical model studies were used to develop insight for prediction of the magnitude and duration of increased sediment concentrations due to tow passage in other pools and for different types of tow passages.

Scope

The modeling effort addressed the entrainment, transport, and deposition of sediment due to several forces. Ambient hydrodynamic forces created by the river at low, medium, and high flow were calculated using a numerical model. Hydrodynamic forces created by the drawdown and return currents were determined by another numerical model and then combined with the ambient hydrodynamic forces. Forces induced by the bow pressure wave and the tow's propeller jet as a function of depth and ambient velocity were determined external to the numerical models using an algorithm developed from experimental techniques (Maynord 2000). Combined bow-pressure-wave and tow-propeller-jet forces were then calculated in the numerical model based on the actual depth and velocity at the specific location in the model. Sediment transport due to advection and diffusion was calculated using the numerical models.

An overall modeling plan was developed in response to the above considerations. A well-tested two-dimensional depth-averaged numerical model, RMA2, was run to simulate the ambient hydrodynamic conditions. A second hydrodynamic numerical model, HIVEL (Stockstill and Berger 1999), was run to

simulate the tow-induced drawdown and return currents. The results of the two models were superimposed upon one another to produce the combined effect of the tow and ambient river currents. SED2D, a two-dimensional depth-averaged unsteady-flow sediment transport numerical model was used to simulate the advection and diffusion of suspended sediment. The SED2D model was modified for this study so that shear stresses created by a moving towboat could be combined with shear stresses produced by the ambient currents to calculate entrainment and transport of sediment.

The upstream passage of a single tow was simulated in the numerical models because velocity differentials and bed shear stresses are greatest under these conditions. The combined size and speed of the tow chosen for the simulation was considered to be a reasonable combination that would produce the maximum sediment entrainment in each of the reaches. Tow passage was simulated in each model for three river discharges that covered the normal range of expected conditions.

2 Numerical Models

Model Descriptions

TABS-MD (Thomas and McAnally 1991) is a suite of generalized numerical models and utility codes, developed at the U.S. Army Engineer Waterways Experiments Station (WES),[1] which are designed to study multidimensional hydrodynamics in rivers, reservoirs, bays, and estuaries. These models can be used to study project impacts on flows, sedimentation, constituent transport, and salinity. In this study, two of the numerical models from TABS-MD were used. These were RMA2 and SED2D.

RMA2 is a two-dimensional depth-averaged finite-element hydrodynamic numerical model. It computes water-surface elevations and horizontal velocity components for subcritical free-surface flow in two-dimensional flow fields. RMA2 uses a finite-element solution technique to solve the Reynolds form of the Navier-Stokes equations for turbulent flows. The effect of friction is accounted for with the Manning's or Chezy equation. Dynamic eddy viscosity coefficients are used to characterize turbulence diffusion characteristics. Both steady- and unsteady-state (dynamic) problems can be analyzed.

RMA2 assumes that the vertical velocity distribution can be represented by an average velocity and that the hydrostatic pressure assumption is reasonable. This means that flow accelerations in the vertical direction should be negligible and that all the water in the water column, at any one location, should be moving in the same direction at any instant in time. The model is not intended to be used for near-field problems where vortices, vibrations, or vertical accelerations are of primary interest.

Input to RMA2 includes bed elevations, hydraulic roughness, downstream water-surface elevation, water discharge at the upstream boundary, dynamic eddy viscosity (turbulent exchange) coefficients, and water temperature. With this input, the computer program calculates water-surface elevations and depth-averaged velocity magnitudes and directions throughout the model grid.

[1] WES became the U.S. Army Engineer Research and Development Center, Vicksburg, MS, on 1 October 1999.

In this study, RMA2 was used to calculate ambient water-surface elevations and velocities at a number of points or nodes. The number of computation points is defined by the level of detail in the numerical grid that describes the model reach.

Tow-induced velocities and depths were calculated using the HIVEL2D two-dimensional unsteady-flow numerical model (Stockstill and Berger 1999). HIVEL2D is a free-surface depth-averaged finite-element model designed specifically to simulate flow in advection-dominated flow fields containing shocks such as those created by drawdown from passing towboats and return currents.

SED2D (older versions of this model were called STUDH) is a two-dimensional depth-averaged finite-element sedimentation numerical model. It uses the same numerical grid as RMA2. The depths and velocities calculated by RMA2 are used as input to SED2D which calculates changes in sediment concentration and bed elevation in space and time using the convection-diffusion equation with bed source-sink terms. The Ackers-White equation (Ackers and White 1973, Ackers 1993) can be used to calculate sediment transport potential for sand. However, for the Upper Mississippi River Study the SED2D code was enhanced to calculate sediment transport using the Garcia-Parker equation (Garcia and Parker 1991). A single representative grain size is used in the sediment calculations for sand. Silt and clay erosion is calculated using Parthenaides' (1965) equation and silt and clay deposition is calculated using Krone's (1962) equation. As with RMA2, both steady- and unsteady-state (dynamic) problems can be analyzed with SED2D.

Assumptions and limitations that apply to RMA2 also apply to SED2D. In addition, SED2D assumes that the sediment diameter and fall velocity can be represented by a characteristic value, thus it may misrepresent sediment entrainment, transport, and deposition where depth and velocity changes are abrupt or highly variable. This makes calculations difficult where bed gradations vary from one part of the channel to another. The model does not account for sediment moving as bed load. SED2D is not implicitly coupled with hydrodynamic calculations, so changes in bed elevation during the simulation period must not be significant. These limitations were acceptable to achieve the general purposes of this study, which were to evaluate general sedimentation process responses for average conditions and then evaluate the magnitude of variability in sedimentation process responses under variable tow passage conditions.

Water-surface elevations and velocities calculated by RMA2 or, in the case of this study, a combination of calculations from RMA2 and HIVEL2D are input to SED2D. Additional input includes the diameter or fall velocity of the characteristic grain size, sediment concentration of the characteristic grain size at the upstream boundary, initial concentration throughout the flow field, erosion and deposition characteristics of the characteristic grain size, density of the bed layers, sediment diffusion coefficients, and water temperature. In order to determine the effects of sediment suspended by navigation tows, the SED2D model was modified to allow for time variable sediment input along a designated

path. With this input, SED2D calculates: (a) bed-shear stresses, (b) depth-averaged sediment concentration, (c) changes in bed elevation, and (d) advective and diffusive transport of suspended sediment at points or nodes throughout the model grid.

Output from the sedimentation studies discussed in this report was used in the system-wide impacts study (Pokrefke et al. in preparation). Critical to the systemwide studies was application of the NAVEFF numerical model (Maynord 1996). NAVEFF, developed at WES, basically calculates drawdown, return current, shear stress, wave height, and scour depth at a given cross section for a given set of tow-traffic characteristics and ambient river conditions. Although NAVEFF was not used in this sedimentation study, algorithms and output generated by this study needed to be consistent with NAVEFF applications.

Modifications to SED2D

The purpose of the sediment modeling was to quantify the entrainment and transport of sediments in the main channel and nearshore due to tow traffic. The existing SED2D numerical model uses calculated ambient hydraulic velocities and depths from RMA2 to calculate bottom shear stresses and sediment entrainment. SED2D was modified to accept calculated bottom shear stresses from a moving tow. Maynord (2000) experimentally determined bottom shear stress distributions for moving tows as a function of local depth and velocity and tow characteristics. These characteristics were the tow length and speed, total draft, propeller diameter, thrust, distance from the propeller to the towboat stern, and distance between propellers. Additionally, it was necessary to know if the tow was upbound on the river or downbound and whether a Kort Nozzle or open-wheel type of propeller was being used. At each time step in the modified version of SED2D, Maynord's algorithm was used to calculate the distribution of tow-induced bed shear stresses. The bed shear stresses calculated using this algorithm represent the cumulative effects of ambient current, return current, and the tow.

In addition, an algorithm was written for SED2D that traces tow movement along a designated ship path at a constant velocity. As the tow moves, the numerical grid coordinates of the bow and stern at each time step are identified. These become the reference points for the tow-induced shear-stress distribution calculated using Maynord's algorithm.

A typical tow-induced shear-stress time series at a point in the river as the tow passes is shown in Figure 1. In Figure 1 these tow-induced bed shear stresses only apply to grid nodes directly under the tow. However, Maynord's algorithm provides values for tow-induced bed-shear stresses as they decay with lateral distance from the tow. Bed shear stress value is computed using velocity and depth data from the hydrodynamic solution for the specified towboat characteristics. Typically, as a tow passes a given location, there are two peaks

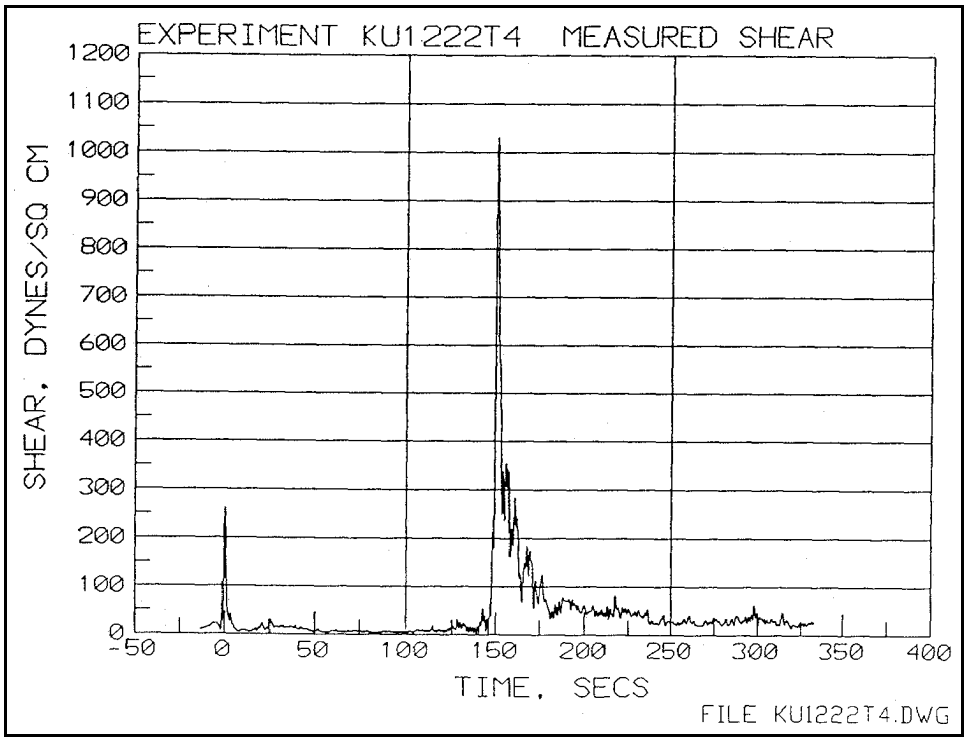

Figure 1. Typical tow shear-stress time series (prototype units)

in the induced bed-shear stress; one as the bow passes at time zero, and the other when the stern and propellers pass at time t. This is shown in Figure 1 where the duration of the bow-induced bed-shear stresses is much shorter than the propeller-induced bed-shear stresses. These relative durations are typical. However, the relative peak magnitudes of the induced bed-shear stresses vary with hydrodynamic conditions and tow characteristics such as speed, draft, direction relative to the flow, and propeller thrust.

In order to determine the appropriate total bed-shear stress at a given numerical grid point, the modified model compares the bed shear produced by the tow, the bed shear produced by return currents (currents produced by the long period wave at the nearshore), and the bed shear produced by the ambient currents. Since the algorithms used to calculate bed-shear stresses are based on cumulative effects, the maximum of these three bed shears is used in the sediment entrainment function for calculating the increase in sediment concentration at each node for each time step. Thus, the effects of the tow in the navigation channel and of the return currents on the nearshore are determined. It should be noted that the three-dimensional propeller currents are not being modeled.

Model Geometry

Numerical computation grids were developed for reaches of Pool 8 and Pool 26 on the Mississippi River and for the LaGrange Pool on the Illinois River. GIS data were provided by the Environmental Management Technical Center (EMTC) in Onalaska, Wisconsin. Aerial photos were used to help delineate the

model boundaries. Elevations were based on surveys conducted between 1989 and 1992 on Pool 8, between 1991 and 1995 on Pool 26, and between 1992 and 1997 on the LaGrange Pool.

The numerical grid for Pool 8 is shown in Figure 2. It consisted of 12,278 elements and 34,772 nodes. The upstream boundary for the Pool 8 model was set at river mile 697.5, at the U.S. highway 61 bridge, and where Baron Island splits the flow into two channels. The downstream boundary is at river mile 688.6, near Brownsville, Wisconsin.

The numerical grid for Pool 26 is shown in Figure 3. It consisted of 4,445 elements and 13,242 nodes. The upstream boundary of the model was set at river mile 232.3, and the downstream boundary was set at river mile 221.2.

The numerical grid for the LaGrange Pool is shown in Figure 4. It consisted of 5,267 elements and 14,373 nodes. The upstream boundary of the model was set at river mile 99.0, and the downstream boundary was just below river mile 93.0.

Hydrodynamic Boundary Conditions

The specified hydrodynamic boundary conditions were discharge at the upstream boundary and water surface elevation at the downstream boundary. Assigned water temperatures varied between 12.8 and 16.0 °C.

For Pool 8, there were two prototype data sets available for numerical model adjustment. These data were collected by WES (Fagerburg and Pratt 1998) on 2 November 1995 and 13 September 1996. U.S. Army Engineer District, St. Paul (*www.ncs-wc.usace.army.mil*), supplied the following river data for those days.

Date	Discharge m^3/sec	Elevation RM 689.0 Brownsville m, NGVD	Elevation RM 697.3 La Crosse m, NGVD
2 November 1995	1,971	192.13	193.27
13 September 1996	589	192.28	192.36

Data from the U.S. Army Engineer District, St. Paul (1994), indicated that an 80/20 percent flow split, around Baron Island, at the upstream boundary of the Pool 8 model, was appropriate for a total discharge of 2,200 m^3/sec (78,000 cfs). This was the only available data, and the same flow distribution was used for all flow conditions. Of the flow, 80 percent enters on the main stem of the Mississippi River, east side of Baron Island, and 20 percent enters in the west channel. The discharge distribution at the upstream boundary of the model was set accordingly.

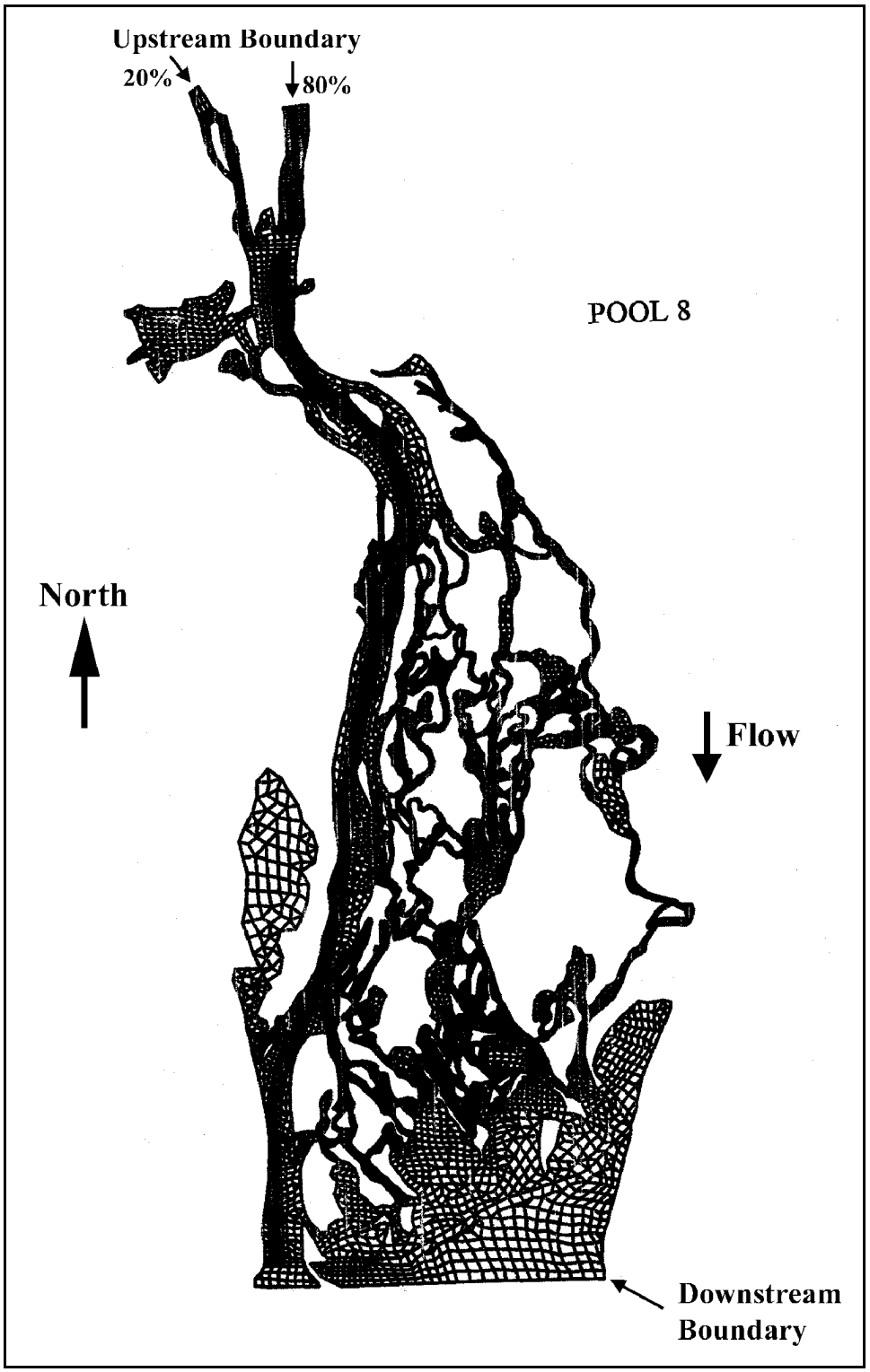

Figure 2. Numerical grid for Pool 8

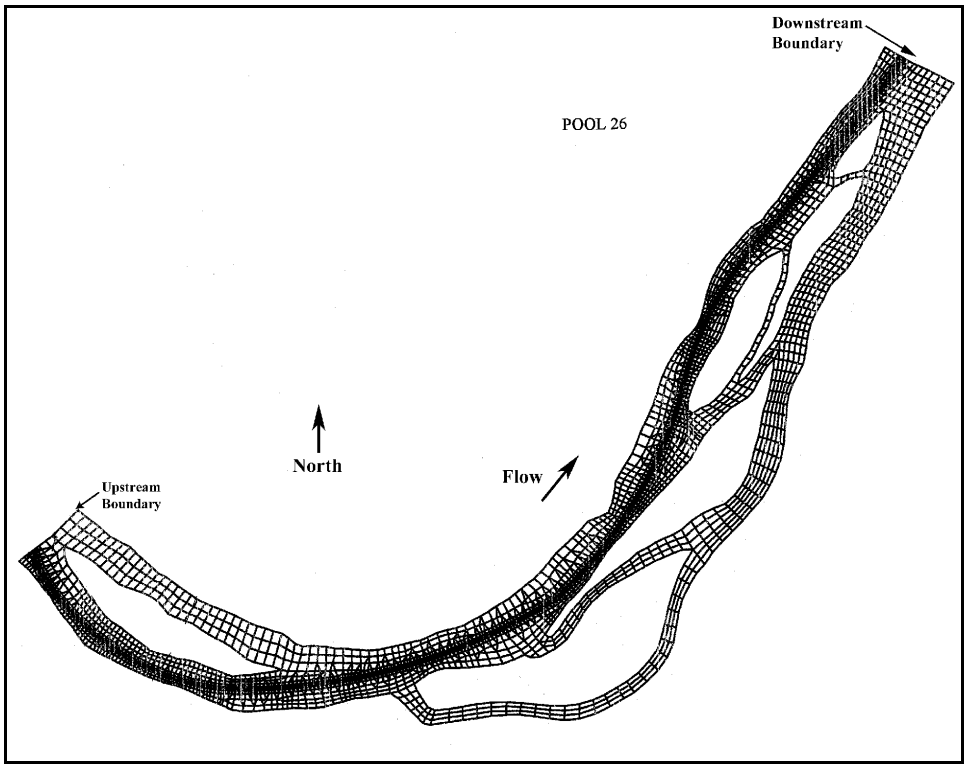

Figure 3. Numerical grid for Pool 26

For Pool 26, prototype data were obtained during a September 1996 WES (Fagerburg and Pratt 1998) field data collection effort. The upstream discharge boundary condition was 1,217.6 m^3 /sec, and the downstream boundary water surface elevation was 128.0 m NGVD.

For the LaGrange pool, prototype data collected on 15 July 1996 were used for numerical model verification. The upstream discharge boundary condition was 305.3 m^3/sec in the main channel and 2.83 m^3/sec in the side channel. The downstream boundary was 131.3 m NGVD at both exit locations.

The adjusted hydrodynamic numerical models were used to calculate ambient velocity patterns and depths in the three study reaches for a range of flow conditions. The 5, 50, and 95 percent duration exceedance stages were selected for each study reach. Flows corresponding to these stages were taken from rating curves at gauges, and profiles between gauges were interpolated. The discharge and stage exceeded 5 percent of the time was designated “high” flow. The discharge and stage exceeded 50 percent of the time was designated “medium” flow. The discharge and stage exceeded 95 percent of the time was designated “low” flow. The high and low flows are within the range of navigable conditions. Table 1 lists the boundary conditions used in the numerical models for each of the numerical simulations.

Hydraulic roughness coefficients and dynamic turbulent eddy viscosity coefficients are assigned for each element of the hydrodynamic model. In this

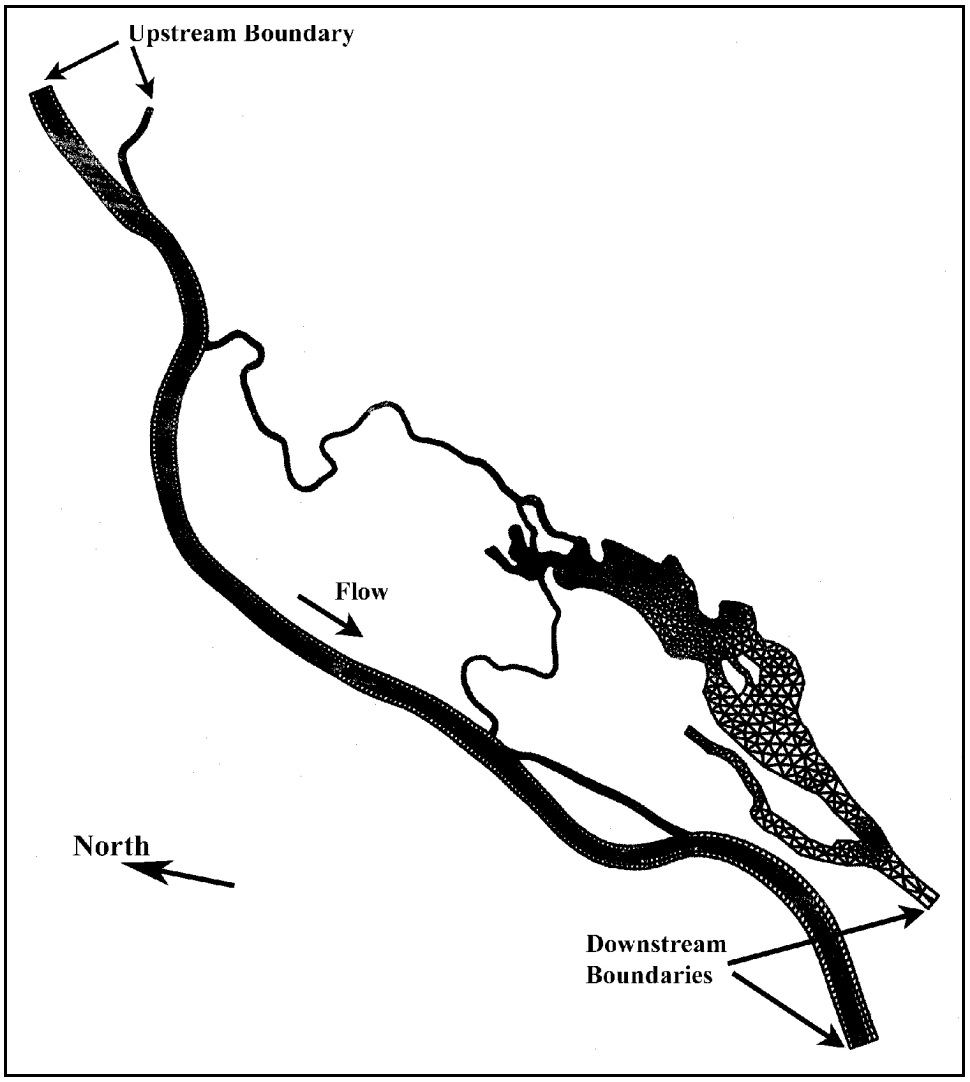

Figure 4. Numerical grid for LaGrange Pool

study, the roughness coefficient was allowed to vary with depth according to Equation 1 which is described in Thomas and McAnally (1991). This empirical equation is a simple representation of Manning's n as a function of depth. It works well with either SI or non-SI units, but the coefficients are different for the different unit systems. This equation allows Manning's n to be greater in areas of shallow water and less in the deepest areas, with a smooth transition between all areas. The equation produced reasonable roughness coefficients for the range of depths simulated in this study. Extremes of zero or infinite depths are prevented from occurring in the model. Elements with depths approaching zero are either removed from the solution by the model's wetting and drying algorithm and/or designated as a marsh porosity element (an element with smaller volume assigned). The bathymetry over the computation domain is, in mathematical terms, a continuous function. Therefore no values of infinity will occur for depth.

Table 1
Hydrodynamic Boundary Conditions

Flow	Downstream Water- Surface Elevation m, NGVD	Upstream Discharge m^3/sec
Pool 8		
Low	192.3	297
Medium	192.1	889
High	192.7	2540
Pool 26		
Low	127.8	623
Medium	128.2	2322
High	129.5	6286
LaGrange Pool		
Low	130.8	136
Medium	131.4	340
High	134.1	1246

$$n = \frac{n_{\max}}{D^a} + n_{veg} \; e^{-\frac{D}{b}} \qquad (1)$$

where

n = Manning's roughness coefficient

n_{max} = Maximum Manning's roughness coefficient without vegetation influence

n_{veg} = Manning's roughness coefficient due to vegetation

D = average depth in the element, ft

a,b = coefficients

The dynamic turbulent eddy viscosity coefficient may be assigned directly in the RMA2 model or it may be allowed to vary with the Peclet number according to Equation 2.

$$\varepsilon = \frac{\rho u \, dx}{P} \qquad (2)$$

where

ε = dynamic eddy viscosity

ρ = fluid density

u = average elemental velocity

dx = length of element in streamwise direction

P = Peclet number

The dynamic turbulent eddy viscosity coefficients were chosen based on experience with similar studies. In the numerical models developed for this study, the primary function of these coefficients is to ensure numerical stability and that the absolute value has an insignificant effect on calculated velocities. At higher flows, the turbulent eddy viscosities used in the numerical model were typically increased for numerical stability purposes.

The numerical grids were divided into characteristic element types, and then appropriate values were chosen for n_{max} and n_{veg}. In Pool 8, only one characteristic element type was assigned. In Pool 26, separate characteristic element types were chosen for the main channel and for the overbanks. In the LaGrange Pool, five characteristic element types were used to differentiate between friction values. These were (a) the main channel, (b) the sides of the main channel, (c) the thin meandering side channels, (d) shallow, relatively flat lakes with low velocities, and (e) the banks of the main river system. The magnitudes of these values were determined during the adjustment phase of the numerical model study.

Simulated Tow Characteristics

In the numerical simulations, it was necessary to select specific characteristics for the tow. The physical effects produced by commercial vessels are related to the following: (a) width and length of the barge train, (b) draft, (c) direction of travel (upbound or downbound), (d) vessel speed relative to ground, (e) propulsion system (Kort nozzle or open wheel), (f) applied horsepower, and (g) lateral location of the vessel in the channel (i.e., sailing line). These variables were evaluated using 1996 traffic data. The MIST study team selected characteristic combinations to be used in the systemwide study and a single combination to be used in this sedimentation study. The NAVEFF computer program was used to calculate tow velocities relative to the ground for the selected conditions. Tow velocities relative to the ground varied with flow conditions in Pool 8 and the LaGrange Pool, but were independent of flow conditions in Pool 26. Thrusts were determined using a method developed by Maynord (in preparation) from analysis of prototype data. In this method, thrust is a function of tow size and speed, ambient velocity and depth, shape of the cross section, and whether the towboat has a Kort nozzle or an open-wheel

propeller. Tow characteristics for each pool were chosen to represent a reasonable combination that would produce the maximum expected shear stress on the bed. In all cases, this would be produced by an upbound tow. A single characteristic tow was simulated in all pools. The towboat was 52 m long and 10 m wide. It had a Kort nozzle with twin 2.74-m-diam propellers. The simulated towboat pushed a 3-barge-wide by 5-barge-long barge train with a combined width and length of 32 m and 297 m, respectively. The draft was 2.74 m (9 ft). The tow speed and propeller thrust were the only two tow characteristics that varied with the three flow conditions.

For Pool 8, tow velocities of 3.4, 2.5, and 2.1 m/sec relative to the ground were simulated for low, medium, and high flow, respectively. This required thrusts of 414,011 N, 268,750 N, and 262,600 N for low, medium, and high flow, respectively.

In Pool 26, a tow velocity of 2.35 m/sec relative to the ground was simulated for all three flow conditions. This required thrusts of 242,225 N, 328,490 N, and 419,677 N for the low-, medium-, and high-flow conditions, respectively.

In the LaGrange Pool, a towboat length of 52 m, pushing a 32-m-wide and 297-m-long barge, with a draft of 2.74 m was simulated. The simulated tow had a Kort nozzle with twin 2.74-m-diam propellers. At low flow, the velocity relative to the ground was 2.0 m/sec which required a prop-thrust of 286,536 N. At medium flow, the velocity relative to the ground was 1.6 m/sec which required a prop-thrust of 283,200 N. At high flow, the velocity relative to the ground was 1.64 m/sec which required a thrust of 191,015 N.

Tow-Induced Hydrodynamics

Tow-induced velocities and depths were calculated using the HIVEL2D two-dimensional unsteady flow numerical model (Stockstill and Berger 1999). The HIVEL2D model was run for the same pools and flow conditions as the RMA2 model. The grid resolution for the HIVEL2D model was much greater than the RMA2 model along the tow path, while the RMA2 model had more grid resolution throughout the remainder of the grid, especially in backwater areas. The HIVEL2D model calculated velocities and depth throughout the numerical grid as a tow with a designated path and speed moved through the study reach. The HIVEL2D model was able to account for the tow-induced drawdown and return currents. Due to the generally greater resolution throughout the model grid, RMA2 ambient currents were considered to be more accurate. So, to obtain a complete hydrodynamic solution, calculated differences between ambient and tow-induced velocities and depths from HIVEL2D were superimposed on the RMA2 ambient velocities and depths.

The numerical grids used in the RMA2 runs were not exactly the same as those used for the HIVEL2D runs. HIVEL2D requires more detailed grid resolution in the ship channel due to the rapid changes in velocity and depth with tow

passage. Therefore, the output files containing the calculated difference file of velocities and water-surface elevations from HIVEL2D were interpolated to the RMA2 geometry and then superimposed upon the steady-state RMA2 values at all nodes. In this way, the tow moving through the channel and the associated waves in the backwater areas were simulated and could be viewed as water-surface elevations changing with time and spatially varying from one end of the model to the other. It was also possible to view velocity changes throughout the domain in the same manner. The combined hydrodynamic files were used as input to drive the sediment transport model.

Sediment Transport Functions

Shear velocity calculations

Shear velocity at the bed of the river is a critical parameter used in many sediment transport functions. It is a function of the intensity of the turbulent velocity fluctuations in the water column. In steady uniform flow, shear velocity may be calculated using the Manning roughness equation.

$$u_* = \frac{\sqrt{g}Un}{R^{1/6}} \tag{3}$$

where

u_* = shear velocity, m/sec

g = acceleration of gravity, m/sec^2

U = depth averaged velocity, m/sec

n = roughness coefficient

R = hydraulic radius, m

This is the equation used in SED2D to calculate shear velocity for ambient conditions for use in the sediment transport equations. It uses the depth-averaged velocity and depths calculated by RMA2 and a user-supplied roughness coefficient. This roughness coefficient represents only the portion of the total roughness that can be attributed to grain roughness and therefore may be less than the roughness used for determining water-surface elevations.

When nonuniform flow conditions occur in the river, such as with the passage of a tow, the Manning roughness equation is not an appropriate predictor for shear velocity. Therefore, in this application of SED2D, the shear velocities created by the moving tow were determined using velocities and depths calculated by RMA2, HIVEL2D, and Maynord's (2000) experimental algorithm,

which calculates shear velocity based on specified tow characteristics, channel cross section, and water depth.

Sediment entrainment function for sand

Existing sediment transport functions have been developed from river and flume data for relatively steady and uniform flow conditions. There is no existing sediment transport function that has been demonstrated to be applicable to the intense and rapidly varying shear stresses and vertical velocity distributions that may be induced by towboat bow pressure and propellor jets. The sediment entrainment function developed by Garcia and Parker (1991) seemed to be promising for this study because sediment entrainment in their equation is a function of only the depth, grain size, and shear stress. These variables are readily available for this study because shear stresses induced by the tow were determined experimentally by Maynord (2000). The Ackers-White equation (Ackers and White 1973, Ackers 1993), which was the only existing sand transport equation in SED2D, calculates sediment transport as a function of depth-averaged water velocity among other variables. Unfortunately, due to the effects of an additional shear plane, draft, and drawdown, water velocity in the vicinity of the towboat is unknown and can only be estimated. Although, neither is considered entirely satisfactory, both the Ackers-White and Garcia-Parker entrainment functions were evaluated in the adjustment phase of the study. Using prototype total sediment concentration measurements, both after tow passage and in ambient flow conditions, it was possible to determine if calculated sediment concentrations were of a reasonable magnitude.

The Garcia-Parker sediment entrainment function is a deterministic equation developed from flume data. As part of this study, experiments were conducted at the University of Illinois by Professor Garcia to determine how to apply the Garcia-Parker sediment transport function for an unsteady flow condition (Garcia, Admiraal, and Rodriguez 1999). Unsteady flows up to 3 m/sec were generated in a closed conduit testing facility with a sand bed. Instantaneous velocities and sediment concentrations were measured with an acoustic doppler velocimeter and an acoustic sediment concentration profiler. Two series of experiments were conducted, one with 0.5-mm sand and one with 0.1-mm sand. The experiments demonstrated that reasonable results could be obtained with unsteady flow using the Garcia-Parker equation without modification. The Garcia-Parker equation (Garcia and Parker 1991) calculates a nondimensional volumetric sediment entrainment.

$$E_s = \frac{A Z_u^5}{1 + \frac{A}{0.3} Z_u^5}$$

$$Z_u = \frac{u_*'}{\omega} \mathbb{R}_*^{0.6} \qquad (4)$$

$$\mathbb{R}_* = \sqrt{gRd}\ \frac{d}{\nu}$$

where

E_s = entrainment (dimensionless concentration by volume at the bed)

$A = 1.30 \times 10^{-7}$

Z_u = Similarity variable for uniform sediment

u_*' = grain shear velocity

ω = fall velocity

$\mathbb{R}_*$ = particle Reynolds number

g = acceleration of gravity

R = Submerged specific gravity of sediment (1.65)

d = median grain size

ν = kinematic viscosity

With steady uniform flow there is a predictable vertical distribution of both velocity and sediment concentration. The sediment concentration distribution under these conditions was described by Rouse (1938). Garcia suggests that the Rouse distribution can be approximated by the following equation which allows depth-averaged concentration and the bed concentration to be related.

$$C_b = r_o C$$

$$r_o = 1.0 + 31.5 \left(\frac{u_*}{\omega} \right)^{-1.46} \qquad (5)$$

where

C_b = bed concentration = E_s at equilibrium

r_o = correction factor

C = depth averaged concentration

u_* = shear velocity

ω = fall velocity

However, when flow is unsteady, as in the case of tow passage, the vertical distribution of both velocity and sediment concentration can only be estimated. Thus, when sediment is entrained by a short burst of shear at the bed, it does not immediately assume a predictable Rouse distribution. In SED2D there is provision to account for this lag in achieving "equilibrium" sediment concentration in the water column. Calculated entrainment at the bed (E_s from Equation 4) is multiplied by the inverse of a characteristic time, t_c, which is the larger of

$$t_c = \Delta t$$

$$t_c = 10\frac{D}{\omega} \qquad entrainment \tag{6}$$

$$t_c = \frac{D}{\omega} \qquad deposition$$

where

t_c = characteristic time

Δt = duration of time step

D = water depth

ω = fall velocity

The value 10 used in Equation 6 is somewhat arbitrary and is based on observations of the time required to establish a fully developed boundary layer. In this study, t_c was always determined using the entrainment or deposition equation because the time steps used in the simulations were very small.

The change in depth-averaged sediment concentration for a time step can then be calculated using the Garcia-Parker entrainment function and by assuming a Rousian vertical velocity distribution to adjust the calculated bed concentration to a depth-averaged concentration. Entrainment or deposition is adjusted by applying the characteristic time damping factor.

$$\frac{\partial C}{\partial t} = \frac{\left(E_s - r_o C\right)}{t_c} \tag{7}$$

Relatively high sediment entrainment rates were calculated by the Garcia-Parker equation compared with other sediment transport equations. One reason may be that this equation has not been verified for deep rivers like the Mississippi River. It is certain that neither this equation nor any other sediment transport equation has been verified for the very large shear velocities imposed by passing towboats. Even though the Ackers-White equation produced results that seemed to be more consistent with measured data, the Garcia-Parker equation was chosen for the production runs for two reasons: (a) it produced sediment concentrations that can be considered representative of the maximum reasonable effect due to tow passage and (b) because its formulation (entrainment is a function of only shear velocity and depth) is well suited for application to generalized relationships to determine sediment entrainment for a variety of hydrodynamic and tow passage conditions defined by the NAVEFF computer program (Maynord 1996). NAVEFF calculates return velocities and drawdown from commercial vessels operating in navigable waterways.

Cohesive sediment entrainment function

The modeling did not attempt to combine noncohesive and cohesive mobile-bed processes in the same run. Entrainment of cohesive sediment is calculated in SED2D using the Parthenaides (1965) equation.

$$\varepsilon = m \left[\frac{\tau_{b\,\max} - \tau_c}{\tau_c} \right] \tag{8}$$

where

ε = erosion rate

m = erosion rate coefficient

$\tau_{b\,max}$ = maximum bed-shear stress due to a tow passage

τ_c = critical bed-shear stress

Bed Material Gradations

Bed sediment samples were collected from Pool 8 and Pool 26 on the Mississippi River and from the LaGrange Pool on the Illinois River by teams from WES, the EMTC, and the State of Illinois Natural History Survey. The data were collected primarily to determine a representative grain size for use in SED2D. However, additional characteristics such as moisture content, bulk density, sand-silt-clay percentages, and loss-on-ignition (a measure of organic content) were determined for many of the samples. A total of 316 samples were collected in the three pools. Laboratory analyses were conducted at WES.

Sampling methods

Three sampling methods were used to collect bed sediment information. Surface samples were collected using two sizes of Ponar-type clam-shell dredges, bed stratification was identified using a core sampler, and a three-prong penetrometer was used to obtain relative density information. Federal Interagency Sedimentation Committee standards for bed material sampling are established for materials finer than medium gravel. The core sampler employed in this sampling effort is similar in form and function to the standard BMH-53 and was useful in shallow areas where the bed material was finer than gravel. The standard BM-54 is designed to collect sand-size bed samples in deep water, however, many of the samples in the deeper channels contained grain sizes too large to use the standard BM-54, and there is no other FISP standard equipment available at this time to sample the larger grain sizes. In such cases the U.S. Geologic Survey (USGS) recognizes that Ponar samplers and pipe dredges can be very useful (Edwards and Glysson 1988). The Ponar-type clam-shell dredge was used in this study to be consistent with existing sampling methodologies used by the EMTC facility of the National Biological Survey. The penetrometer is not a standardized tool at this time. Limited sampling was done using the penetrometer as requested by EMTC researchers who are collecting data to analyze its applicability in different environments.

Each bed material sample was classified based on its location. Major zones of hydraulic and geographic importance were established. These were:

a. navigation channel - the center line of the channel between the navigation buoys

b. main channel - includes the navigation channel and samples shoreward, excluding the channel border samples

c. main channel borders - include the samples taken at approximately 1.0-m depth and those at the waters edge

d. Side channels

(1) primary - branch off of the main channel and then reconnect to the main channel at some point downstream.
(2) secondary - branch off and return to the primary side channels or other secondary side channels but are not directly connected to the main channel, with possible exceptions at flood stages.

e. backwaters - areas that have only one inlet/outlet during normal discharges, making them a “dead-end” off of side channels.

The following paragraphs give a summary of the sediment analysis results pool by pool.

In Pool 8, when water depths were greater than 3 m, samples were collected using a small (15.24- by 15.24-cm, 9-kg) clam-shell dredge that was deployed and lifted by hand as the boat drifted with the current over the sampling location. In Pool 26 and LaGrange Pool, a larger clam-shell dredge (22.86 by 22.86 cm, 27 kg), operated with a winch system, was used to accommodate the higher velocities and depths. When either dredge was brought to the surface, it was emptied into a large plastic bucket so that the contents could be described and photographed. In some cases, after excess water was allowed to drain off, the entire sample was returned in a ziploc bag to the lab for analysis. In the case of large, homogeneous samples, the contents were mixed well and a subsample was returned to the lab. These methods are not inconsistent with standardized methods described by Edwards and Glysson (1988).

For samples in water 3 m deep or less, a hand-operated core sampler, about 5.1 cm in diameter and 7.6 cm long, with a removable inner sleeve, was used. Obvious stratification was noted in a field book, and the top 10 cm of the sample was preserved in a whirl-pak plastic bag. In a few cases, obvious stratification of clay and sand in the top 10 cm was separated into subsamples for analysis.

The penetrometer was used on a trial basis in Pool 8 side-channel and back-water areas. It was determined, by simultaneously sampling with the clam-shell dredge, that the penetrometer was giving similar nil readings for a variety of impenetrable materials such as clays and gravels, at which point its use was discontinued. The penetrometer data were passed on to the EMTC where extensive penetrometer work has been done in the past. The results presented herein do not include penetrometer data.

Sampling locations for the three trend pools included: (a) the main channel at the original upper, midway, and lower boundaries of the numerical model area, (b) midchannel at locations between the boundaries, and (c) adjacent to entrances into backwater and side-channel areas. The goal was to define the grain size distributions present on the bed that might be entrained by a passing tow and transported both in the main channel and possibly into side-channel and backwater areas. Samples were taken in the backwater and side-channel areas to determine if there was any correlation between the materials available for entrainment by vessels and those actually deposited in those off-channel areas. A second sampling trip to the LaGrange Pool was conducted to determine the extent of mussel shell coverage on the main channel bed. Outline maps showing sample locations are given in Figures 5, 6, and 7. Most of the samples were located spatially using GPS coordinates; however, a few are estimated based on aerial photo and topographic maps when the GPS unit failed.

Laboratory analysis and data

Samples composed primarily of sand and gravel were analyzed using standard dry sieving procedures at the WES Coastal and Hydraulics Laboratory. The entire sample was oven dried, weighed, and then processed through a stack of

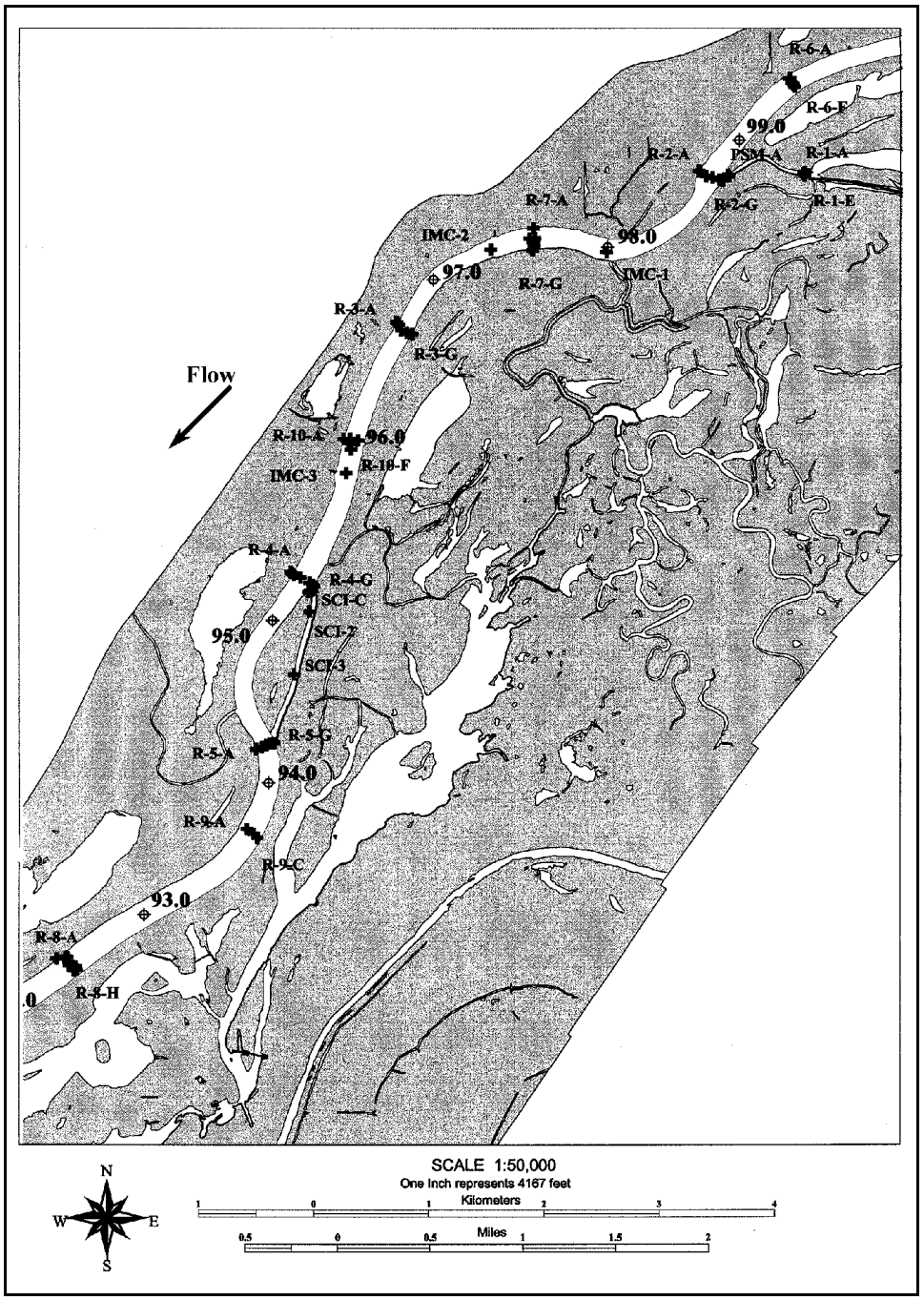

Figure 5. Bed-material sample locations on LaGrange Pool

sieves including the following mesh sizes: 19.1, 9.52, 4.76, 3.36, 2.0, 0.84, 0.42, 0.210, 0.149, 0.074, and 0.063 mm. The size fractions were calculated from the weight retained on each sieve. A spreadsheet was then used to calculate percentiles, the arithmetic and geometric means, and standard deviations for each sample. Large shell fragments and debris were removed from the sample before sieving, however, small shell fragments remained in the sieved samples.

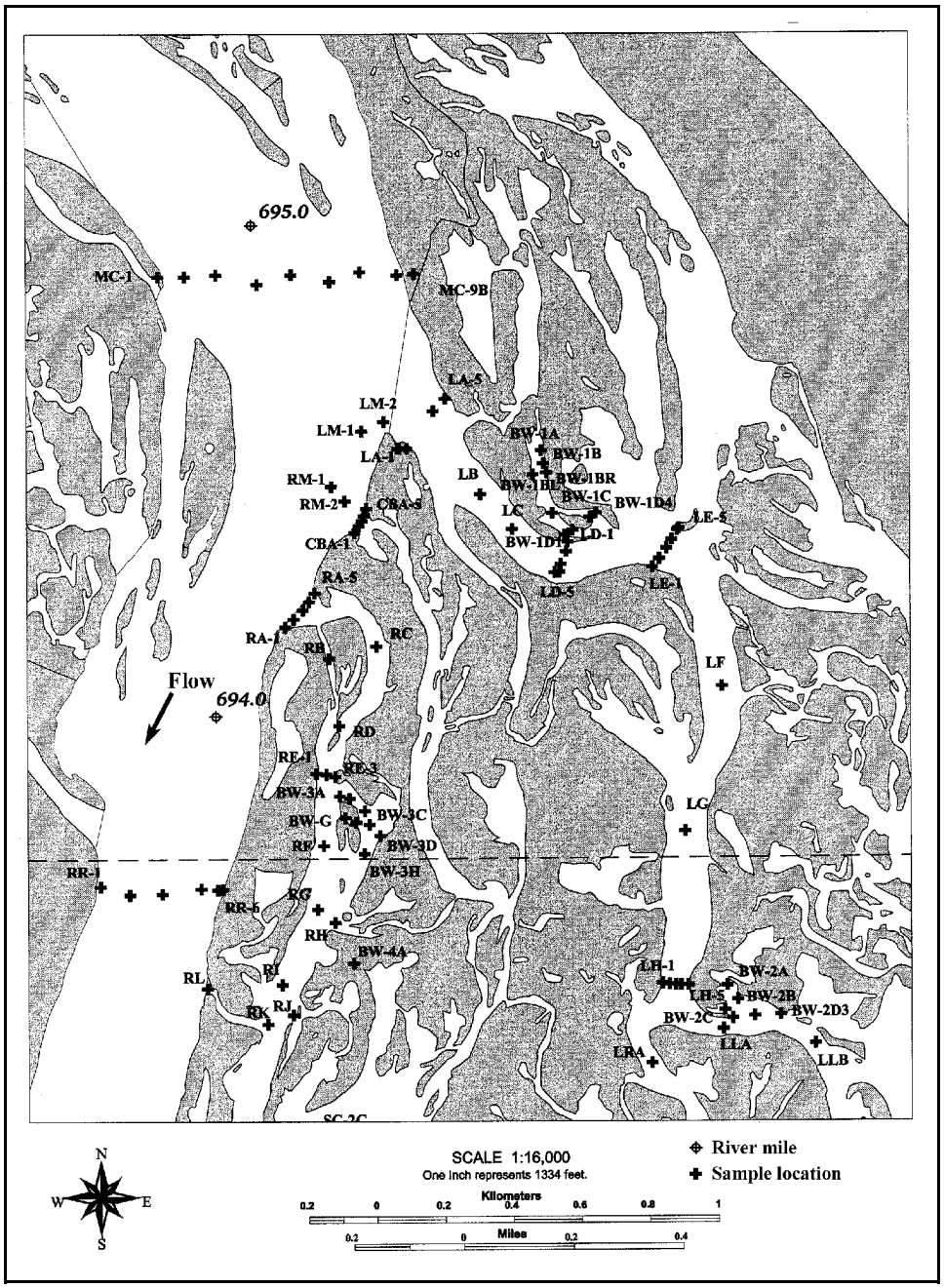

Figure 6. Bed-material sample locations on Pool 8 (Continued)

Samples composed primarily of fine sand, silt, and clay were processed at the WES Environmental Laboratory. A hydrometer was used to determine sand, silt, and clay percentages. Boundary values of 2 microns for the silt-clay cutoff and 50 microns for the sand-silt cutoff were used. All material greater than 5 mm was removed before the hydrometer analysis was run. In addition, these samples are processed to determine moisture content, a rough bulk density, and organic content using a loss-on-ignition measurement. It is important to note that the moisture content and bulk density of the samples are dependent on the

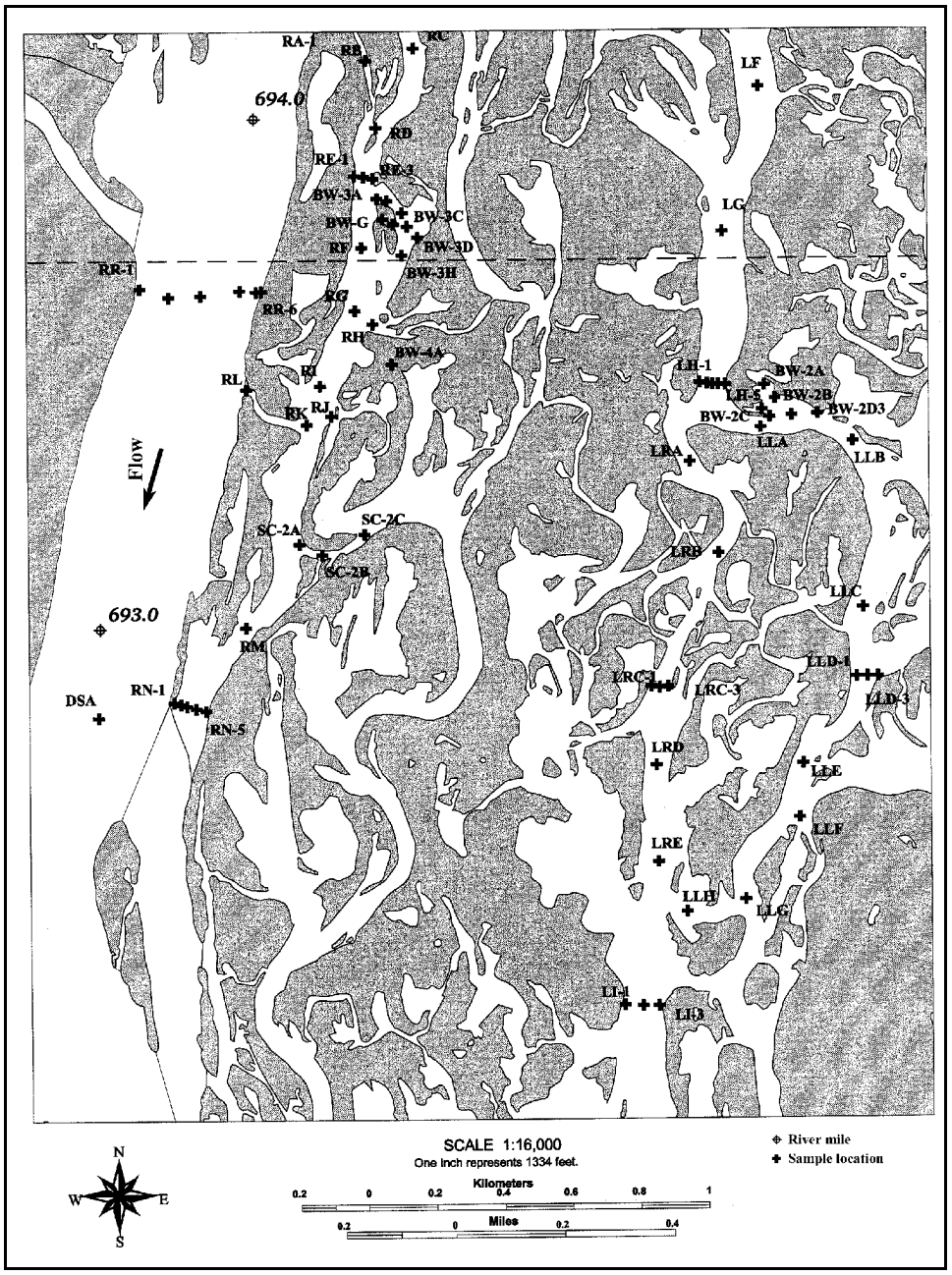

Figure 6. (Concluded)

sampling and storage methods. Clam-shell dredge samples will not give reliable values for either of these parameters, as the sample is highly disturbed. Core samples stored in the whirl-paks may give a more reliable value for the moisture content, but the reported bulk density does not represent undisturbed or in situ conditions because the sample was mixed by kneading before subsampling. Therefore, it will not reflect the packing or structural density of the natural river bed material, but rather the density of the disturbed particle mixture.

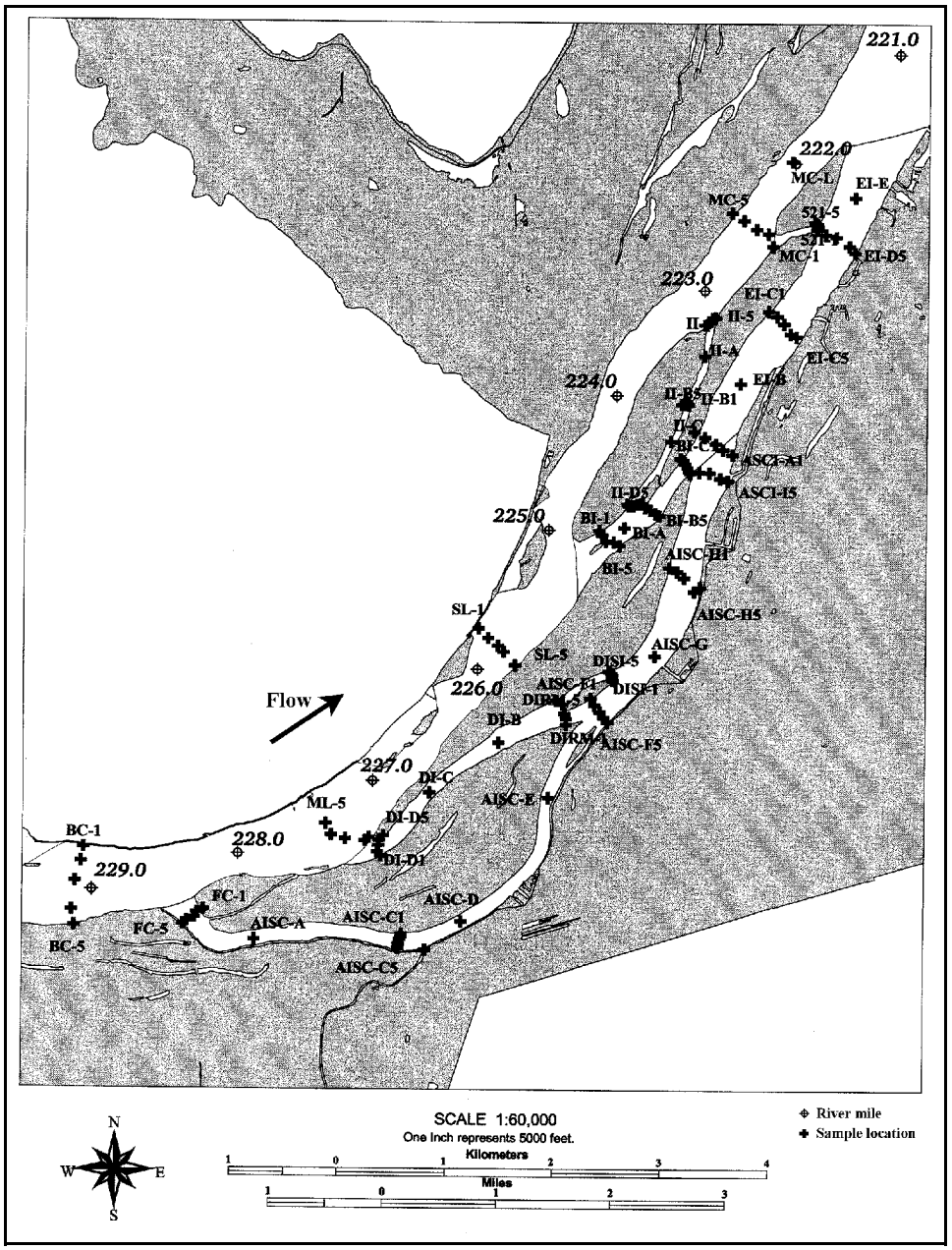

Figure 7. Bed-material sample locations on Pool 26

Finally, some samples were processed by both labs, using the methods described above, so that the final results included the complete set of data including: a sieve analysis, a hydrometer sand-silt-clay classification, an organic content, a moisture content, and a bulk density.

LaGrange Pool

A more detailed sampling program was conducted on the LaGrange Pool than on the Mississippi River pools due to the high degree of variability identified after the first sampling expedition. A total of nine cross sections and three midchannel locations were sampled for grain size information on the Illinois Waterway in the LaGrange Pool between river miles 93 and 100 during two sampling expeditions. Complete results are given in Table 2. Bed characteristics from the samples collected during the first trip (Ranges 1-5, Panther Slough Mouth (PSM), Sugar Creek Island side channel (SCI), and in-main-channel (IMC) were analyzed for sand, silt, and clay percentages and for percentiles and the presence or absence of shells. The second data set, Ranges 6 through 10, was collected 4 February 1998. The average velocity, taken at 0.6-m depth, on Range 6 was between 0.4 and 0.5 m/sec in the mid- and right-quarter channel, respectively. Depths in the navigation channel were around 6 m at mid-channel, 4.5 m at the quarter-channel location, and 1.8 to 3 m at the outer one-eighth channel location. A detailed laboratory analysis was performed on a subset of the 4 February 1998 samples to quantify the sediment characteristics of samples associated with mussel shells. Values in Table 2 for percentages of shells, sand, silt, and clay that are visual estimates are recorded in bold type. Quantitative sieve analysis is in plain type. The purpose of collecting data on Ranges 6 to 10 was to determine the approximate coverage of the bed by intact mussel shells and gravels. A statistical summary of the LaGrange sediment data is given in the following tabulation.

Statistics on Median Sediment Grain Sizes for Sub-Areas of LaGrange Pool

					Side Channels		Mussel Shell Area Analysis	
	Navigation Channel	Main Channel Without Gravel	Main Channel	Main Channel Border	Primary	Secondary	Without Intact Shells	With Intact Shells
Average, mm	2.39	0.22	2.37	0.02	0.037	0.004	0.31	1.36
Std. Dev., mm	5.13	0.20	5.94	0.02	0.074	0.001	0.32	3.55
Maximum, mm	16.71	0.65	24.91	0.10	0.22	0.005	1.23	16.74
Minimum, mm	0.12	0.007	0.01	0.003	0.003	0.003	0.03	0.03

Mussel-shell beds are typically found on either side of the center channel line, but at two locations the muscle beds actually straddled the center line rather than being on only one side. Cross-section sampling revealed that most of the LaGrange Pool study reach had intact shell coverage over one-eighth to one-fourth of the bed. Coverage expanded to around half of the channel in areas where there were large active mussel beds. This expanded shell coverage extended downstream at least 100 m from the focus of the mussel bed. The upstream extent was not determined. The maximum area covered by shells at a single cross section was approximately 60 percent. In contrast, one range had no intact shells.

Table 2
LaGrange Pool Bed Material Characteristics

SAMPLE ID	METHOD	DEPTH ft	LOCATION	SHELL CONTENT %	MOISTURE CONTENT %	BULK DENSITY g/mL	% OF SEDIMENT > 50u	% OF SEDIMENT 2u<X<50u	% OF SEDIMENT < 2u	LOSS-ON IGNITION (%)	**d95** mm	**d84** mm	**d65** mm	**d50** mm	**d35** mm	**d30** mm	**d16** mm	**d5** mm	**Geo. Mean** mm	**Geo. Std. Dev.** mm
R-1-A	SCOOP	0	SCRDB		47.0	0.751	2.50	67.5	30.0	5.5	0.0450	0.0265	0.0106	0.0051	0.0025	0.0020	0.0010	0.0006	0.0052	5.0870
R-1-B	PONAR	3	SCRQC		53.1	0.611	7.51	52.5	40.0	6.9			0.0300	0.0092	0.0036	0.0016	0.0014	0.0009	0.0006	0.0045	6.2612
R-1-C	PONAR	4.2	SCCC		58.8	0.536	2.50	56.3	41.3	7.2	0.0439	0.0232	0.0077	0.0032	0.0016	0.0013	0.0008	0.0006	0.0040	5.5215
R-1-D	PONAR	2.6	SCLQC		59.8	0.509	10.01	55.0	35.0	6.5		0.0356	0.0116	0.0048	0.0020	0.0016	0.0009	0.0006	0.0054	6.3279
R-1-E	SCOOP	0	SCLDB		40.9	0.914	5.01	65.0	30.0	5.7	0.0508	0.0293	0.0113	0.0053	0.0025	0.0020	0.0010	0.0006	0.0054	5.3508
PSM-A	SCOOP	0	SCRDB		30.3	1.195	35.00	41.2	23.7	5.4			0.0508	0.0155	0.0047	0.0032	0.0012	0.0007		
PSM-B	PONAR	4.1	SCCC		54.3	0.621	10.00	52.5	37.5	7.2		0.0350	0.0108	0.0042	0.0018	0.0015	0.0009	0.0006	0.0051	6.5286
PSM-C	SCOOP	0	SCLDB		38.3	0.994	22.50	47.5	30.0	6.5			0.0215	0.0077	0.0028	0.0020	0.0010	0.0006		
R-2-A	SCOOP	0	MCRDB		39.7	0.912	8.75	65.0	26.3	5.0		0.0353	0.0136	0.0064	0.0030	0.0024	0.0011	0.0006	0.0064	5.5727
R-2-B	PONAR	3	MCRNS		34.0	1.100	30.00	55.0	15.0	3.3			0.0377	0.0155	0.0064	0.0047	0.0021	0.0008		
R-2-C	PONAR	14	MCRQC		31.6	1.184	32.51	52.5	15.0	3.4			0.0435	0.0171	0.0068	0.0050	0.0021	0.0008		
R-2-D *	PONAR	13	NAV	**50 +**	25.8	1.386	83.75	8.8	7.5	4.8	28.0816	14.5839	6.6390	3.4351	0.4103	0.2689	0.1014	0.0017	1.7188	19.0672
R-2-E	PONAR	3.2	MCLQC		37.3	0.983	24.99	55.0	20.0	4.2			0.0281	0.0115	0.0047	0.0035	0.0015	0.0007		
R-2-F	PONAR	3	MCLNS		43.1	0.879	25.00	50.0	25.0	5.0			0.0265	0.0100	0.0037	0.0027	0.0012	0.0006		
R-2-G	SCOOP	0	MCLDB		39.5	0.954	17.49	60.0	22.5	4.7			0.0196	0.0087	0.0038	0.0029	0.0013	0.0007		
IMC-1 *	PONAR	20	NAV	**50 +**	31.0	1.229	70.00	22.5	7.5	2.6	0.6685	0.3343	0.1851	0.1234	0.0787	0.0625	0.0072	0.0012	0.0668	9.8873
IMC-2 *	PONAR	16	NAV	**50 +**	18.6	1.630	90.00	5.0	5.0	2.0	43.6122	40.2053	30.4231	16.7130	8.8141	6.3073	0.7006	0.1060	7.7791	13.1313
R-3-A	SCOOP	0	MCRDB*		37.3	1.046	17.49	57.5	25.0	4.3			0.0188	0.0080	0.0034	0.0026	0.0012	0.0006		
R-3-B	PONAR	3	MCRNS		36.1	1.094	34.98	43.8	21.3	4.1			0.0506	0.0166	0.0054	0.0037	0.0014	0.0007		
R-3-C *	PONAR	11.8	MCRQC	**30 +**	21.4	1.545	87.50	7.5	5.0	3.2	30.0641	26.2075	15.0027	10.6365	6.9834	5.9954	1.6823	0.0324	7.7692	4.3932
R-3-D *	PONAR	17	NAV	**50 +**	17.2	1.627	93.75	2.5	3.8	2.6	10.0470	3.0705	1.1219	0.6537	0.4234	0.3430	0.1815	0.0162	0.7142	4.1492
R-3-E	PONAR	10.5	MCLQC		48.9	0.755	18.76	56.3	25.0	4.4			0.0198	0.0083	0.0035	0.0026	0.0012	0.0006		
R-3-F	PONAR	3	MCLNS		40.7	0.932	7.51	67.5	25.0	4.4		0.0337	0.0135	0.0065	0.0032	0.0025	0.0012	0.0006	0.0064	5.3334
R-3-G	SCOOP	0	MCRDB		40.2	0.948	10.00	67.5	22.5	3.0		0.0380	0.0152	0.0074	0.0036	0.0028	0.0013	0.0007	0.0072	5.3940
IMC-3 *	PONAR	14	NAV	**50 +**	19.9	1.539	95.00	0.0	5.0	2.8	8.2391	2.9297	1.0488	0.6072	0.3915	0.3458	0.2443	0.0783	0.7574	3.6556
R-4-A	SCOOP	0	MCRDB		31.2	1.197	26.26	48.7	25.0	4.8			0.0283	0.0104	0.0038	0.0027	0.0012	0.0006		
R-4-B	PONAR	3	MCRNS		44.2	0.856	4.99	62.5	32.5	5.1	0.0507	0.0286	0.0106	0.0049	0.0022	0.0018	0.0010	0.0006	0.0051	5.4574
R-4-C	PONAR	8.5	MCRQC		36.5	1.032	13.75	58.7	27.5	4.7		0.0448	0.0156	0.0068	0.0030	0.0022	0.0011	0.0006	0.0069	6.4056
R-4-D *	PONAR	12.7	NAV	yes	20.8	1.611	92.50	2.5	5.0	2.2	3.5284	1.4819	0.5913	0.3727	0.2493	0.2180	0.1539	0.0020	0.4397	3.1987
R-4-E *	PONAR	5.3	MCLQC	yes	26.0	1.359	85.00	7.5	7.5	1.6	10.6626	1.4121	0.3570	0.2759	0.2132	0.1857	0.0843	0.0013	0.3202	4.1955
R-4-F	PONAR	3	MCLNS		29.0	1.267	50.00	35.0	15.0	2.9	0.3636	0.2275	0.1095	0.0625	0.0142	0.0086	0.0022	0.0008	0.0313	16.3118
R-4-G	SCOOP	0	MCLDB		50.8	0.693	-2.51	62.5	40.0	6.6	0.0387	0.0213	0.0076	0.0034	0.0016	0.0014	0.0009	0.0006	0.0039	5.1445
SCI-A	SCOOP	0	SCRDB		26.2	1.398	25.00	52.5	22.5	5.7	0.0909	0.0660	0.0273	0.0108	0.0042	0.0031	0.0013	0.0007	0.0098	7.1770
SCI-B	PONAR	3	SCRNS		37.9	1.012	42.50	32.5	25.0	4.3	0.0965	0.0799	0.0577	0.0239	0.0053	0.0032	0.0012	0.0006	0.0131	11.7631
SCI-C	SCOOP	0	SCLDB		51.0	0.726	2.50	52.5	45.0	7.7	0.0435	0.0220	0.0068	0.0027	0.0014	0.0012	0.0008	0.0006	0.0036	5.7895
SCI-2	PONAR	5.5	SCCC		25.1	1.354	80.00	12.5	7.5	1.8	0.4445	0.3606	0.2738	0.2203	0.1590	0.1283	0.0206	0.0012	0.1179	6.1620
SCI-3	PONAR	4	SCCC		35.2	1.132	21.25	61.3	17.5	3.9	0.0886	0.0607	0.0244	0.0110	0.0050	0.0038	0.0017	0.0007	0.0105	5.9307
R-5-A	SCOOP	0	MCRDB		26.7	1.350	35.01	45.0	20.0	3.8			0.0508	0.0171	0.0058	0.0040	0.0015	0.0007		
R-5-B	PONAR	4.5	MCRNS		34.9	1.066	57.50	27.5	15.0	3.0	9.4071	0.3986	0.1870	0.1005	0.0305	0.0157	0.0025	0.0008	0.0462	22.4086
R-5-C *	PONAR	13	MCRQC	yes	21.7	1.497	90.91	3.0	6.1	1.8	44.0636	41.5520	35.7683	24.9094	16.7746	13.6456	7.3478	3.4038	19.6655	2.5291
R-5-D	PONAR	14.4	NAV		20.5	1.602	95.00	2.5	2.5	0.5	0.7770	0.5992	0.3998	0.3311	0.2742	0.2575	0.2160	0.0625	0.3499	1.6712
R-5-E	PONAR	12.2	MCLQC		38.8	0.969	32.50	46.2	21.2	4.8			0.0427	0.0148	0.0052	0.0036	0.0014	0.0007		
R-5-F	PONAR	3	MCLNS		39.2	0.990	12.50	65.0	22.5	4.4		0.0426	0.0164	0.0078	0.0037	0.0028	0.0013	0.0007	0.0076	5.7095
R-5-G	SCOOP	0	MCLDB		40.7	0.947	25.00	53.8	21.3	4.2			0.0276	0.0111	0.0045	0.0033	0.0014	0.0007		
R-6-A	PONAR	16	MCRQC	frags				**50.0**	**50.0**											
R-6-B	PONAR	20	MCRIEC	30.55		1.169	30.00	55.0	15.0	3.2	1.0076	0.1633	0.0456	0.0325	0.0195	0.0151	0.0029	0.0013	0.0248	8.1728
R-6-C	PONAR	19	NAV	69.24			**68.00**	**16.0**	**16.0**		0.3840	0.3048	0.1933	0.1504	0.0995	0.0724	0.0619	0.0537	0.1416	2.2271
R-6-D	PONAR	20	MCLISC	34.31		1.044	94.99	3.8	1.3	5.1	3.2375	1.4511	0.3917	0.3206	0.2496	0.2259	0.1722	0.0488	0.4311	3.1940
R-6-E	PONAR	18	MCLIEC	20		1.006	65.00	22.5	12.5	3.1	0.4052	0.3438	0.2377	0.1765	0.0740	0.0393	0.0095	0.0014	0.0831	10.2966
R-6-F	PONAR	14	MCLQC	**0**				**50.0**	**50.0**											
R-7-A	PONAR	11	MCROEC					**50.0**	**50.0**											
R-7-B	PONAR	15	MCRQC	frags			**50.00**	**50.0**												
R-7-C	PONAR	19	MCRIEC	frags			**50.00**	**50.0**												
R-7-D	PONAR	19	NAV	17.2		1.452	95.00	3.8	1.3	1.6	1.7009	1.0430	0.3861	0.3269	0.2677	0.2480	0.1887	0.0488	0.4007	2.4615
R-7-E	PONAR	16	MCLIEC	**75**			**25.00**													
R-7-F	PONAR	15	MCLQC	**25**			**75.00**													
R-7-G	PONAR	7	MCLOEC	minor			**50.00**	**50.0**												

Table 2
LaGrange Pool Bed Material Characteristics

SAMPLE ID	METHOD	DEPTH ft	LOCATION	SHELL CONTENT %	MOISTURE CONTENT %	BULK DENSITY g/mL	% OF SEDIMENT > 50u	% OF SEDIMENT 2u<X<50u	% OF SEDIMENT < 2u	LOSS-ON IGNITION (%)	**d95** mm	**d84** mm	**d65** mm	**d50** mm	**d35** mm	**d30** mm	**d16** mm	**d5** mm	**Geo. Mean** mm	**Geo. Std. Dev.** mm
R-8-A	PONAR		MCROEC	**5**			**5.00**	**45.0**	**45.0**											
R-8-B	PONAR		MCROSC	**10**			**10.00**	**40.0**	**40.0**											
R-8-C	PONAR		MCRQC	29.37		1.262	82.50	12.5	5.0	1.8										
R-8-D	PONAR		MCRIEC	**50**			**50.00**													
R-8-E	PONAR	15	NAV	**50**		1.520	97.50		2.5	1.8	6.2465	3.5305	1.7307	1.2342	0.7376	0.5720	0.3034	0.1615	1.0975	3.4641
R-8-F	PONAR		MCLIEC	22.48		1.556	97.50	2.5	0.0	2.3	1.8274	1.4478	0.7921	0.4015	0.3357	0.3138	0.2524	0.1808	0.5274	2.5985
R-8-G	PONAR	11	MCLQC	**35**			**65.00**			0.9	1.7386	1.1634	0.4015	0.3434	0.2853	0.2659	0.2117	0.0707	0.4389	2.5051
R-8-H	PONAR	6	MCLOEC	1.2		1.562	97.50	2.5	0.0	0.6	1.7101	1.0724	0.3938	0.3431	0.2923	0.2754	0.2280	0.1541	0.4378	2.3153
R-9-A	PONAR		MCRQC				**90.00**	**10.0**												
R-9-B	PONAR		NAV	frags			**90.00**													
R-9-C	PONAR		MCLQC			1.206	27.50	60.0	12.5	2.9	0.2811	0.0687	0.0440	0.0320	0.0200	0.0160	0.0048	0.0014	0.0219	4.4070
R-10-A	PONAR		MCROEC					**50.0**	**50.0**											
R-10-B	PONAR		MCRQC	24.1		0.860	35.00	50.0	15.0	3.8	3.1205	0.6894	0.0740	0.0356	0.0212	0.0164	0.0030	0.0013	0.0417	15.6957
R-10-C	PONAR		MCRIEC	**50**				**25.0**	**25.0**											
R-10-D	PONAR		MCRISC	frags			**90.00**	**10.0**												
R-10-E	PONAR		NAV	minor frags					**95.0**											
R-10-F	PONAR		MCLQC				**90.00**	**10.0**												
AVERAGES						**1.12**	**46.51**	**38.27**	**22.36**	**3.91**	**6.43**	**3.54**	**1.77**	**1.13**	**0.68**	**0.54**	**0.22**	**0.08**	**1.06**	**6.65**

NOTE:

MC	MAIN CHANNEL
SC	SIDE CHANNEL
SSC	SECONDARY SIDE CHANNEL
NAV	IN NAVIGATION PATH BETWEEN BOUYS
BW	BACKWATER AREAS ARE OFF OF A CHANNEL AND HAVE A DEAD END AT FLAT POOL.
LDB	LEFT DESCENDING BANK
RDB	RIGHT DESCENDING BANK
CC	CENTER OF CHANNEL
QC	QUARTER CHANNEL USED GENERICALLY FOR SAMPLES TAKEN BETWEEN CENTER OF CHANNEL AND THE BANKS
NS	NEARSHORE : SAMPLE IS TAKEN SUBAQUEOUSLY IN 1 METER OR LESS DEPTH OF WATER
IEC	INNER 1/8TH OF THE CHANNEL FROM THE CC
OEC	OUTER 1/8TH OF THE CHANNEL FROM THE QC
ISC	INNER 1/16TH OF THE CHANNEL FROM THE CC

****BOLD PERCENTAGE VALUES ARE VISUAL ESTIMATES ONLY !!**

In some cases it was difficult to determine if an intact mussel bed existed or how effective it would be in terms of armoring the bed. This difficultly arose because the clam-shell dredge disturbed the samples as they were collected. When both bed sediment and shells were collected, it was difficult to determine if the bed sediment had been above, below, above and below, or mixed with the shells.

All of the samples contained some shell fragments of various sizes and percentages. These shell fragments were well mixed with the other bed sediments and did not form an "armoring" as the intact shells might. However, shells did create a shift in mean effective particle size as some samples were more than 50 percent shells. This shift is reflected in the median values shown in the preceding statistical summary tabulation for the LaGrange Pool. In this tabulation, the sample medians were 0.31 mm with shells removed, and 1.36 mm with the shells included. The standard deviation of the samples also increased from 0.32 mm without shells to 3.55 mm with shells. The bed sediment collected with the shells varied from coarse sand to silty clays and sands. Sand was predominant in the main channel samples associated with intact shells. However, 6 of the 12 samples analyzed were 30 percent silt and clay when the shells were removed from the analysis. One sample was collected off of hard-packed clay that the clam-shell sampler brought up in rigid clumps with the shells.

The shorelines were composed primarily of hard-packed clays and silts. However, a sandbar was evident on the left descending bank just upstream of Range 7 near the mouth of the Old Sangamon River. The sandbar was pointed out by an employee of the Illinois State Water Survey as the site of an extensive mussel bed.

The Sangamon River was diverted between 40 and 50 years ago and used to contribute significant gravel and sand to the Illinois River. These remnant gravels were of sufficient quantity to affect the grain size distributions of the bed material downstream from the old Sangamon River confluence. Samples taken from this area indicated a bed that was coarser than the average bed determined for the Illinois River. Assuming that these gravels are immobile under current hydraulic conditions and represent only a localized anomaly, a more representative grain size distribution can be achieved by removing samples that contain large percentages of gravel when calculating the average. The preceding statistical summary tabulation for the LaGrange Pool has a column in which the statistical parameters were calculated excluding samples that contained gravels. The adjusted average d_{50} is only 0.22 mm with a minium d_{50} of 0.007 compared to 2.39 mm and 0.12 mm for the unadjusted navigation channel average and minimum. This adjustment puts the grain size distributions more in line with the observed fine nature of most of the channel and channel borders.

For the LaGrange Pool, the water's edge samples were typically 50 to 100 percent finer than those at the 1-m depth. The main channel border data given in the preceding statistical summary tabulation for the LaGrange Pool are an average of these finer waters-edge samples and those at the 1-m depth.

In general, the main channel and the navigation channel showed similar characteristics until the depth became 1 m or less, at which point the grain size distribution fined from the sand range to the silt range. There is an additional fining trend from the main channel into the primary (83 percent) and further into the secondary (98 percent) side-channel areas. The sorting increases as well, as evidenced by the decreasing standard deviation of d_{50} as samples are taken farther from the center of the main channel. The bed sediment for areas where mussel shells were identified was somewhat coarser (0.31 mm) compared to the main channel samples (0.22 mm). This may be due to the fact that mussel shells were located most often within the inner one-fourth of the channel and the main channel samples extend out to the outer one-eighth of the channel and so are influenced by the fining profile toward the channel borders.

Five cohesive samples were selected from those collected during the first sampling trip for laboratory analysis of cohesive bed characteristics. The WES Coastal and Hydraulics Laboratory determined bed-material gradations, critical shear stresses, and erosion rates for the cohesive samples. Size class distributions were determined using a laser particle size analyzer. The critical shear stress and erosion rates were measured in both a Particle Entrainment Simulator (PES) device and a Vertical Loop Sediment Water Tunnel (VOST) device. Values determined using the different devices produced slightly different results which is typical of laboratory test results with cohesive sediments. Measured results are shown in Table 3.

Table 3
Laboratory Determined Cohesive Bed Characteristics, LaGrange Pool

					PES Device		VOST Device	
Sample No.	Moisture Content Percent	Bulk Weight Density gm/cm^3	Percent Organics	Median Grain Size mm	Critical Shear Stress Pa	Erosion Rate g/m^2/min	Critical Shear Stress Pa	Erosion Rate g/m^2/min
1	33.8	1.699	4.0	0.012	x	x	x	x
2	31.7	1.738	3.7	0.013	0.46	27.7	x	x
3	29.9	1.762	3.6	0.013	x	x	2.20	7.44
4	30.4	1.754	3.6	0.012	0.44	5.2	x	x
5	35.3	1.672	4.2	0.010	0.45	3.7	2.24	165.0

Note: x = not determined in laboratory

Pool 8

Samples collected on the Mississippi River in Pool 8 between river miles 695 and 692.5, 5-7 June 1995, consisted of 16 cross sections and 47 single samples from midbackwater or center-channel areas for a total of 121 samples. Sample locations are shown in Figure 6. Two major side channels were sampled and

four backwaters with cross sections across the mouth and single samples in the center extending to the back edge. Two cross sections were taken in the main channel, MC(1-9) and RR(1-6). MC stands for main channel and was the upstream-most cross section sampled before the channel began splitting around islands. RR stands for root river which is just upstream of where the cross section was sampled. Sample DSA (stands for downstream) was also in the main channel on the navigation line and is the downstreammost sample taken in this study. The side-channel samples are named using (L)eft and (R)ight for the left side channel when facing downstream and rightmost side channel. Both side channels were on the left descending bank of the river. Alphabetical progression was followed from upstream to downstream and numbers were added to the name in the case of cross sections. For example, RA5 is the fifth and left descending bank sample taken on the upstreammost cross section at the entrance of the right side channel from the main channel. RB would be a single sample in the middle of the channel next downstream from RA(1-5), etc. The left side channel bifurcates into LL (left branch of left channel) A through H and LR (right branch of left channel).

Eighty-three samples were analyzed completely by both the sieve analysis and the hydrometer analysis for grain size distributions. An additional 22 samples were analyzed using the hydrometer method alone. Fourteen of the remaining samples were sampled only by penetrometer method with some visual estimates of grain size on nine of those samples. The complete results are given in Table 4. The following statistical summary tabulation for Pool 8 presents the statistics on the median (d_{50}) grain sizes for selected channel environments found in Pool 8.

Statistics on Median Sediment Grain Sizes for Sub-Areas of Pool 8

				Side Channels		Backwater Areas	
	Navigation Channel	Main Channel	Main Channel Border	Primary	Secondary	All Samples	Borders
Average, mm	0.44	0.43	0.24	0.38	0.36	0.1	0.12
Std. Dev., mm	0.105	0.11	0.14	0.45	0.087	0.097	0.04
Maximum, mm	0.64	0.64	0.39	2.87	0.52	0.34	0.16
Minimum, mm	0.34	0.23	0.092	0.024	0.24	0.0051	0.062

As in the case of the LaGrange Pool, there is a close similarity between the navigation channel and more complete sampling of navigable waters of the main channel excluding the borders. The fining trend from the main channel out through the side channels and into the backwater areas also continued. The main channel borders are 44 percent finer than the main channel in contrast to the 91 percent decrease in d_{50} for the LaGrange Pool. In Pool 8, the primary and secondary side channels had similar mean values for d_{50}, but the secondary side

Table 4
Pool 8 Bed Material Characteristics

SAMPLE ID	METHOD	DEPTH ft	LOCATION	MOISTURE CONTENT %	BULK DENSITY g/mL	% OF SEDIMENT > 50u	% OF SEDIMENT 2u<X<50u	% OF SEDIMENT < 2u	LOSS-ON IGNITION (%)	d95 mm	d84 mm	d65 mm	d50 mm	d35 mm	d30 mm	d16 mm	d5 mm	Geo. Mean mm	Geo. Std. Dev. mm
MC 1	CORE	2.7	MCRDB	27.13	1.44	95.00	2.50	2.50	0.21	0.8224	0.6814	0.4925	0.3866	0.3106	0.2888	0.2355	0.0625	0.3959	1.7023
MC 2	CORE	8.9		14.80	1.74	97.50	2.50	0.00	0.28	1.5865	0.8407	0.6252	0.4949	0.3780	0.3362	0.2423	0.1512	0.4654	1.8708
MC 3	CORE	8	NAV	11.84	1.73	95.00	2.50	2.50	0.42	1.4357	0.7754	0.5400	0.4048	0.2983	0.2694	0.1941	0.0625	0.3935	2.0004
MC 4	PONAR	20.6	NAV	12.40	1.51	97.50	2.50	0.00	0.22	1.4332	0.7908	0.6336	0.5318	0.4464	0.4211	0.2941	0.2214	0.4982	1.6478
MC 5	PONAR	21.6	NAV	14.40	1.50	97.50	2.50	0.00	0.19	0.8561	0.6955	0.4995	0.3926	0.3211	0.3003	0.2489	0.2148	0.4081	1.6743
MC 6	PONAR	21.3	NAV	16.91	1.60	97.50	2.50	0.00	0.23	0.8940	0.6870	0.4790	0.3740	0.3014	0.2805	0.2293	0.1635	0.3891	1.7341
MC 7	PONAR	9		77.16	0.24	67.50	20.00	12.50	6.20	0.7735	0.4976	0.3095	0.2269	0.0899	0.0405	0.0036	0.0009	0.0740	32.7691
MC 8	PONAR	10		14.29	1.55	97.50	2.50	0.00	0.27	0.7994	0.6199	0.4095	0.3425	0.2864	0.2699	0.2284	0.1626	0.3647	1.6548
MC 9	CORE	0.4	MCLDB	16.58	1.56	97.50	2.50	0.00	0.29	0.8321	0.6874	0.4942	0.3827	0.2985	0.2748	0.2180	0.1249	0.3856	1.7761
MC 9B	CORE	0.4		17.60	1.53	95.00	2.50	2.50	0.56	0.2894	0.1871	0.1456	0.1218	0.1018	0.0959	0.0812	0.0508	0.1228	1.5181
RR 1	CORE	2.1	MCRDB	17.72	1.56	72.50	22.50	5.00	1.61	0.5874	0.3746	0.2715	0.2107	0.0933	0.0680	0.0106	0.0020	0.0943	10.7967
RR 2	PONAR	15		14.19	1.55	97.50	2.50	0.00	0.28	0.7970	0.6417	0.4413	0.3602	0.2994	0.2815	0.2369	0.1856	0.3797	1.6509
RR 3	PONAR	21.5	NAV	14.11	1.58	97.50	2.50	0.00	0.36	1.9882	1.3488	0.7810	0.6409	0.5259	0.4924	0.3819	0.2265	0.6912	1.8913
RR 4	PONAR	13.5	NAV	14.33	1.50	97.50	2.50	0.00	0.09	0.7997	0.6834	0.5209	0.4204	0.3348	0.3104	0.2510	0.2124	0.4162	1.6503
RR 5	PONAR	15.2	NAV	18.02	1.59	87.50	7.50	5.00	1.49	7.6838	1.6477	0.4777	0.3405	0.2584	0.2357	0.1529	0.0020	0.4410	3.5332
RR 6	CORE	1.6	MCLDB	28.37	1.20	62.50	27.50	10.00	2.86	0.3137	0.1913	0.1304	0.0923	0.0456	0.0243	0.0042	0.0010	0.0419	12.1254
LA 1	CORE	1.5	SCRDB	18.62	1.52	92.50	5.00	2.50	0.63	0.3866	0.3141	0.2195	0.1862	0.1615	0.1539	0.0994	0.0110	0.1798	1.7802
LA 2	PONAR	16		13.83	1.51	97.50	0.00	2.50	0.31	1.5670	0.8011	0.6226	0.5103	0.4169	0.3738	0.2756	0.2168	0.4830	1.7109
LA 3	PONAR	12.3	MCSC	19.46	1.59	97.50	0.00	2.50	0.29	1.3658	0.7537	0.5382	0.4136	0.3280	0.3036	0.2445	0.1803	0.4239	1.7570
LA 4	PONAR	12.1		13.43	1.54	97.50	2.50	0.00	0.33	1.2833	0.7586	0.5624	0.4441	0.3388	0.3085	0.2374	0.1232	0.4308	1.7895
LA 5	CORE	2	SCLDB	24.12	1.31	77.50	15.00	7.50	1.44	0.2091	0.1678	0.1249	0.1021	0.0834	0.0780	0.0139	0.0012	0.0620	4.4889
LM 2	PONAR	15.8	SCEMC	16.71	1.54	97.50	2.50	0.00	0.30	1.7416	1.0884	0.7129	0.5890	0.4866	0.4565	0.3254	0.2238	0.5931	1.8289
LM 1	PONAR	20	SCEMC	13.82	1.63	97.50	2.50	0.00	0.21	0.9550	0.6832	0.4639	0.3660	0.2984	0.2788	0.2304	0.1651	0.3862	1.7277
LB	PENE	19.6	SCCC																
LC	PONAR	22.4	SCCC	15.29	1.85	90.00	5.00	5.00	0.88	8.2754	4.6941	0.6106	0.3814	0.2538	0.2216	0.1196	0.0021	0.5982	7.7488
LD 1	CORE/PEI	1.8	SCLDB	20.50	1.34	95.00	2.50	2.50	0.43	0.2447	0.1986	0.1774	0.1623	0.1479	0.1314	0.0942	0.0625	0.1448	1.4731
LD 2	PONAR/PI	8		17.31	1.55	97.50	0.00	2.50	0.16	0.5019	0.3877	0.3286	0.2884	0.2531	0.2423	0.2145	0.1576	0.2884	1.3442
LD 3	PONAR	19.2		23.01	1.45	72.50	17.50	10.00	2.50	0.8258	0.6277	0.3844	0.2431	0.1004	0.0712	0.0064	0.0010	0.0993	20.2596
LD 4	PONAR	22		46.22	0.75	87.50	7.50	5.00	2.65	0.3316	0.2022	0.1624	0.1317	0.1030	0.0949	0.0755	0.0020	0.1262	1.6405
LD 5	CORE/PEI	2	SCRDB	26.16	1.28	72.50	20.00	7.50	1.71	0.3007	0.1925	0.1462	0.1092	0.0815	0.0740	0.0085	0.0012	0.0564	7.2899
BW1A	CORE/PEI	2.4	BWCC	45.09	0.84	47.50	40.00	12.50	6.10				0.0414	0.0122	0.0081	0.0026	0.0009		
BW1B	CORE	3	BWCC	61.78	0.51	9.99	57.50	32.50	8.04		0.0360	0.0123	0.0052	0.0022	0.0018	0.0010	0.0006	0.0057	6.1439
BW1BR	PENE	1.3	BWRDB																
BW1BL	PENE	1.8	BWLDB																
BW1C	CORE	3.7	BWCC	64.88	0.42	2.50	67.50	30.00	9.04	0.0450	0.0265	0.0106	0.0051	0.0025	0.0020	0.0010	0.0006	0.0052	5.0870
BW1D 1	CORE	2.8	BWLDB	40.51	0.91	72.50	20.00	7.50	4.76	0.2442	0.1572	0.1171	0.0949	0.0769	0.0685	0.0085	0.0012	0.0503	6.3985
BW1D 2	CORE	2.9		29.23	1.24	82.50	10.00	7.50	2.02	0.3312	0.2048	0.1704	0.1457	0.1038	0.0926	0.0372	0.0012	0.1035	2.6635
BW1D 3	CORE	2.4		21.63	1.46	70.00	22.50	7.50	2.22	0.3333	0.2052	0.1672	0.1312	0.0833	0.0625	0.0072	0.0012	0.0580	9.8531
BW1D 4	CORE	1.9	BWRDB	35.39	1.07	80.00	12.50	7.50	3.94	0.3684	0.2189	0.1739	0.1487	0.1034	0.0917	0.0206	0.0012	0.0875	4.3417
LE 1	CORE	2	SCRDB	19.97	1.53	87.49	10.01	2.50	1.13	0.3496	0.2279	0.1802	0.1573	0.1212	0.1079	0.0779	0.0046	0.1408	1.7336
LE 2	PONAR	12.2		15.86	1.67	92.29	5.14	2.57	1.22	4.1485	2.1437	0.9574	0.6784	0.5174	0.4727	0.2684	0.0101	0.7308	2.8439
LE 3	PONAR	18.3		9.68	1.70	97.50	0.00	2.50	0.38	6.0164	5.0788	1.6545	0.6725	0.4790	0.4278	0.2784	0.1739	0.9833	4.9840
LE 4	PONAR	8.9		20.34	1.54	90.00	5.00	5.00	1.21	0.6585	0.3658	0.2603	0.2027	0.1697	0.1599	0.0978	0.0020	0.1935	1.9385
LE 5 TOP	CORE	2.3	SCLDB	24.34	1.11	52.50	35.00	12.50	6.36	0.2367	0.1567	0.1007	0.0697	0.0181	0.0110	0.0028	0.0009	0.0311	13.7402
LE 5 SAN	CORE	2.3	SCLDB	47.65	0.86	39.68	44.23	16.08	5.68				0.0237	0.0079	0.0054	0.0019	0.0008		
LF	PONAR	9.1	SCCC	12.12	1.47	97.50	2.50	0.00	0.33	1.4841	0.8028	0.6459	0.5440	0.4582	0.4328	0.3038	0.2225	0.5100	1.6331
LG	PONAR	11.6	SCCC	9.46	1.73	95.00	2.50	2.50	0.33	0.9903	0.6327	0.3968	0.3294	0.2734	0.2570	0.2160	0.0625	0.3557	1.7230
LH 1	CORE	2	SCRDB	24.27	1.38	70.01	20.00	10.00	3.28	0.1829	0.1369	0.1070	0.0881	0.0712	0.0625	0.0055	0.0010	0.0405	8.7446
LH 2	PONAR	11.8		15.75	1.63	97.50	2.50	0.00	0.26	1.5912	0.7898	0.5846	0.4611	0.3567	0.3262	0.2539	0.1984	0.4522	1.7645
LH 3	PONAR	10.6		14.59	1.50	97.50	2.50	0.00	0.18	1.0315	0.7191	0.5317	0.4190	0.3336	0.3092	0.2500	0.2115	0.4223	1.6962
LH 4	PONAR	9.4		18.36	1.63	97.50	2.50	0.00	0.21	1.1174	0.7374	0.5552	0.4438	0.3483	0.3206	0.2544	0.2120	0.4366	1.7032
LH 5	CORE	5.8	SCLDB	16.37	1.52	95.00	2.50	2.50	0.35	0.3888	0.3257	0.2399	0.1964	0.1689	0.1606	0.1142	0.0625	0.1940	1.6889
LRA	PONAR	7.6	SCCC	21.67	1.49	97.50	2.50	0.00	0.40										
LRB	PONAR	6.6	SCCC	13.94	1.61	97.50	0.00	2.50	0.42										
LRC 1	CORE	1.4	SCRDB	23.20	1.37	87.50	5.00	7.50	1.26								0.0012		
LRC 2	PONAR	6.8	SCCC	26.56	1.32	87.50	7.50	5.00	1.48								0.0020		
LRC 3	CORE	1.6	SCLDB	22.47	1.34	82.50	10.00	7.50	1.23							0.0311	0.0012		
LRD	CORE	2.6	SCCC	17.07	1.53	97.50	2.50	0.00	0.28	0.8043	0.6470	0.4442	0.3601	0.2978	0.2795	0.2341	0.1730	0.3793	1.6674
LRE	CORE	2	SCCC	11.57	1.52	97.50	2.50	0.00	0.20	0.7204	0.4853	0.3492	0.2900	0.2409	0.2264	0.1795	0.1140	0.2934	1.6446
LI 1	CORE	1.3	SCRDB	38.71	0.96	67.50	22.50	10.00	6.52					0.0522	0.0353	0.0047	0.0010		
LI 2	PONAR	7.8	SCCC	13.83	1.49	97.50	2.50	0.00	0.27	0.8774	0.6437	0.4100	0.3334	0.2712	0.2531	0.2070	0.1498	0.3542	1.7709
LI 3	CORE	2.5	SCLDB	18.84	1.58	92.50	2.50	5.00	1.11	0.4105	0.3402	0.2459	0.1965	0.1652	0.1559	0.1002	0.0020	0.1885	1.8461
LLA	PONAR	7.2	SCCC	16.55	1.62	97.28	2.72	0.00	0.35										
BW2A	CORE	2	BWCC	65.74	0.43	17.51	57.49	25.00	10.98	0.0854	0.0541	0.0188	0.0081	0.0034	0.0026	0.0012	0.0006	0.0080	6.7519
BW2B	CORE	1	BWCC	54.61	0.62	27.50	52.50	20.00	8.64	0.0921	0.0688	0.0319	0.0126	0.0050	0.0036	0.0015	0.0007	0.0109	6.9833
BW2C	CORE	1.5	BWCC	56.21	0.58	37.50	45.00	17.50	8.65	0.0954	0.0771	0.0533	0.0205	0.0069	0.0048	0.0017	0.0007	0.0140	7.7970
BW2D 1	CORE	1.5	BWLDB	51.02	0.66	50.00	35.00	15.00	6.58	0.2030	0.1595	0.1019	0.0625	0.0142	0.0086	0.0022	0.0008	0.0278	15.7674

Table 4
Pool 8 Bed Material Characteristics

SAMPLE ID	METHOD	DEPTH ft	LOCATION	MOISTURE CONTENT %	BULK DENSITY g/mL	% OF SEDIMENT > 50u	% OF SEDIMENT 2u<X<50u	% OF SEDIMENT < 2u	LOSS-ON IGNITION (%)	d95 mm	d84 mm	d65 mm	d50 mm	d35 mm	d30 mm	d16 mm	d5 mm	Geo. Mean mm	Geo. Std. Dev. mm
BW2D 2	CORE	3.4	BWCC	49.06	0.74	17.50	67.50	15.00	6.00	0.1377	0.0665	0.0254	0.0118	0.0055	0.0042	0.0021	0.0008	0.0117	5.6891
BW2D 3	CORE	1.5	BWRDB	50.54	0.70	65.00	25.00	10.00	5.37	0.2070	0.1634	0.1166	0.0909	0.0625	0.0312	0.0045	0.0010	0.0405	11.0288
LLB	PONAR	6.5	SCCC	14.17	1.55	97.50	2.50	0.00	0.30	1.4345	0.7898	0.5944	0.4749	0.3697	0.3367	0.2590	0.2107	0.4597	1.7485
LLC	CORE	7.3	SCCC	17.11	1.58	97.50	2.50	0.00	0.34	0.8266	0.6890	0.5031	0.3967	0.3217	0.3000	0.2467	0.2115	0.4070	1.6725
LLD 1	CORE	6	SCRDB	16.16	1.66	92.50	7.50	0.00	0.56	1.5163	0.8054	0.5087	0.3698	0.2821	0.2577	0.1968	0.1506	0.3884	2.0286
LLD 2	CORE	4	SCCC	15.68	1.65	97.50	2.50	0.00	0.33	0.6865	0.4117	0.3083	0.2454	0.1922	0.1751	0.1131	0.0197	0.2252	1.9240
LLD 3	CORE	1.5	SCLDB	25.48	1.44	95.00	5.00	0.00	0.57	0.8149	0.5594	0.3634	0.2960	0.2411	0.2252	0.1752	0.1014	0.3073	1.7899
LLE	PONAR	14.5	SCCC	16.04	1.66	97.50	2.50	0.00	0.47	2.1917	1.1555	0.6768	0.5256	0.4048	0.3633	0.2684	0.2116	0.5463	2.0783
LLF	PONAR	16	SCCC	9.46	1.69	97.50	2.50	0.00	0.33	1.0736	0.7006	0.4816	0.3762	0.3065	0.2862	0.2363	0.1714	0.3964	1.7271
LLG	PONAR	14	SCCC	17.00	1.55	97.50	0.00	2.50	0.21	0.4602	0.3876	0.3334	0.2960	0.2628	0.2525	0.2260	0.1789	0.2960	1.3095
LLH	CORE	2.2	SCCC	18.52	1.48	92.50	2.50	5.00	0.64								0.0020		
RM 1	PONAR	20	ESCMC	13.24	1.52	97.50	2.50	0.00	0.28	2.7560	0.8172	0.6646	0.5646	0.4796	0.4542	0.3310	0.2259	0.5345	1.5766
RM 2	PONAR	23	ESCMC	13.77	1.59	97.52	2.48	0.00	0.30	1.8536	0.7648	0.5080	0.3829	0.3055	0.2833	0.2294	0.1560	0.4065	1.8331
CBA 1	CORE	4.2	BWRDB	21.54	1.48	80.00	12.50	7.50	1.49	0.4903	0.3294	0.2067	0.1613	0.1096	0.0941	0.0206	0.0012	0.1031	4.9333
CBA 2	PONAR	5.5		14.20	1.40	97.50	0.00	2.50	0.21	0.7040	0.4284	0.3333	0.2764	0.2291	0.2153	0.1673	0.0926	0.2706	1.6011
CBA 3	PONAR	6.5	BWCC	15.25	1.63	97.50	0.00	2.50	0.22	1.4025	0.6677	0.4139	0.3352	0.2715	0.2531	0.2051	0.1299	0.3581	1.8133
CBA 4	CORE	4.1		24.15	1.40	90.00	2.50	7.50	0.63	0.8304	0.5249	0.3064	0.2165	0.1676	0.1543	0.0909	0.0012	0.2178	2.4026
CBA 5	CORE	1	BWLDB	17.45	1.54	92.50	2.50	5.00	1.08	0.2871	0.1975	0.1672	0.1448	0.1134	0.1045	0.0832	0.0020	0.1335	1.5520
RA 1	PONAR	5	SCRDB	29.28	1.23	52.50	32.50	15.00	3.23	0.2064	0.1454	0.0950	0.0668	0.0165	0.0097	0.0022	0.0008	0.0276	16.4634
RA 2	PONAR	15.5		9.57	1.95	97.69	2.31	0.00	0.71	9.9864	6.8789	4.0171	2.8693	2.0494	1.5764	0.6367	0.2440	2.3250	3.4518
RA 3	PONAR	7	SCCC	13.26	1.57	97.50	2.50	0.00	0.59	0.9686	0.7113	0.5187	0.4064	0.3278	0.3051	0.2496	0.2132	0.4163	1.6892
RA 4	PONAR	6.2		14.13	1.39	97.50	2.50	0.00	0.26	0.6134	0.4034	0.3449	0.3049	0.2694	0.2586	0.2304	0.2105	0.3049	1.3231
RA 5	CORE	0.5	SCLDB	18.85	1.53	97.50	2.50	0.00	0.37	0.3779	0.2986	0.2065	0.1861	0.1678	0.1621	0.1389	0.0821	0.1976	1.4722
RB	PONAR	7.5	SCCC	15.49	1.58	97.50	2.50	0.00	0.69	1.92422	1.621177	1.205811	0.954534	0.727613	0.654821	0.487465	0.251171	0.910308066	1.828277654
RC	CORE	4.5	SCCC	15.50	1.56	95.00	5.00	0.00	0.70	1.3203	0.7435	0.5132	0.3835	0.2873	0.2609	0.1896	0.0625	0.3781	1.9806
RD	CORE	4.5	SCCC	14.71	1.69	)O MANY ROCKS			0.49	1.8603	0.8096	0.5993	0.4727	0.3643	0.3316	0.2547	0.1953	0.4602	1.7843
RE 1	CORE	3.5	SCRDB	29.10	1.23	72.50	17.50	10.00	2.64	0.4141	0.2830	0.1665	0.1169	0.0813	0.0704	0.0064	0.0010	0.0596	10.3310
RE 2	PONAR	9.6	SCCC	13.65	1.47	97.50	2.50	0.00	0.30	0.7660	0.5958	0.4026	0.3382	0.2842	0.2681	0.2279	0.1635	0.3581	1.6229
RE 3	CORE	3	SCLDB	20.39	1.48	85.00	12.50	2.50	1.49	0.3807	0.2630	0.1823	0.1533	0.1121	0.1000	0.0687	0.0039	0.1405	1.9733
BW3A	CORE	1.5	BWCC	52.88	0.61	35.00	50.00	15.00	7.14			0.0508	0.0191	0.0072	0.0052	0.0021	0.0008		
BW3B	CORE	2	BWCC	22.81	1.42	85.00	10.00	5.00	1.49								0.0020		
BW3C	CORE	3	BWCC	45.62	0.78	55.00	35.00	10.00	5.39					0.0200	0.0126	0.0034	0.0010		
BW3D	CORE	0	BWCC	21.06	1.49	87.50	10.00	2.50	1.71								0.0044		
BW3E	CORE		BWCC	26.30	1.29	75.00	17.50	7.50	2.34							0.0095	0.0012		
BW3F	PENE	3	BWCC																
BW3G	PENE	1.5	BWCC																
BW3H	PENE	5.6	BWCC																
RF	PENE/VIS	4.8	SCCC																
RG	PENE/VIS	4	SCCC																
RH	PENE/VIS	3.3	SCCC					15.00											
RI	CORE	4.7	SCCC	14.44	1.66	97.50	2.50	0.00	0.28										
RJ	PENE/VIS	0	SCCC																
SCA	PONAR	6.8	ESCMC	13.25	1.59	97.50	2.50	0.00	0.27										
RK	CORE	6	SCRDB	17.77	1.49	95.00	5.00	0.00	0.38								0.0508		
RL	PENE/VIS		SCCC																
SC2A	PENE/VIS	4.8	SCLDB																
SC2B	PENE/VIS	1.5	SCLDB																
SC2C	CORE	5.5	SCCC	32.01	1.12	77.50	17.50	5.00	2.52							0.0151	0.0020		
BW4A	PENE/VIS	3	BWCC																
RM	PENE/VIS	6	SCCC																
RN 1	CORE	1.5	SCRDB	17.97	1.55	92.50	5.00	2.50	0.84								0.0100		
RN 2	CORE	4.7		20.18	1.43	95.00	2.50	2.50	0.53								0.0508		
RN 3	PONAR	5.4	SCCC	13.98	1.66	92.50	7.50	0.00	0.49								0.0171		
RN 4	CORE	4		15.10	1.63	97.50	2.50	0.00	0.28	1.6636	0.7808	0.5690	0.4432	0.3460	0.3186	0.2530	0.2111	0.4440	1.7567
RN 5	CORE	1.5	SCLDB	18.29	1.47	92.50	7.50	0.00	0.70	0.3353	0.2047	0.1672	0.1396	0.1101	0.1017	0.0815	0.0197	0.1325	1.5898
DSA	PONAR	11	ESCMC	13.33	1.54	97.50	2.50	0.00	0.34										

channels and backwaters showed a higher degree of sorting. The d_{50} fined from the main channel to side channels by approximately 30 percent and 35 percent into the backwater areas.

Pool 26

Pool 26 was sampled 18-19 July 1995 between river miles 222.5 and 228.5 on the Mississippi River. Twenty-two cross sections were sampled from water's edge to water's edge and 12 samples were collected in the middle of the channel for a total of 120 clam-shell dredge and core samples. There were no dead-end backwaters in this reach of the river, and the side channels were much less complicated than those found on Pool 8. Comparing Figure 7 to Figure 6, we see that there were fewer anabranches in Pool 26 and the flow through the side-channels was actually flow around and within islands. The labeling scheme for Pool 26 was based on the names of the islands. For instance, AISC stands for Apple Island side channel, DI is Dardenne Island, EI is Enterprise Island, etc.

Table 5 lists all of the samples collected and gives the results of the hydrometer and sieve analyses. Gaps in the record reflect selective sieving to reduce costs. Very fine samples were only analyzed using the hydrometer method, whereas very coarse samples were only analyzed using the sieve process. Hydrometer results are given for 52 of the samples, and complete sieve results are available for 74 of the 120 samples. The following tabulation presents the summary statistics on the median (d_{50}) grain sizes for portions of the main channel and side channel areas of Pool 26.

Statistics on Median Sediment Grain Sizes for Sub-Areas of Pool 26

				Side Channels	
	Navigation Channel	**Main Channel**	**Main Channel Border**	**Primary**	**Secondary**
Average, mm	0.47	0.48	0.35	0.42	0.35
Std. Dev., mm	0.14	0.14	0.15	0.40	0.62
Maximum, mm	0.77	0.77	0.5	1.57	3.47
Minimum, mm	0.34	0.31	0.1	0.015	0.007

As in the other two pools, the navigation and main channel samples are similar in average d_{50} sizes of around 0.47 mm. Pool 8 and Pool 26 show more general similarity for sorting (standard deviation) and maximum and minimum values than LaGrange Pool. In Pool 26, the main channel border is only 25 percent finer than the middle channel samples. Fining into the primary side channels is less pronounced at 10.6 percent than the other two pools, and, in this case, the side channels are not as well sorted, containing material that is both coarser and finer than that found in the main channel. The secondary side channels are finer than the main channel by 25 percent.

Table 5
Pool 26 Bed Material Characteristics

SAMPLE ID	METHOD	LOCATION	BULK DENSITY g/mL	% OF SEDIMENT > 50u	% OF SEDIMENT 2u<X<50u	% OF SEDIMENT < 2u	LOSS-ON IGNITION (%)	d95 mm	d84 mm	d65 mm	d50 mm	d35 mm	d30 mm	d16 mm	d5 mm	Geo. Mean mm	Geo. Std. Dev. mm
BC 1	PONAR	MCLDB	1.20	75.00	15.00	10.00	1.74	0.8059	0.5697	0.3287	0.2216	0.1573	0.1162	0.0078	0.0010	0.0995	15.4655
BC 2	PONAR	NAV						1.0059	0.6849	0.4635	0.3662	0.2991	0.2796	0.2315	0.1732	0.3872	1.7262
BC 3	PONAR	MCCC						1.2823	0.7667	0.6049	0.5017	0.4134	0.3732	0.2803	0.2238	0.4759	1.6591
BC 4	PONAR	MCRQC						3.0823	1.4852	0.7943	0.6588	0.5464	0.5134	0.4312	0.2632	0.7500	1.8912
BC 5	CORE	MCRDB	1.47	80.00	15.00	5.00	1.66	1.9825	1.1688	0.6491	0.4715	0.2663	0.2098	0.0248	0.0020	0.2391	10.7436
ML 1	PONAR	MCRDB						0.7815	0.6265	0.4276	0.3573	0.3008	0.2840	0.2419	0.2132	0.3783	1.6153
ML 2	PONAR	MCRQC						1.4498	0.8012	0.6293	0.5201	0.4299	0.3922	0.2910	0.2301	0.4950	1.6639
ML 3	PONAR	MCCC						2.4223	1.3541	0.7465	0.5854	0.4591	0.4233	0.3009	0.2294	0.6202	2.1294
ML 4	PONAR	NAV						1.9105	1.0574	0.6971	0.5760	0.4759	0.4466	0.3237	0.2373	0.5820	1.8075
ML 5	PONAR	NAV						6.2225	2.8870	1.2152	0.7696	0.5912	0.5415	0.4234	0.2576	0.9798	2.7845
SL 1	CORE	MCLDB	1.50	97.50	0.00	2.50	0.33	0.7288	0.4608	0.3552	0.3056	0.2629	0.2500	0.2172	0.1567	0.3127	1.4574
SL 2	PONAR	MCLQC						0.8369	0.6232	0.4022	0.3448	0.2956	0.2808	0.2433	0.2173	0.3739	1.6123
SL 3	PONAR	NAV						2.0545	0.8406	0.6287	0.4998	0.3909	0.3541	0.2685	0.2160	0.4832	1.7716
SL 4	PONAR	NAV						1.3343	0.7575	0.5539	0.4326	0.3448	0.3200	0.2596	0.2202	0.4398	1.7089
SL 5	PONAR	MCRDB	1.72	97.50	0.00	2.50	0.47	10.3395	4.6331	0.9034	0.4976	0.3161	0.2757	0.1847	0.0960	0.7524	6.0021
MC 1	CORE	MCRDB						0.1667	0.1366	0.1146	0.0997	0.0867	0.0828	0.0722	0.0616	0.0995	1.3753
MC 2	PONAR	MCRQC						6.3439	0.4143	0.3501	0.3066	0.2684	0.2568	0.2268	0.1841	0.3066	1.3515
MC 3	PONAR	NAV						0.8209	0.6234	0.4061	0.3459	0.2947	0.2793	0.2405	0.2138	0.3729	1.6203
MC 4	PONAR	NAV						1.3388	0.7661	0.5698	0.4510	0.3552	0.3278	0.2617	0.2193	0.4489	1.7110
MC 5	CORE	MCLDB						2.9265	0.9926	0.6206	0.4727	0.3555	0.3223	0.2448	0.1729	0.4861	2.0154
MC L	PONAR	NAV						1.3424	0.6714	0.4081	0.3471	0.2951	0.2796	0.2403	0.2134	0.3826	1.6893
FC 1	CORE	SCLDB	1.34	62.50	25.00	12.50	3.05	0.2511	0.1707	0.1121	0.0804	0.0367	0.0191	0.0031	0.0009	0.0348	14.1093
FC 2	PONAR	SCLQC						1.3408	0.7673	0.5910	0.4810	0.3816	0.3477	0.2680	0.2184	0.4624	1.6950
FC 3	PONAR	SCCC						1.1496	0.7391	0.5554	0.4432	0.3496	0.3226	0.2577	0.2160	0.4387	1.6937
FC 4	PONAR	SCRQC	1.66	100.00	0.00	2.50	0.63	3.4559	2.3158	1.4277	1.0147	0.7167	0.6367	0.4571	0.2391	1.0241	2.2509
FC 5	CORE	SCRDB	1.09	37.50	50.00	12.50	3.22	0.2369	0.1378	0.0672	0.0263	0.0093	0.0066	0.0025	0.0009	0.0208	7.9002
AISC A	PONAR	SCCC						1.1900	0.7597	0.5991	0.4966	0.4069	0.3690	0.2808	0.2265	0.4732	1.6491
AISC B	PONAR	SCCC	0.66	5.01	82.49	12.50	5.79	0.0508	0.0329	0.0155	0.0086	0.0047	0.0039	0.0022	0.0009	0.0086	3.8296
AISC C1	PONAR	SCLDB	1.54	82.50	12.50	5.00	1.16	0.3680	0.2061	0.1622	0.1273	0.0956	0.0868	0.0412	0.0020	0.1027	2.3531
AISC C2	PONAR	SCLQC						1.4263	0.7751	0.5697	0.4467	0.3525	0.3259	0.2618	0.2203	0.4492	1.7209
AISC C3	PONAR	SCCC						0.8750	0.7138	0.5347	0.4257	0.3422	0.3182	0.2597	0.2213	0.4289	1.6581
AISC C4	PONAR	SCRQC															
AISC C5	PONAR	SCRDB	1.30	22.49	60.01	17.50	3.88			0.0257	0.0114	0.0051	0.0038	0.0017	0.0007		
AISC D	PONAR	SCCC	1.14	37.50	45.00	17.50	5.52				0.0205	0.0069	0.0048	0.0017	0.0007		
AISC E	PONAR	SCCC						0.7854	0.6595	0.4878	0.3916	0.3242	0.3044	0.2553	0.2222	0.4040	1.6092
AISC F1	CORE	SCLDB	1.15	42.50	45.00	12.50	3.73	0.2011	0.1343	0.0811	0.0351	0.0110	0.0075	0.0026	0.0009	0.0229	8.7719
AISC F2	PONAR	SCLQC						0.7862	0.6372	0.4433	0.3655	0.3078	0.2906	0.2476	0.2183	0.3863	1.6099
AISC F3	PONAR	SCCC						1.2719	0.7759	0.6190	0.5178	0.4332	0.3980	0.2924	0.2295	0.4898	1.6346
AISC F4	PONAR	SCRQC						0.8370	0.7117	0.5379	0.4313	0.3404	0.3144	0.2516	0.2112	0.4258	1.6823
AISC F5	CORE	SCRDB	1.32	62.50	30.00	7.50	2.73	0.1996	0.1538	0.1085	0.0829	0.0468	0.0263	0.0052	0.0012	0.0405	8.8789
AISC G	PONAR	SCCC															
AISC H1	CORE	SCLDB	1.16	42.50	42.50	15.00	4.45				0.0286	0.0090	0.0062	0.0021	0.0008		
AISC H2	PONAR	SCLQC															
AISC H3	PONAR	SCCC															
AISC H4	PONAR	SCRQC															
AISC H5	CORE	SCRDB	1.21	24.99	50.00	25.00	4.34			0.0264	0.0100	0.0037	0.0027	0.0012	0.0006		
AISC I1	CORE	SCLDB	0.92	29.99	50.01	20.00	4.72	0.1482	0.0974	0.0442	0.0156	0.0055	0.0039	0.0015	0.0007	0.0131	8.3929
AISC I2	PONAR	SCLQC						1.4228	0.7543	0.5320	0.4075	0.3292	0.3066	0.2512	0.2148	0.4258	1.7365
AISC I3	PONAR	SCCC						7.4724	3.1803	0.6576	0.4842	0.3672	0.3377	0.2671	0.2222	0.7437	4.1905
AISC I4	PONAR	SCRQC						2.3671	1.5293	0.8797	0.6944	0.5609	0.5224	0.4280	0.2646	0.7689	1.9124
AISC I5	CORE	SCLDB	1.00	35.00	50.00	15.00	4.07	0.1632	0.1083	0.0625	0.0221	0.0078	0.0055	0.0021	0.0008	0.0171	7.7280
EI A1	CORE	SCRDB	1.17	62.50	27.50	10.00	3.24	0.2573	0.1754	0.1188	0.0868	0.0456	0.0243	0.0042	0.0010	0.0399	11.4453
EI A2	PONAR	SCRQC						8.8435	4.3744	1.5667	0.8316	0.6130	0.5537	0.4118	0.2506	1.1443	3.6397
EI A3	PONAR	SCCC						1.2156	0.7521	0.5734	0.4628	0.3666	0.3375	0.2677	0.2231	0.4533	1.6770
EI A4	PONAR	SCLQC						1.9550	1.2354	0.7429	0.6144	0.5081	0.4769	0.3645	0.2471	0.6516	1.8482
EI A5	CORE	SCLDB	1.19	50.00	35.00	15.00	4.50				0.0625	0.0142	0.0086	0.0022	0.0008	0.0301	16.1145
EI B	PONAR	SCCC															
EI C1	CORE	SCLDB	1.11	27.49	52.50	20.00	4.34			0.0319	0.0126	0.0050	0.0036	0.0015	0.0007		
EI C2	PONAR	SCLQC															
EI C3	PONAR	SCCC															
EI C4	PONAR	SCRQC															
EI C5	PONAR	SCRDB	1.32	90.00	5.00	5.00	0.86								0.0020		
EI D1	CORE	SCLDB	0.88	20.51	57.56	21.93	5.34			0.0224	0.0096	0.0041	0.0031	0.0013	0.0007		
EI D2	PONAR	SCLQC	1.53	97.50	0.00	2.50	0.24										
EI D3	PONAR	SCCC	1.54	97.50	0.00	2.50	0.34	1.7980	1.1535	0.7344	0.6123	0.5105	0.4804	0.3697	0.2308	0.6392	1.7700
EI D4	PONAR	SCRQC															
EI D5	CORE	SCRDB	1.12	27.49	47.50	25.00	5.10			0.0303	0.0108	0.0039	0.0028	0.0012	0.0006		

Table 5
Pool 26 Bed Material Characteristics

SAMPLE ID	METHOD	LOCATION	BULK DENSITY g/mL	% OF SEDIMENT > 50u	% OF SEDIMENT 2u<X<50u	% OF SEDIMENT < 2u	LOSS-ON IGNITION (%)	**d95** mm	**d84** mm	**d65** mm	**d50** mm	**d35** mm	**d30** mm	**d16** mm	**d5** mm	**Geo. Mean** mm	**Geo. Std. Dev.** mm
EI E	PONAR	SCCC															
DI D1	CORE	SSCRDB	1.25	45.00	35.00	20.00	4.02	0.4010	0.2988	0.1626	0.0381	0.0086	0.0053	0.0015	0.0007	0.0256	16.7896
DI D2	PONAR	SSCRQC	0.74	32.50	47.50	20.00	4.88	0.2088	0.1497	0.0521	0.0174	0.0058	0.0041	0.0015	0.0007	0.0157	10.1811
DI D3	PONAR	SSCCC						0.7656	0.6157	0.4225	0.3569	0.3021	0.2858	0.2446	0.2165	0.3774	1.5920
DI D4	PONAR	SSLQC						1.7217	0.9308	0.6781	0.5620	0.4658	0.4376	0.3145	0.2341	0.5480	1.7214
DI D5	CORE	SSCLDB	1.09	57.50	32.50	10.00	3.03	0.3102	0.1900	0.1256	0.0835	0.0281	0.0165	0.0037	0.0010	0.0389	12.4081
DI C	PONAR	SSCCC															
DI B	PONAR	SSCCC															
DIRM 1	CORE	SSCRDB	0.97	22.50	60.00	17.50	5.46	0.1440	0.0779	0.0304	0.0128	0.0054	0.0040	0.0017	0.0007	0.0120	6.7313
DIRM 2	PONAR	SSCRQC						0.9927	0.7127	0.5185	0.4067	0.3325	0.3110	0.2577	0.2223	0.4211	1.6653
DIRM 3	PONAR	SSCCC						1.7051	0.8838	0.6747	0.5625	0.4690	0.4414	0.3204	0.2376	0.5421	1.6633
DIRM 4	PONAR	SSCLQC						1.6016	0.8523	0.6700	0.5587	0.4659	0.4385	0.3186	0.2384	0.5333	1.6396
DIRM 5	CORE	SSCLDB	1.23	32.50	52.50	15.00	3.60	0.2439	0.1376	0.0530	0.0197	0.0073	0.0053	0.0021	0.0008	0.0178	8.2137
DISI 1	CORE	SSCRDB	1.10	47.50	40.00	12.50	3.13				0.0414	0.0122	0.0081	0.0026	0.0009		
DISI 2	PONAR	SSCRQC	1.67	100.00	0.00	0.00	0.24										
DISI 3	PONAR	SSCCC															
DISI 4	PONAR	SSCLQC						11.2594	8.4530	5.4549	3.4737	1.7885	1.3402	0.6091	0.2958	2.6151	4.0684
DISI 5	CORE	SSCLDB	1.20	50.00	35.00	15.00	3.05				0.0508	0.0126	0.0079	0.0021	0.0008		
BI 1	CORE	SSCLDB	1.12	62.50	25.00	12.50	2.55	0.2215	0.1686	0.1158	0.0867	0.0442	0.0221	0.0032	0.0009	0.0359	14.6278
BI 2	PONAR	SSCLQC	1.60	90.00	0.00	20.00	0.78	0.8882	0.7224	0.5511	0.4451	0.3116	0.2719	0.0349	0.0019	0.2239	7.1857
BI 3	PONAR	SSCCC						1.2390	0.7726	0.6289	0.5347	0.4545	0.4306	0.3071	0.2291	0.5024	1.5931
BI 4	PONAR	SSCRQC						1.7674	0.9662	0.7011	0.5941	0.5034	0.4764	0.3799	0.2508	0.6019	1.5951
BI 5	CORE	SSCRDB	1.06	32.50	47.50	20.00	5.99	0.2931	0.1655	0.0521	0.0174	0.0058	0.0041	0.0015	0.0007	0.0162	10.6369
BI A	PONAR	SSCCC															
BI B1	CORE	SSCLDB	1.07	25.00	50.00	25.00	5.37			0.0265	0.0100	0.0037	0.0027	0.0012	0.0006		
BI B2	PONAR	SSCLQC															
BI B3	PONAR	SSCCC															
BI B4	PONAR	SSCRQC	1.48	92.50	0.00	17.50	0.58								0.0008		
BI B5	CORE	SSCRDB	0.94	0.00	82.50	17.50	3.84	0.0417	0.0270	0.0127	0.0070	0.0039	0.0032	0.0017	0.0007	0.0069	3.9466
BI C1	CORE	SSCRDB	1.23	65.00	27.50	7.50	2.05	0.2056	0.1677	0.1184	0.0900	0.0625	0.0333	0.0057	0.0012	0.0441	8.8238
BI C2	PONAR	SSCRQC						0.9402	0.7245	0.5511	0.4440	0.3528	0.3263	0.2621	0.2207	0.4385	1.6628
BI C3	PONAR	SSCCC						1.0975	0.7556	0.6011	0.5018	0.4179	0.3781	0.2858	0.2293	0.4767	1.6309
BI C4	PONAR	SSCLQC						1.9562	1.3031	0.7612	0.6175	0.5010	0.4672	0.3393	0.2353	0.6488	1.9650
BI C5	CORE	SSCLDB	1.09	42.50	45.00	12.50	3.68	0.1682	0.1181	0.0738	0.0351	0.0110	0.0075	0.0026	0.0009	0.0220	8.5418
II D1	CORE	SSCRDB	1.20	27.49	55.00	17.50	4.28			0.0325	0.0134	0.0055	0.0041	0.0017	0.0007		
II D2	PONAR	SSCRQC															
II D3	PONAR	SSCCC															
II D4	PONAR	SSCLQC															
II D5	CORE	SSC3DB	1.40	87.50	7.50	5.00	1.22								0.0020		
II C	PONAR	SSCCC															
II B1	CORE	SSCRDB	0.92	37.49	50.01	12.50	3.80	0.1484	0.1096	0.0662	0.0263	0.0093	0.0066	0.0025	0.0009	0.0193	7.3617
II B2	PONAR	SSCRQC	1.70	100.00	0.00	0.00	0.56	4.4279	2.3663	1.3288	0.9068	0.6728	0.6133	0.4733	0.2924	1.0051	2.2628
II B3	PONAR	SSCCC						1.9018	0.8648	0.6299	0.4991	0.3909	0.3566	0.2756	0.2251	0.4918	1.7718
II B4	PONAR	SSCLQC															
II B5	CORE	SSCLDB	1.44	82.50	12.50	5.00	1.37							0.0343	0.0020		
II A	PONAR	SSCCC															
II 01	CORE	SSCLDB	0.95	37.50	45.00	17.50	4.44	0.1404	0.1071	0.0632	0.0205	0.0069	0.0048	0.0017	0.0007	0.0156	8.5274
II 02	PONAR	SSCLQC	1.39	100.00	0.00	0.00	0.27	0.6778	0.4164	0.3464	0.2995	0.2590	0.2467	0.2154	0.1546	0.2995	1.3904
II 03	PONAR	SSCCC															
II 04	CORE	SSCRQC	1.72	100.00	0.00	0.00	0.44										
II 05	CORE	SSCRDB	1.16	29.99	55.01	15.00	5.78			0.0377	0.0155	0.0064	0.0047	0.0021	0.0008		
521-1		SSCRDB	1.07	54.99	35.00	10.00	2.84					0.0200	0.0126	0.0034	0.0010		
521-2	PONAR	SSCRQC															
521-3	PONAR	SSCCC															
521-4	PONAR	SSCLQC															
521-5	CORE	SSCLDB	1.22	60.00	27.50	12.50	2.45					0.0281	0.0155	0.0030	0.0009		
AVERAGE			**1.24**	**56.21**	**32.02**	**12.20**	**2.98**	**1.6854**	**0.9247**	**0.4923**	**0.3477**	**0.2551**	**0.2299**	**0.1667**	**0.1183**	**0.3947**	**4.5000**
ST. DEV.			0.25	29.05	22.95	7.12	1.81	2.2534	1.2399	0.6531	0.4243	0.2632	0.2255	0.1585	0.1131	0.3826	4.2607
MAX			1.72	100.00	82.50	25.00	5.99	11.2594	8.4530	5.4549	3.4737	1.7885	1.3402	0.6091	0.2958	2.6151	16.7896
MIN			0.66	0.00	0.00	0.00	0.24	0.0417	0.0270	0.0127	0.0070	0.0037	0.0027	0.0012	0.0006	0.0069	1.3515
COUNT			52.00	52.00	52.00	52.00	52.00	74.00	74.00	82.00	87.00	89.00	89.00	90.00	93.00	75.00	75.00

Application to numerical models

Since the sediment transport model is a single grain size code, the median grain size, d_{50}, is the best choice for a representative grain size for noncohesive sediments. The field data indicated that almost all of the numerical grid in Pools 8 and 26 on the Mississippi River could be represented by a uniform sand grain size. The median grain size in Pool 8 was 0.43 mm, and in Pool 26, it was approximately 0.5 mm. In the LaGrange Pool, it was determined that the navigation channel bed consisted primarily of sand with a median grain size of 0.1 mm. This value is smaller than the calculated average values for the navigation and main channel found in Table 4 to balance the wide range of median sizes found and the influence of probably immobile coarse material remaining from earlier tributary input. Cohesive sediments were found to dominate the bed adjacent to the navigation channel and along the shoreline of the LaGrange Pool. Consequently, only sand was modeled in the Mississippi River pools and both sand and cohesive sediment were modeled in the LaGrange Pool.

Erosion of cohesive sediment is determined by the Parthenaides equation in SED2D. This equation requires that the erosion rate coefficient and the critical bed shear stress of the cohesive bed material be known. Five surface samples were collected from the LaGrange Pool and laboratory tests were conducted to determine these characteristics. Critical shear stresses ranged between 0.44 and 2.24 Pa. Erosion rates varied between 3.7 and 165 g/m^2 /min. This range is typical of cohesive sediment deposits and demonstrates the level of uncertainty associated with calculation of cohesive sediment erosion.

Sediment Boundary Conditions

Initial ambient sediment concentrations throughout the numerical grid are required input for SED2D. Initial values for sediment concentrations are calculated using the numerical model iteratively. First, initial conditions were uniformly assigned, based on a calculated average concentration using the average hydraulic parameters and the appropriate sediment transport function. Second, the model was run with a steady discharge for a sufficient length of time to allow the model to attain an equilibrium concentration. Third, the calculated equilibrium concentrations were used as initial conditions for another steady-state run. Finally, when the final and initial calculated concentrations were identical, the process was complete. This concentration is then the equilibrium concentration and represents the ambient concentration. These calculated values then became the initial conditions at each node in the model domain as start-up values for the dynamic runs.

Sediment diffusion coefficients in the numerical models were chosen based on experience from previous similar studies. Values between 0.022 and 10 m^2/sec were selected. Anisotropic diffusion was not simulated, as the same values were selected for lateral and streamwise directions. No attempt was made to optimize these values. They were used primarily for numerical stability.

3 Model Adjustment

Hydrodynamic Model

The RMA2 model is adjusted by matching calculated water-surface elevations to measured stages at some point upstream from the downstream boundary. Adjustment of the model in this study was achieved by matching calculated and measured stages from gaging station rating curves. Model verification was achieved by comparing measured and calculated velocities measured away from the upstream and downstream boundaries.

Adjustment variables in the numerical model are the magnitude and distribution of maximum Manning's roughness coefficients without the influence of vegetation, and the Manning's roughness coefficient due to vegetation. These values were adjusted until reasonable water-surface elevations and velocity magnitudes and patterns were calculated. The composite roughness coefficient is given by Equation 9. Final adjusted input values for roughness coefficients are given in Table 6.

$$n = \frac{n_{\max}}{D^{a}} + n_{veg}\ e^{-\frac{D}{b}} \tag{9}$$

where

n = Manning's roughness coefficient

n_{max} = Maximum Manning's roughness coefficient without vegetation influence

D = average depth in the element, ft

a,b = coefficients

n_{veg} = Manning's roughness coefficient due to vegetation

Table 6
Model Adjustment Coefficients for RMA2

Characteristic Element Type	n_{max}	a	n_{veg}	b
Pool 8				
1	0.020	0.167	0.040	3
Pool 26				
1	0.028	0.080	0.026	2
2	0.025	0.080	0.026	4
3	0.040	0.167	0.040	0.3
4	0.025	0.167	0.040	0.2
LaGrange Pool				
1	0.025	0.167	0.040	2
2	0.030	0.080	0.026	1
3	0.030	0.080	0.026	1
4	0.025	0.167	0.040	2
5	0.025	0.167	0.040	1

In Pool 8, the final adjusted channel Manning's roughness coefficients varied as a function of depth. Throughout most of the model, the roughness coefficient varied between 0.039 (at a depth of 0.6 m) to about 0.017 (at a depth of 2.4 m). At a depth of 1.2 m, the value was 0.026. A dynamic turbulent eddy viscosity coefficient of 900 Pascal-sec was used throughout the model domain. In order to attain model stability at the high flow condition, the dynamic turbulent eddy viscosity coefficient was increased to 960 Pascal-sec. With a discharge of 589 m^3/sec, the water-surface slope was 0.000007 based on the field data and 0.000013 based on calculated water-surface elevations. This translates to an error of 8.2 cm over 13.3 km. For the flowrate of 1,971 m^3/sec, the field-data slope was 0.000086, and the model calculated value was 0.000091. The error in water-surface slope here is 6 cm over 13.3 km. These errors in slope are very small and indicate a well-adjusted model with respect to flow and channel resistance.

Prototype velocity data were collected at Range 3 on 2 November 1995. Total discharge was 1,971 m^3 /sec,and the downstream stage was 192.13 m NGVD. Using the roughness coefficient values from Table 6 and a dynamic turbulent eddy diffusion coefficient of 900 Pascal-sec, velocities at Range 3 were calculated. The magnitudes of the calculated depth-averaged velocities were ±15 percent of the measured ones.

In Pool 26, the final adjusted Manning's roughness coefficients varied between 0.025 in the channel and 0.040 in the backwater areas. Convergence was achieved for the steady-state condition using a convergence criterion of 0.001 m change in water-surface elevation per iteration cycle. This convergence

criterion applies to the single nodal location at which the greatest variation was recorded from the last iteration.

Verification data in Pool 26 were obtained during the WES field data collection effort of September 1996. The upstream discharge boundary condition was 1,218 m^3/sec, and the downstream boundary water-surface elevation was 128.0 m NGVD. Prototype velocity data were collected at four ranges. The magnitudes of the calculated depth-averaged velocities were ±15 percent of the measured data.

Prototype velocity data were collected at three ranges in the LaGrange Pool during the WES field data collection effort of 15 July 1996 and were used for model verification. The upstream flow boundary condition was 305.3 m^3/sec in the main channel and 2.83 m^3/sec in the side channel. The downstream boundary for this inflow condition was 131.3 m NGVD at both exit points. The model was run assuming a steady-state condition and converged well. The convergence criterion was 0.001 m change in water-surface elevation per iteration cycle. The magnitudes of the calculated depth-averaged velocities were ±15 percent of the measured ones.

Sedimentation Model

SED2D is adjusted by matching calculated sediment concentrations to measured sediment concentrations. Given adequate field data, the only adjustment parameters in the SED2D model are sediment diffusion coefficients, which govern the rate of sediment diffusion, and the characteristic time, which governs the rate that sediment concentrations approach equilibrium. The sediment transport function itself may be considered an adjustment factor in this study, because there are two sand transport functions available. Lacking adequate field data, the sediment boundary conditions, including sediment inflow concentration and bed material characteristics, may also become adjustment parameters. In those cases, reliability of model results depends on both the uncertainty associated with input boundary conditions and the technical experience and judgment of the modeler.

The available suspended sediment data do not differentiate among sand, silt, and clay size classes. Thus, it was not possible to adjust the numerical model to known sand or known silt and clay concentrations. By observation of the relative fall velocities of the collected samples, it was determined that the measured sediment load contained all three sediment classifications. Therefore, the available data are useful only as they set an upper limit for total suspended sediment concentration.

Sand entrainment, transport, and deposition are governed primarily by the flow shear velocity and the grain size of the sand particle. Adjustment parameter values that had been successfully used in similar studies at WES were applied in this study. Based on experience from other similar sediment studies, assigned sediment diffusion coefficients generally varied between 0.022 and 1.0 m^2 /sec.

In Pool 26, at high flow, a value of 10.0 m^2 /sec was used to attain numerical stability. Initial values for sediment diffusion coefficients were estimated using Equation 10 and then raised if necessary to achieve numerical stability.

$$D_s = 0.23 D u_* \tag{10}$$

where

D_s = sediment diffusion coefficient, m^2 /sec

D = local water depth, m

u_* = local shear velocity, m/sec

Sediment diffusion coefficients were applied uniformly throughout the numerical grid. Sediment diffusion coefficients used in the study are shown in Table 7. Sensitivity studies were conducted to determine the effect of sediment diffusion coefficients on the calculated sediment concentrations at several locations in the various grids. It was determined that, within the range of coefficients used in this study, calculated variations were insignificant. Sand transport was calculated in the numerical models using both the Ackers-White (Ackers 1993, Ackers and White 1973) and Garcia-Parker (Garcia and Parker 1991) equations. Significantly greater sand sediment concentrations were calculated using the Garcia-Parker equation. Prototype total suspended sediment concentration data were available in all three trend reaches. Data were taken for ambient flow conditions and a series of samples were taken behind passing tows. Using these data, it was not possible to conclusively establish one equation as more representative than the other, although it appeared that the Ackers-White equations predicted more representative sediment concentrations. However, considering the high degree of uncertainty associated with sediment transport predictions, it was deemed appropriate to use the Garcia-Parker equation in this study to represent the very high range of expected sediment concentrations.

Table 7
Sediment Diffusion Coefficients, m^2/sec

Low Flow		Medium Flow		High Flow	
Sand	**Fines**	**Sand**	**Fines**	**Sand**	**Fines**
LaGrange Pool					
0.022	0.33	0.022	0.33	0.022	0.33
Pool 26					
0.022		0.11		10.0	
Pool 8					
0.5		0.15		1.0	

Silt and clay entrainment, transport, and deposition are governed primarily by the characteristics of the cohesive sediment deposit, the flow shear velocity, and the characteristics of the suspended sediment. In this study, silt and clay sedimentation was considered only for the LaGrange Pool where cohesive sediment deposits were found adjacent to the navigation channel. Prototype data included measured total suspended sediment concentrations in the LaGrange Pool at Valley City (RM 61.3) for a wide range of discharges, measured total suspended sediment concentrations associated with boat passage and for ambient conditions during two prototype data collection surveys conduced by WES, and five experimental determinations of cohesive sediment deposit characteristics.

Critical erosion shear stress was the adjustment parameter used to limit ambient sediment concentrations to the range of total sediment concentrations observed at Valley City. This required increasing the critical shear stresses for the high flow condition. It is not unusual for the upper layers of cohesive sediment deposits to be eroded by antecedent flows, exposing deeper layers of the deposit which may have higher critical shear stresses. Assigned critical erosion shear stress for low and medium flow was 0.3 Pa and 1.15 Pa for high flow. These values are within the range of critical shear stresses determined from laboratory analyses of five samples taken from the LaGrange Pool.

Fall velocity is the adjustment parameter that determines the duration of sediment suspension. Fall velocity of the silt and clay mixture was assigned so that limited measurements of increased concentrations along the shoreline, due to tow passage, were simulated in the numerical sedimentation model. A fall velocity of 0.0025 m/sec was assigned for the silt and clay mixture.

With these adjustment parameters, two sand-bed numerical sedimentation models of the Mississippi River, one through Pool 8 and one through Pool 26, were ready for experimental calculations for a range of flow conditions. Two numerical sedimentation models of the LaGrange Pool, one with a sand bed in the channel and one with a fine bed adjacent to the channel, were also ready for experimental calculations for a range of flow conditions.

4 Model Results

Simulation Conditions

The adjusted hydrodynamic (RMA2) and sedimentation (SED2D) numerical models were used to calculate ambient velocity patterns, depths, and sediment concentrations in the three trend reaches for a range of flow conditions. Three stage conditions and corresponding average discharges determined from rating curves were selected based on a statistical analysis of prototype data. The discharge and stage that is exceeded 5 percent of the time was designated "high" flow. The discharge and stage exceeded 50 percent of the time was designated "medium" flow. The discharge and stage exceeded 95 percent of the time was designated "low" flow.

In Pool 8, the flowrates were 297 m^3/sec for the low-flow case, 889 m^3/sec for the medium-flow case, and 2,540 m^3/sec for the high-flow case. Roughness coefficients were automatically calculated, and varied between 0.039 at a depth of 0.6 m and 0.017 at a depth of 2.4 m. For the high-flow case, the roughness coefficient was set at 0.025 everywhere in order to help achieve numerical stability. Dynamic turbulent eddy viscosity coefficients of 900 Pascal-sec were used throughout the model domain for the low- and medium-flow cases, and 1,000 Pascal-sec for the high-flow case. The higher value was used strictly to achieve numerical stability and had no significant effect on calculated results.

In Pool 26, the flow rates were 623 m^3/sec for the low-flow case, 2,322 m^3/sec for the medium-flow case, and 6,286 m^3/sec for the high-flow case. Roughness coefficients were automatically calculated, and varied between 0.017 and 0.045. Dynamic turbulent eddy viscosity coefficients were also calculated, and varied between 520 and 9,620 Pascal-sec. This large variation in the magnitudes of dynamic turbulent eddy viscosity coefficients is due to both the large range in the numerical grid cell sizes and velocity variations with discharge and location. Additional data from Pool 26 were available for verification of the calculated water-surface elevations. The St. Louis District had calculated water-surface elevations using the HEC-2 backwater program. The RMA2 and HEC-2 calculated stage at the end of the 11-km study reach compared within 0.11 m.

In the LaGrange Pool, the flow rates were 136 m^3/sec for the low-flow case, 340 m^3/sec for the medium-flow case, and 1,246 m^3/sec for the high-flow case.

Roughness coefficients and dynamic turbulent eddy viscosity coefficients were automatically calculated. Manning's roughness coefficients varied between 0.018 and 0.053, and the dynamic turbulent eddy viscosity varied between 30 and 970 Pascal-sec.

In the SED2D numerical model, bed shear stresses for sediment transport calculations are calculated as a function of Manning's roughness coefficient. The SED2D code is not outfitted with a depth function to calculate the roughness coefficient as is RMA2. Therefore, it was not possible to explicitly assign an identical set of Manning's roughness values to the SED2D and RMA2 numerical models. However, the values used in the SED2D models were chosen to be close to those calculated by RMA2.

The dynamic hydrodynamic and sedimentation calculations were separated into two parts. A first run was produced to show the effect of the return currents caused by the drawdown due to the tow, and a second run was produced to show the effect of increased boat shear under the tow. The two types of runs are referred to in this report as return-current runs and boat-shear runs. These process-separation runs were not necessary for the specific reaches simulated in this study because the two-dimensional models could have integrated the induced shear stresses. However, separate process runs were required in order to apply results to variable channel geometries in the subsequent systemswide impact study (Pokrefke et al. in preparation). Comparisons of total sediment concentration calculated using the integrated approach and the separate-process approach showed good agreement close to the tow where tow effects dominate and also close to the shore where return-current effects dominate. In between, the comparison was fair. Return-current shear stresses were determined from the combined RMA2 and HIVEL2D numerical model calculations, and the boat shear stresses were determined from Maynord's (2000) experimental algorithm. In general, the sum of the calculated concentrations at each node at a specified time step is the predicted total concentration due to tow passage. The exception is for nodes directly under or within one tow width of the passing tow. In this region, HIVEL2D calculations are not applicable.

Time histories of sediment concentration at each node in the numerical grids are calculated and may be displayed from output files. In this report, time histories at two selected locations are presented. New Gauge 1 is located at a location in each grid where relatively high sediment concentrations were calculated along the tow path. New Gauge 2 is located near the shore at the entrance to a backwater channel.

Pool 8 Sediment Modeling

The modified version of SED2D, as described in Chapter 2, was used for the sediment modeling. The input requirements for running the model for steady-state (ambient) conditions consisted of a hydrodynamic output file from RMA2 and a run control file from SED2D. The sediment was characterized as having a

d_{50} of 0.439 mm in a 1-m-thick bed. The fall velocity was determined to be 0.06 m/sec, assuming a shape factor of 0.7. The temperature of the water was assumed constant at 12.8°C (55°F).

Using guidance found in the SED2D manual and previous experience, the sediment diffusion coefficient was estimated at 0.15 m^2/sec. Boundary conditions were calculated, using the Garcia-Parker equation, at each node along the upstream boundary, using the field-determined d_{50} grain size and calculated velocities and water depths from RMA2. The initial ambient sediment concentrations, at each node, were determined by iterative calculations, starting with a constant value at all nodes and running the numerical model with steady-flow conditions until changes with each subsequent time step were insignificant. A Manning n value of 0.03 was assigned for the determination of bed shear stress. The time step for the steady-state simulation was set to 0.5 hr, and it was run for 8 hr, resulting in 16 time steps. The above sediment parameters were used for the low-, medium-, and high-flow steady-state initial runs, the only exception being that the initial inflowing concentrations at the inflow boundary nodes and initial ambient concentrations at each node were adjusted for the different flow rates. The results of the three simulations all showed that an equilibrium concentration was obtained within 2 simulation hours.

The second step in the sediment modeling process was running the dynamic simulations. That is, moving the tow and/or drawdown wave through the system and observing its effects on entrainment and transport. In addition to the normal SED2D input files containing the sediment parameters required for the steady state runs, time-dependent hydrodynamic files, as well as boat path and boat information (tow characteristics) files, were also necessary for the dynamic runs. An upbound towboat pushing barges in a 3 by 5 barge train, with a draft of 2.74 m, and a Kort nozzle with twin 2.74-m-diam propellers, was simulated in the numerical model. The tow speed, and thus its propeller thrust, were the only two parameters that changed for the low-, medium-, and high-flow runs. Its path was the navigation channel, best viewed in the numerical grid of Figures 2 and 8. It was determined from initial numerical simulations using the HIVEL numerical model that return currents would not be significant for the medium-flow and high-flow conditions. Therefore, return-current calculations were only made for the low-flow condition in Pool 8. Observations of the simulation results for the three flows are discussed separately below.

Ambient sand concentrations were 0 mg/ℓ near the banks of the river and in the channel for the low-flow case. The low-flow boat-shear simulation showed localized entrainment of sand in the channel with the highest concentrations being in the channel directly beneath the tow as it passed. The peak instantaneous calculated concentration was 28,000 mg/ℓ. Although this value is very high, its duration is extremely short and most of the sediment falls out within approximately 18 sec. Figure 9 shows the spatial extent of the highest concentrations. Figure 10 shows the time history of entrained sand concentrations in the channel, as well as the fact that it took only 18 sec to go from highest values back to background values. This figure also shows a smaller peak concentration of about 4,000 mg/ℓ which precedes the maximum peak. This initial peak

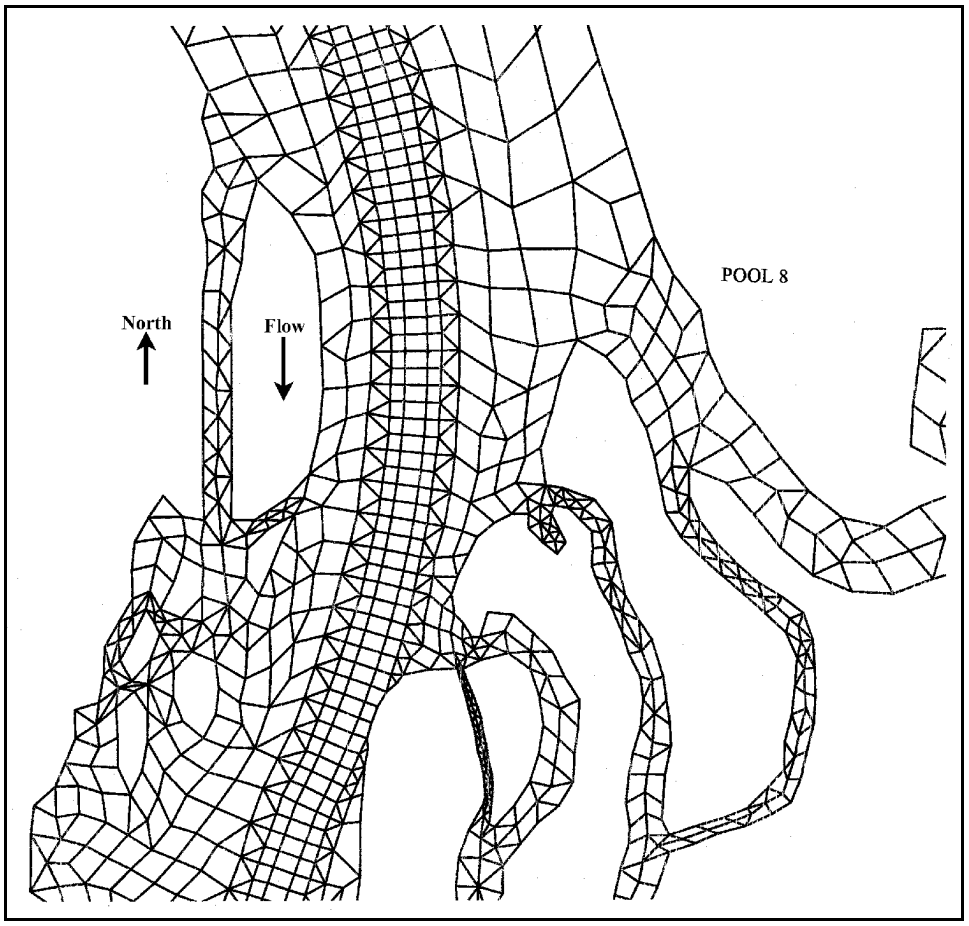

Figure 8. Numerical grid for Pool 8, enlarged section

concentration represents the sediment entrained by the passage of the barge bow, while the larger peak concentration represents the sediment entrained by the passage of the towboat stern and its propeller-induced bed shear. Figure 11 shows the entrained sand concentrations for the entrance to a backwater area identified as new Gauge 2 in Figure 9. The figure shows less than 0.1 mg/ℓ increase in sand concentration near the backwater entrance due to the boat-shear-induced entrained sediment.

The low-flow return-current simulation shows a maximum resuspension of about 0.2 mg/ℓ near the backwater entrance (Figure 12).

Ambient sand concentrations varied between 0.1 mg/ℓ, near the banks of the river, and 0.8 mg/ℓ, in the channel, for the medium-flow case. The medium-flow boat-shear simulation showed much lower localized entrainment in the channel than the low-flow case, with the highest concentrations being in the channel directly beneath the tow as it passed. The peak concentration was about 8,000 mg/ℓ. As in the low-flow case, this value is much higher than ambient conditions, but of short duration and thus not transported any significant distance. In the first 12 sec the concentration of 8,000 mg/ℓ dropped to about 2,000 mg/ℓ, and within 72 sec had dropped to the ambient condition. The

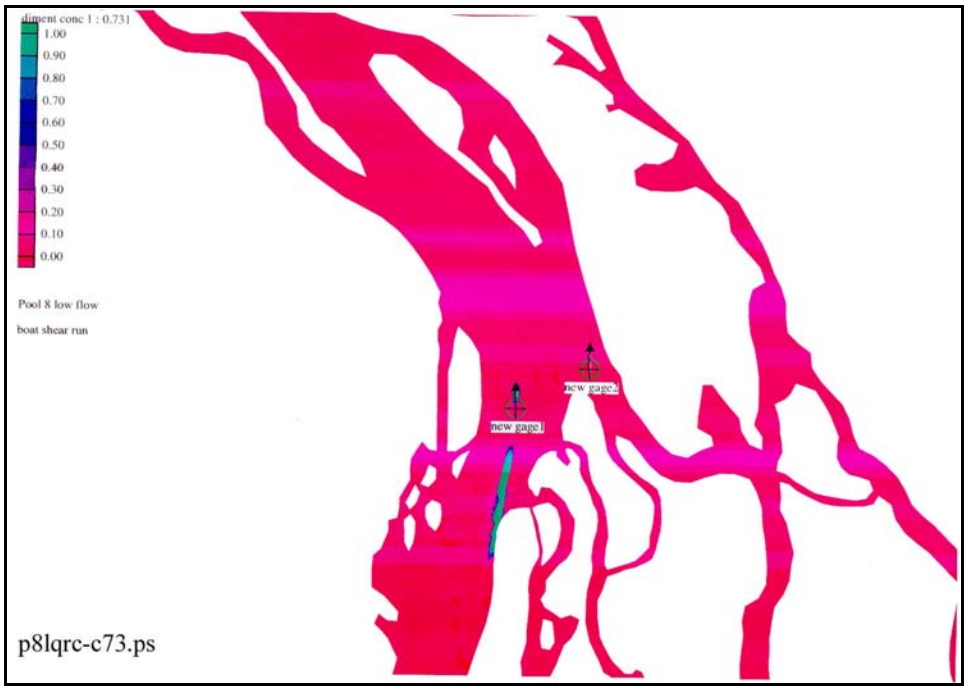

Figure 9. Sediment concentration contours, Pool 8, low flow, boat-shear stresses

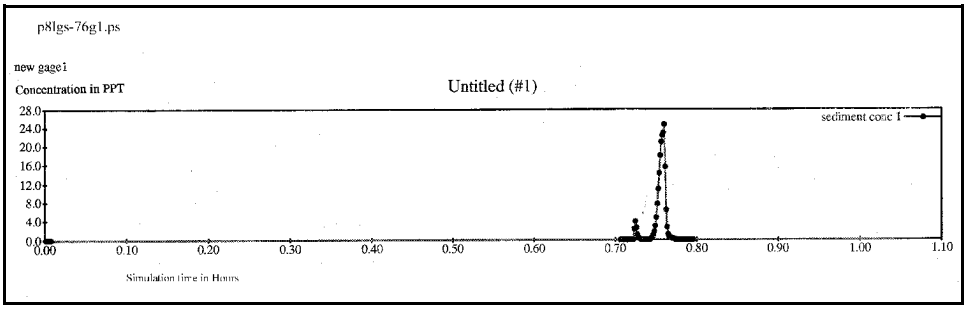

Figure 10. Sediment concentration time history at new Gauge 1, Pool 8, low flow, boat-shear stresses

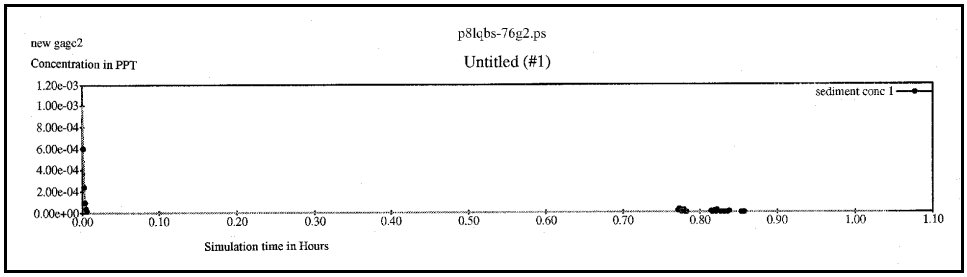

Figure 11. Sediment concentration time history at new Gauge 2, Pool 8, low flow, boat-shear stresses

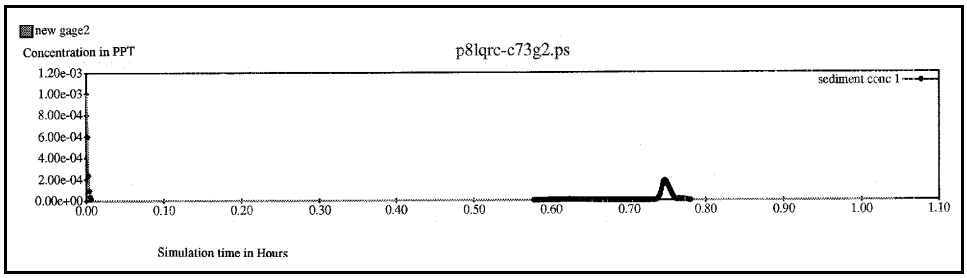

Figure 12. Sediment concentration time history at new Gauge 2, Pool 8, low flow, shear stresses from return current

sediment plume was slightly wider than for the low-flow case, but the plume still did not produce any significant increase in sand concentration near the shores or backwater entrances. Figure 13 shows the spatial extent of the highest concentrations. Figure 14 shows the time history of entrained sand concentrations in the channel, as well as the fact that it settled out very quickly. In this case, the time step was 6 sec, which means that in about 12 time steps, or approximately 72 sec, most of the entrained sediment had settled out. Figure 15 shows the entrained sediment concentrations for the entrance to the backwater area identified as new Gauge 2. No significant sediment was entrained due to tow passage.

Ambient sand concentrations varied between 0.6 mg/ℓ, near the banks of the river, and 18.5 mg/ℓ in the channel, for the high-flow case. The high-flow boat-shear simulation showed peak sand concentrations of 560 mg/ℓ in the channel, which were even lower than for the medium-flow case. The duration of the increased sediment concentration was 85 sec for the high-flow case, which is slightly longer than for the medium-flow case. The spatial extent is shown in Figure 16. The time history plot at new Gauge 1 is shown in Figure 17. In this case, the peak concentration is caused by bed shear stresses induced by the passage of the barge bow rather than bed shear stresses induced by the tow propellers. The time history at the entrance to the backwater at new Gauge 2 is shown in Figure 18.

General conclusions for the three flow conditions in Pool 8 are that, for the low-flow condition, more sand-sized sediment is entrained both underneath the vessel and at the backwater entrance than for the medium- and high-flow cases. The amount entrained near the backwater entrance is negligible for all conditions. Under the tow, high quantities of sediment entrainment were calculated with low-flow conditions, but the sediment falls out more quickly than at higher flows. The medium- and high-flow simulations show much less entrainment under the tow. The material entrained under the tow stays in suspension slightly longer (72 sec in the medium flow and 85 sec in the high flow), but still not long enough to be transported any considerable distance.

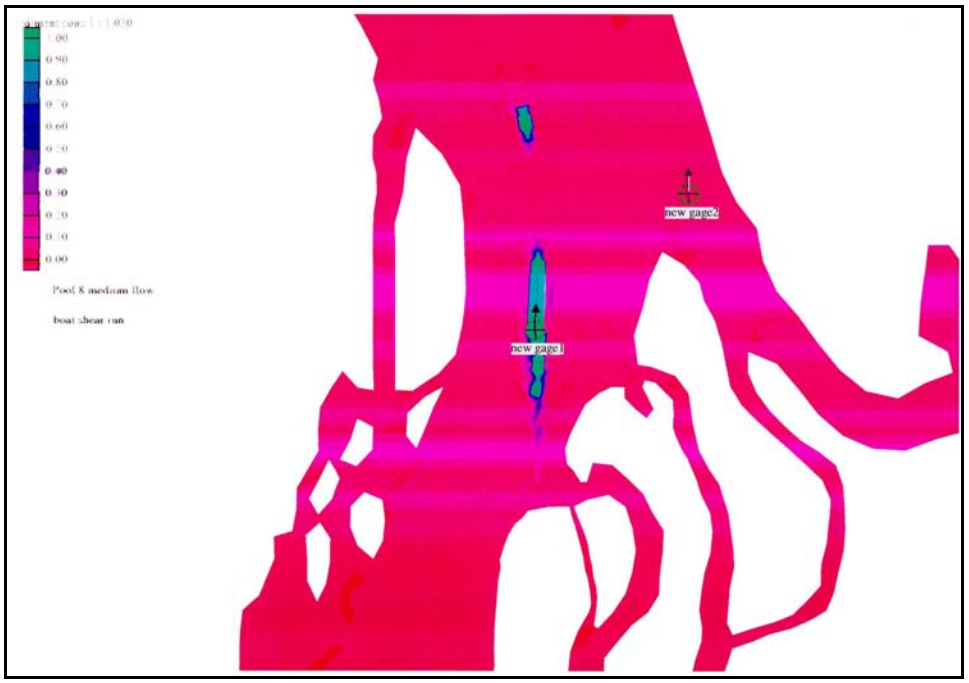

Figure 13. Sediment concentration contours, Pool 8, medium flow, boat-shear stresses

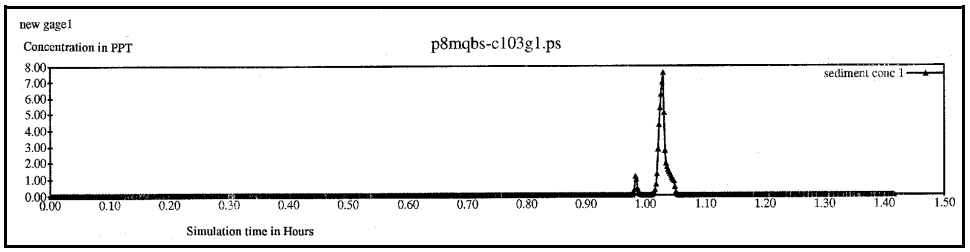

Figure 14. Sediment concentration time history at new Gauge 1, Pool 8, medium flow, boat-shear stresses

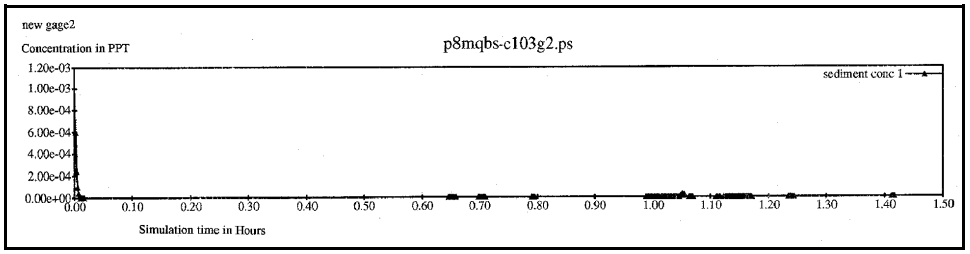

Figure 15. Sediment concentration time history at new Gauge 2, Pool 8, medium flow, boat-shear stresses

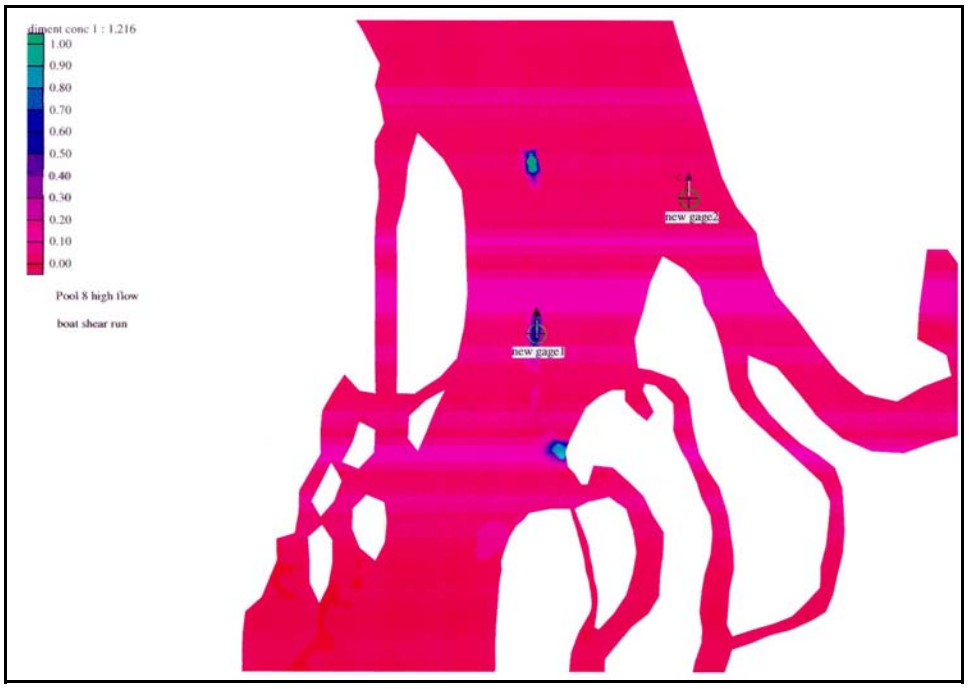

Figure 16. Sediment concentration contours, Pool 8, high flow, boat-shear stresses

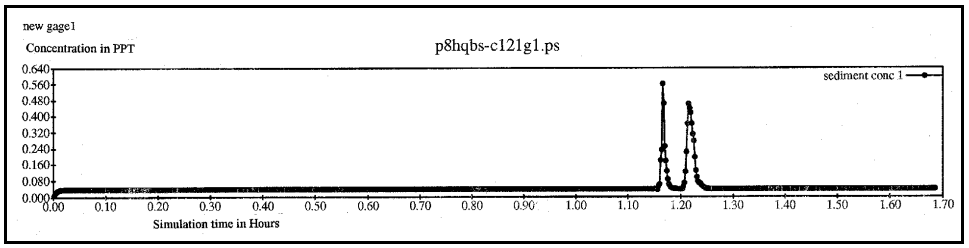

Figure 17. Sediment concentration time history at new Gauge 1, Pool 8, high flow, boat-shear stresses

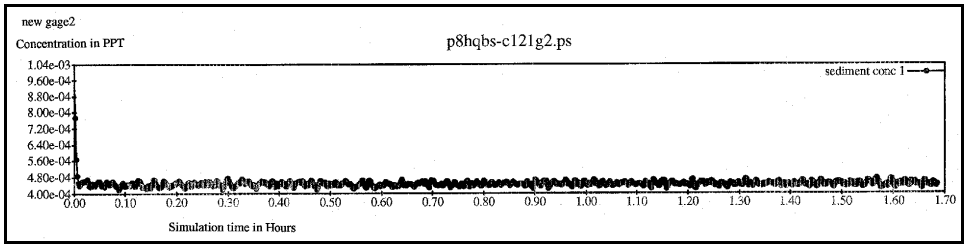

Figure 18. Sediment concentration time history at new Gauge 2, Pool 8, high flow, boat-shear stresses

Pool 26 Sediment Modeling

The modified version of SED2D, as described in Chapter 2, was used for the sediment modeling. The input requirements for running the model for steady-state conditions consisted of a hydrodynamic output file from RMA2 and a run control file for SED2D. Pool 26 sediment was characterized as having a d_{50} of 0.5 mm in a 1-m-thick bed. The fall velocity was determined to be 0.06 m/sec, assuming a shape factor of 0.7. The temperature of the water was assumed constant at 16°C (60.8°F).

The initial conditions for ambient sediment concentrations were calculated iteratively assuming steady-state flow conditions. Boundary conditions were calculated, using the Garcia-Parker equation, at each node along the boundary, using the field-determined d_{50} grain size, and calculated velocities and water depths from RMA2. Using guidance found in the SED2D manual and previous experience, the diffusion coefficient was estimated at 0.022 m^2/sec. A Manning n value of 0.025 was assigned for the determination of bed shear stress in the channel, 0.028 outside of the main channel, and 0.03 in the nearshore areas. The time step for the steady state simulation was 0.05 hr, and it was run for 15 hr, resulting in 300 time steps. For high flow it was necessary to use 0.001-hr time steps for 0.3 hr, also resulting in 300 time steps.

The above sediment parameters were used for the low-, medium-, and high-flow steady-state initial runs. The only exception was that the initial inflowing concentrations at the inflow boundary nodes were adjusted for the differing flow rates. The results of all three simulations showed that, after an equilibrium concentration was obtained, the deposition and scour patterns were consistent with the river's bathymetric features and hydraulic conditions.

The second step in the sediment modeling process was running the dynamic simulations. It was determined that the return current effects were negligible in Pool 26, so no return-current runs were made . The dynamic changes in bed shear stress were totally due to the boat shear. An upbound tow pushing a 3 by 5 barge train, with a draft of 2.74 m, and a Kort nozzle with twin 2.74-m-diam propellers was simulated in the numerical model. The tow speed and thus its propeller thrust were the only two parameters that changed for the low-, medium-, and high-flow runs. The tow path was the navigation channel, best viewed in the numerical grid of Figures 3 and 19. Observations of the simulation results for the three flows are discussed separately in the following paragraphs.

Ambient sand concentrations were determined to be essentially zero for the low-flow case both near the banks of the river and in the channel. The low-flow boat-shear simulation showed localized sand entrainment in the channel with the highest values being in the channel directly beneath the tow as it passed. The peak concentration was 13,000 mg/ℓ. Although this concentration is high, its duration is extremely short and most of the sediment falls out within approximately 72 sec. Figure 20 shows the spatial extent of the highest concentrations. Figure 21 shows the time history of entrained sand concentrations in the channel,

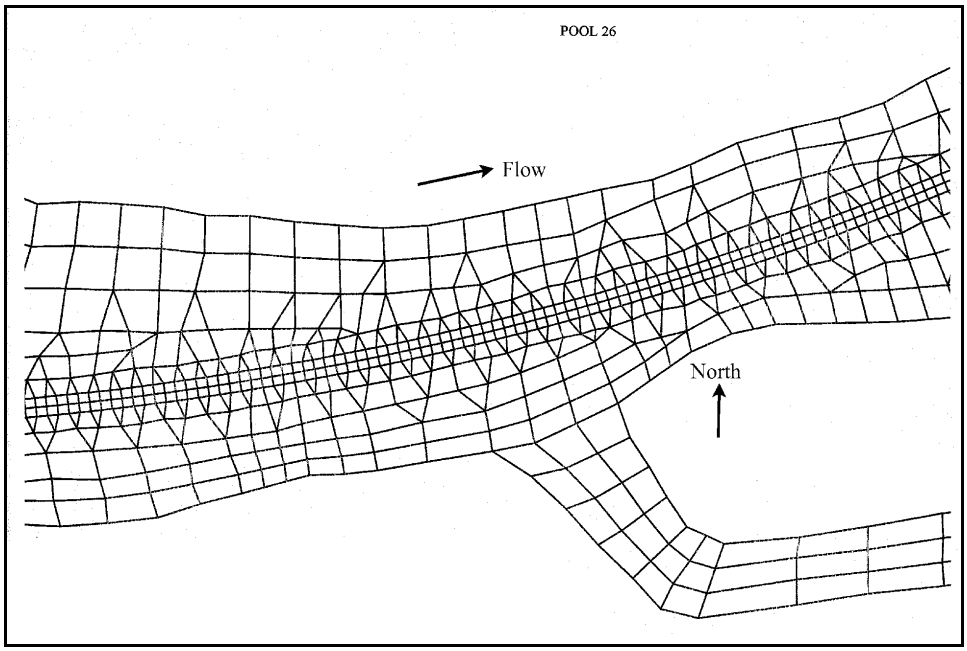

Figure 19. Numerical grid for Pool 26, enlarged section

Figure 20. Sediment concentration contours, Pool 26, low flow, boat-shear stresses

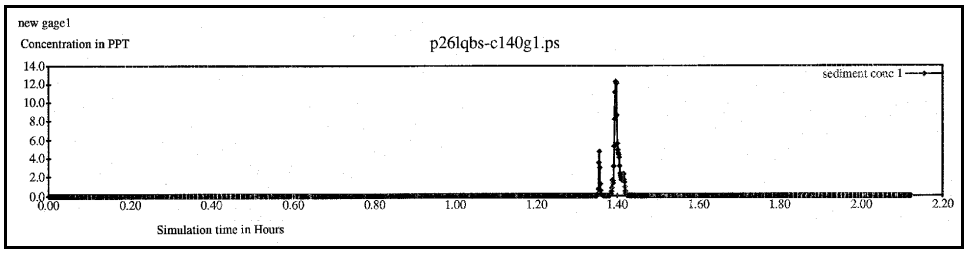

Figure 21. Sediment concentration time history at new Gauge 1, Pool 26, low flow, boat-shear stresses

as well as the fact that it took about 18 time steps to go from highest concentrations back to background values. Figure 22 shows the entrained sand concentrations for the entrance to a backwater area identified as new Gauge 2 in Figure 20. Although some sediment activity due to the passing of the tow is shown, the concentrations were very small, about 0.2 mg/ℓ, indicating no significant effect near the backwater entrance due to the boat-shear-induced entrained sediment.

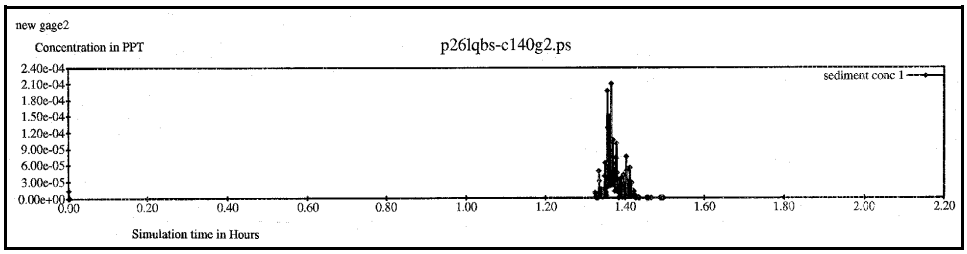

Figure 22. Sediment concentration time history at new Gauge 2, Pool 26, low flow, boat-shear stresses

Ambient sand concentrations varied between 0.7 mg/ℓ, near the banks of the river, and 8 mg/ℓ, in the channel, for the medium-flow case. The medium-flow boat-shear simulation showed much lower localized sand entrainment in the channel than the low-flow case, with the highest concentrations being in the channel directly beneath the tow as it passed. The peak concentration was about 3,500 mg/ℓ. As in the low-flow case, this concentration is much higher than ambient conditions, but of short duration and thus not transported any significant distance. The sediment plume was less noticeable than in the low-flow condition and had no effect near the shores or backwater entrances. Figure 23 shows the spatial extent of the highest concentrations. Figure 24 shows the time history of entrained sand concentration in the channel, as well as the fact that it settled out very quickly. In this simulation, most of the entrained sand had settled out after about 48 sec. Figure 25 shows the entrained sand concentrations for the entrance to the backwater area identified as new Gauge 2. No significant sand was entrained due to tow passage, even though a very small blip (0.8 mg/ℓ) in the data does show its passage.

Ambient sand concentrations varied between 20 mg/ℓ, near the banks of the river, and 350 mg/ℓ, in the channel, for the high-flow case. The high-flow

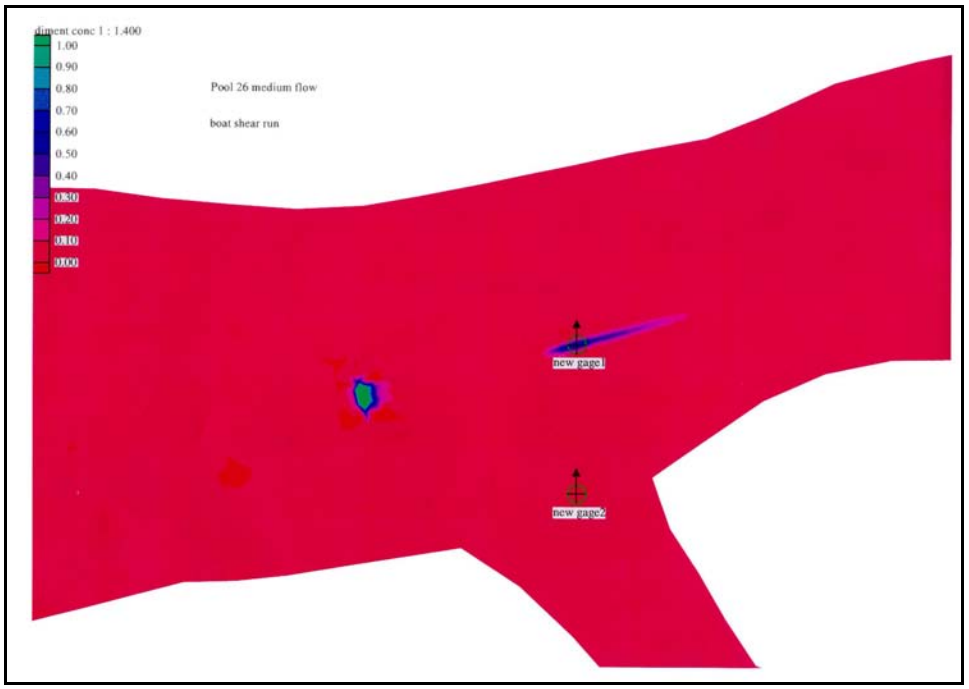

Figure 23. Sediment concentration contours, Pool 26, medium flow, boat-shear stresses

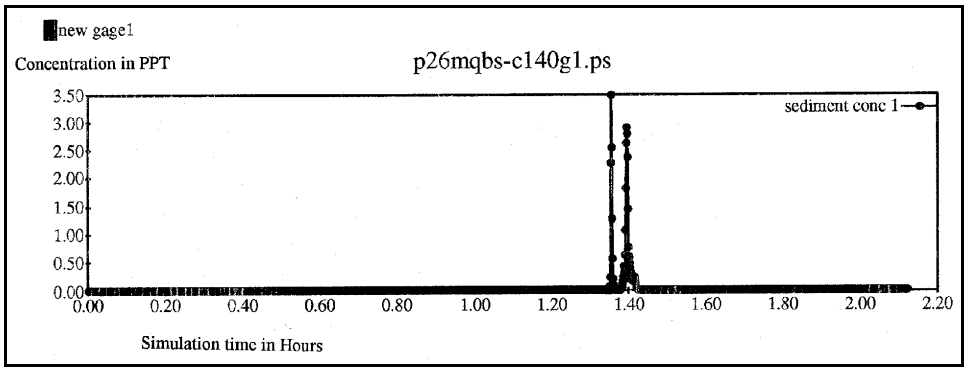

Figure 24. Sediment concentration time history at new Gauge 1, Pool 26, medium flow, boat-shear stresses

boat-shear simulation showed yet lower peak concentrations in the channel. The spatial extent is shown in Figure 26. Note that the entrainment due to the propellers (boat shear) is no longer distinguishable from the ambient entrainment due to the high flow. The peak concentrations due to the bow of the tow are discernable with values up to 1,800 mg/ℓ, as can be seen in the time history plot of Figure 27. The time history of entrained sand for this high-flow condition in the entrance to the backwater at new Gauge 2 is shown in Figure 28. No effect of the passing tow is visible. These figures show the magnitude of increased sediment concentration due to tow passage compared to ambient sediment

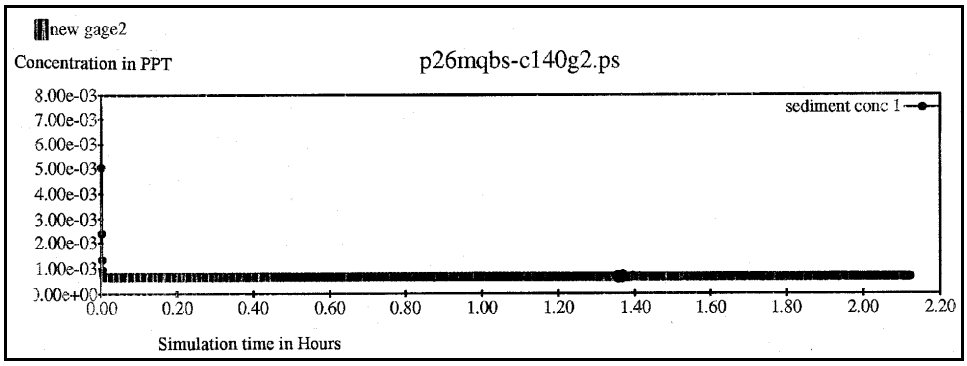

Figure 25. Sediment concentration time history at new Gauge 2, Pool 26, medium flow, boat-shear stresses

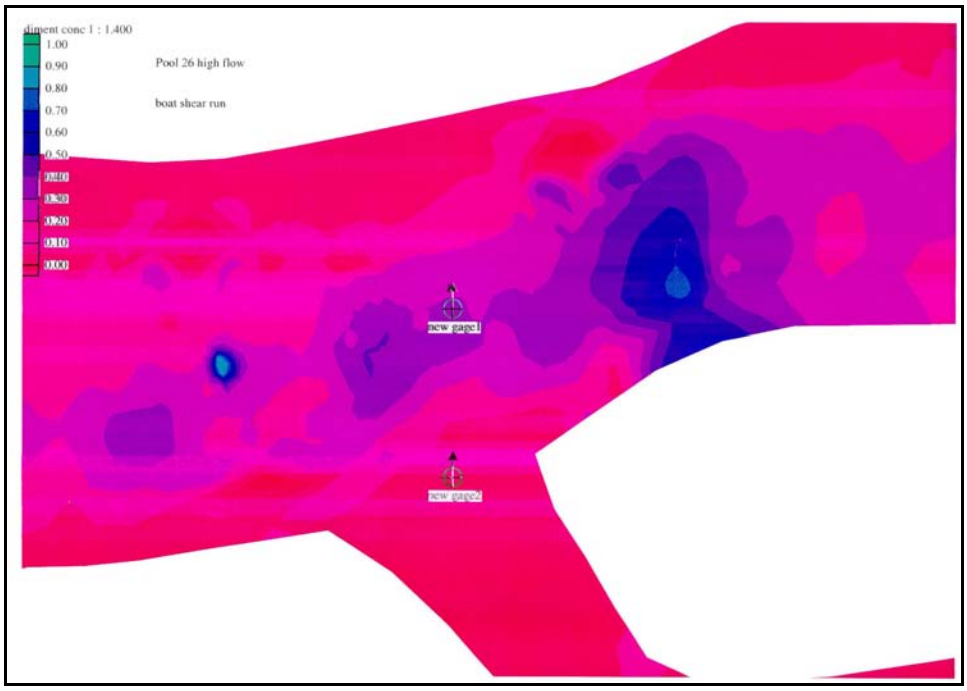

Figure 26. Sediment concentration contours, Pool 26, high flow, boat-shear stresses

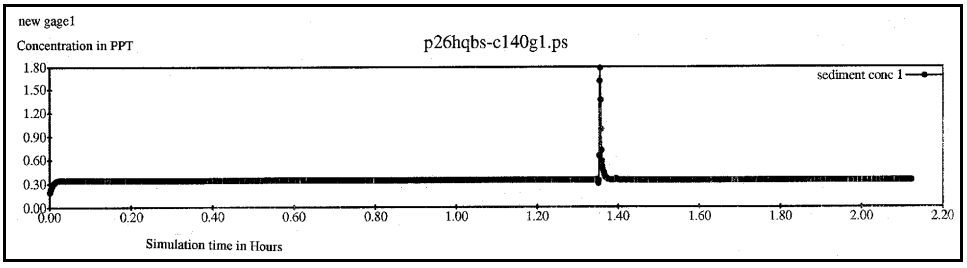

Figure 27. Sediment concentration time history at new Gauge 1, Pool 26, high flow, boat-shear stresses

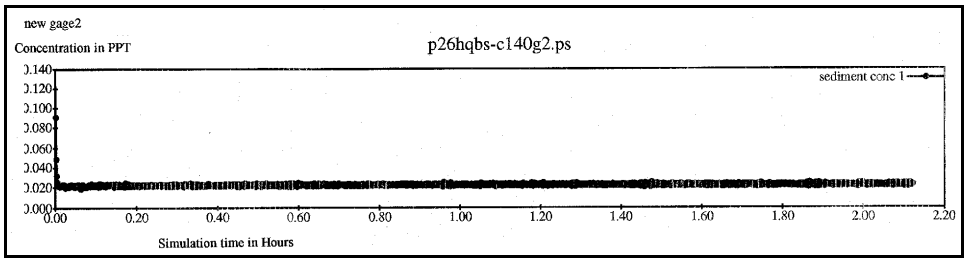

Figure 28. Sediment concentration time history at new Gauge 2, Pool 26, high flow, boat-shear stresses

concentration and also its relatively brief duration compared to the total simulation time.

General conclusions for the three flow conditions in Pool 26 are that, for the low-flow condition, more sand-sized sediment is entrained underneath the vessel than for the other two higher-flow cases. In addition, the sand remains in suspension for the longest period of time (72 sec) in the low-flow condition. The backwater entrance is virtually unaffected at any of the flow conditions.

LaGrange Pool Sediment Modeling

Sand bed

The modified version of SED2D, as described in Chapter 2, was used for the sediment modeling of the LaGrange Pool. The input requirements for running the model for steady-state conditions consisted of a hydrodynamic output file from RMA2 and a run control file for SED2D. The LaGrange Pool sediment was characterized as having a d_{50} of 0.1-mm sand in a 1-m-thick bed. The fall velocity was determined to be 0.0065 m/sec, assuming a shape factor of 0.7. The temperature of the water was assumed constant at 16 °C (60.8 °F).

The initial conditions for ambient sediment concentrations were calculated iteratively assuming steady-state flow conditions. Initial boundary conditions were calculated, using the Garcia-Parker equation, at each node along the boundary, using field-determined d_{50} grain size and calculated velocities and water depths from RMA2. Using guidance found in the SED2D manual and previous experience, the diffusion coefficient was estimated at 0.022 m^2/sec. A Manning n value of 0.025 was assigned for the determination of bed shear stress in the channel, 0.030 in the nearshore areas, and 0.040 in the backwater areas.

The above sediment parameters were used for the low-, medium-, and high-flow steady-state initial runs. The only exception was that the initial inflowing concentrations at the inflow boundary nodes were adjusted for the differing flow rates. The results of the three simulations all showed that when an equilibrium concentration was obtained, the deposition and scour patterns were consistent with the river's bathymetric features and hydraulic conditions.

The second step in the sediment modeling process was running the dynamic simulations. That is, moving the tow and/or long-period wave through the system and observing its effects on entrainment and transport. These were the boat-shear runs and return-current runs. In addition to the normal SED2D input files containing the sediment parameters required for the steady-state runs, time dependent hydrodynamic files, as well as boat path and boat information (tow characteristics) files, were also necessary for the dynamic runs. An upbound tow pushing a 3 by 5 barge train, with a draft of 2.74 m, and a Kort nozzle with twin 2.74-m-diam propellers was simulated in the numerical model. The tow speed and thus its propeller thrust were the only two parameters that were changed for the low-, medium-, and high-flow runs. The tow's path was the navigation channel, best viewed in the numerical grid of Figures 4 and 29. Observations of the simulation results for the three flows are discussed separately in the following paragraphs.

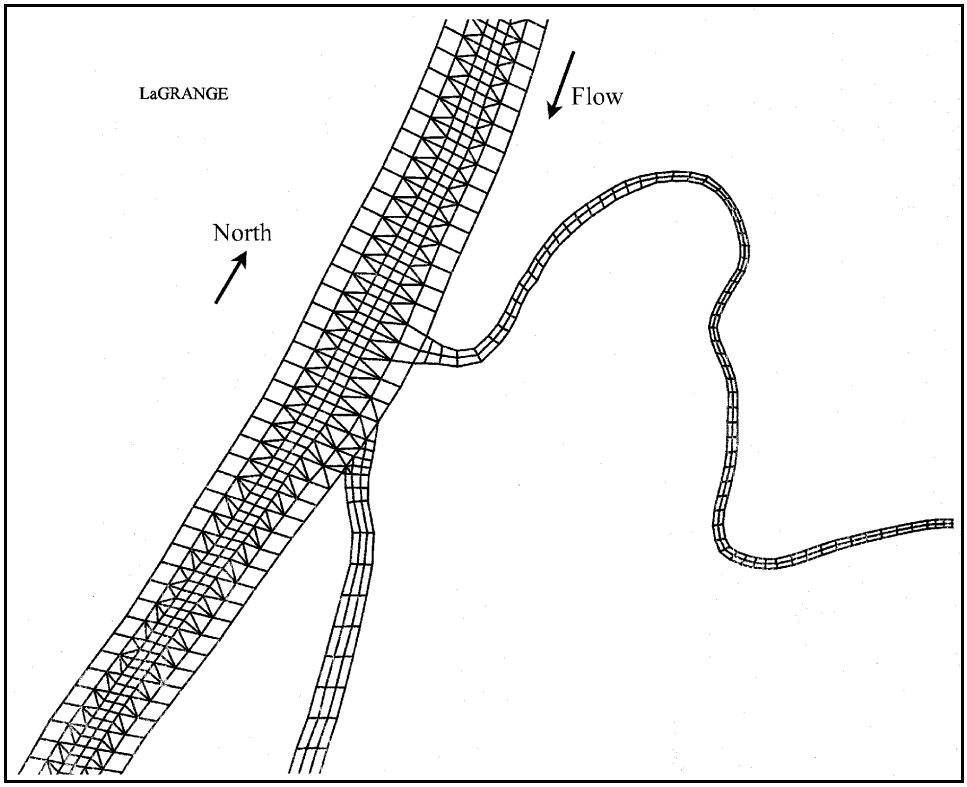

Figure 29. Numerical grid for LaGrange Pool, enlarged section

Ambient sand concentrations varied between 0.005 mg/ℓ, near the banks of the river, and 2.0 mg/ℓ, in the channel, for the low-flow case. The low-flow boat-shear simulation was run with a boat speed relative to the ground of 2.0 m/sec and a propeller thrust of 286,500 N. Calculated results showed localized sand entrainment in the channel with the highest values being directly beneath the tow as it passed. The peak value was 3,750 mg/ℓ. Although this value is high, its

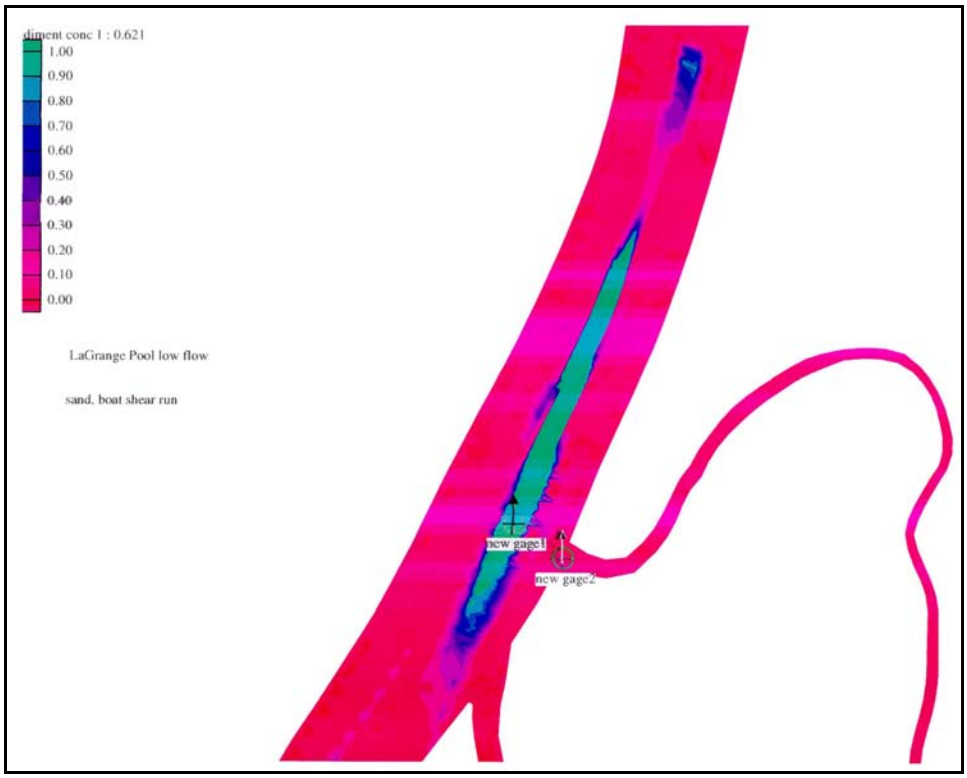

Figure 30. Sediment concentration contours, LaGrange Pool, sand, low flow, boat-shear stresses

duration is extremely short and most of the sand falls out within approximately 130 sec. Figure 30 shows the spatial extent of the highest sand concentrations due to boat shear. Figure 31 shows the time history of entrained sand concentrations due to boat shear in the channel, as well as the fact that it took about 130 sec to go from highest values back to background values. Figure 32 shows the entrained sand concentrations due to boat shear for the entrance to a backwater area identified as new Gauge 2 in Figure 30. Some sediment activity due to the passing of the tow was indicated; the magnitude was 49 mg/ℓ.

A return-current simulation was produced for the LaGrange low-flow condition. Figure 33 shows that at the near shore the maximum amount entrained by the return current was 47 mg/ℓ compared with 49 mg/ℓ entrained due to the boat shear. Note that these concentration peaks occurred at different times and therefore the total maximum concentration is still about 49 mg/ℓ. The increase in sand concentrations due to return-currents lasted longer than the increase due to boat shear.

Ambient sand concentrations varied between 0.006 mg/ℓ, near the banks of the river, and 1.9 mg/ℓ, in the channel, for the medium-flow case. The medium-flow simulation used a boat speed of 1.6 m/sec, relative to the ground, and a propellor thrust of 283,200 N. Calculated results of the medium-flow boat-shear run showed slightly higher localized sand entrainment in the channel than results from the low-flow run, with the highest concentrations being in the channel

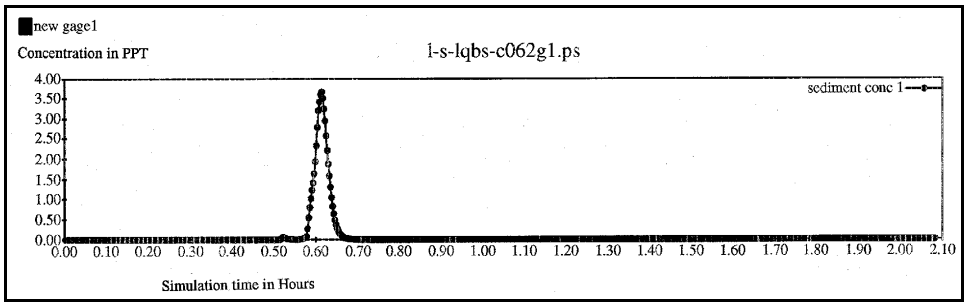

Figure 31. Sediment concentration time history at new Gauge 1, LaGrange Pool, sand, low flow, boat-shear stresses

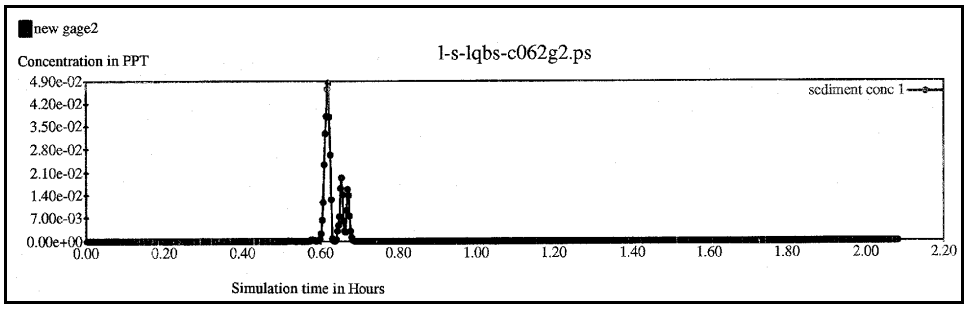

Figure 32. Sediment concentration time history at new Gauge 2, LaGrange Pool, sand, low flow, boat-shear stresses

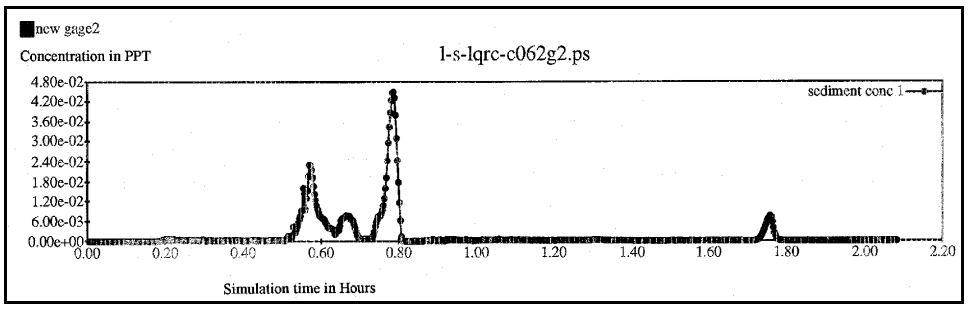

Figure 33. Sediment concentration time history at new Gauge 2, LaGrange Pool, sand, low flow, shear stress from return current

directly beneath the tow as it passed (Figure 34). The peak concentration was about 5,300 mg/ℓ and is shown in Figure 35. As in the low-flow case, this value is much higher than ambient conditions, but, unlike the low-flow case, the suspended sand did not drop out as quickly and was transported for about 4.2 min. This is enough time to move more of the entrained sand in both the streamwise and lateral directions. Figure 36 shows a maximum sand concentration of about 60 mg/ℓ at the backwater entrance as the tow passes.

A return-current run for the medium-flow sand condition showed less entrainment in the backwater entrance, with a maximum sand concentration of 28 mg/ℓ (Figure 37), than the boat-shear run. However, the duration of suspension was

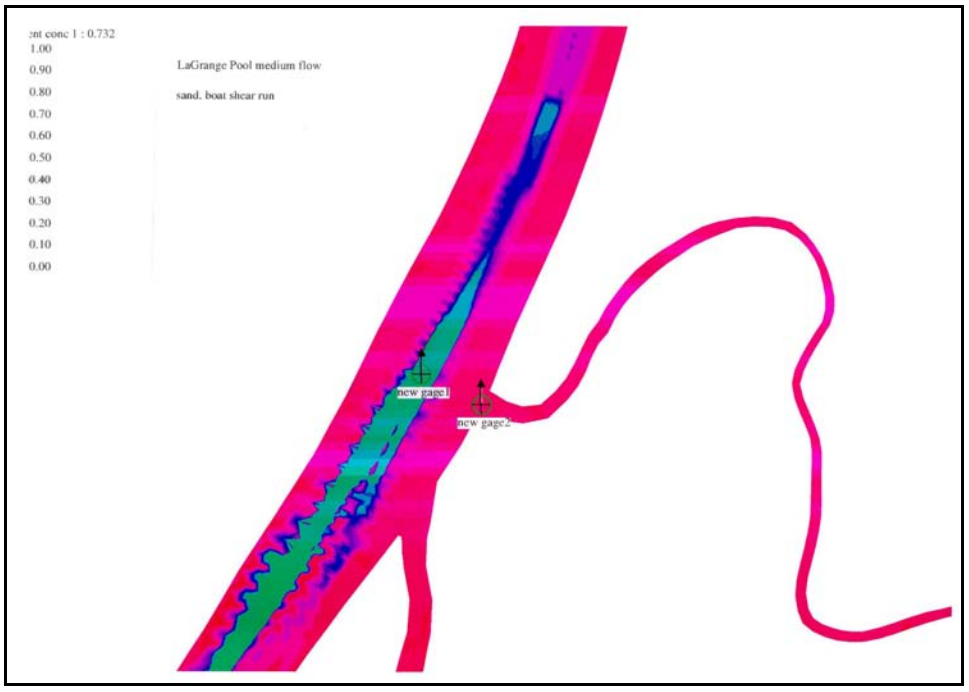

Figure 34. Sediment concentration contours, LaGrange Pool, medium flow, boat-shear stresses

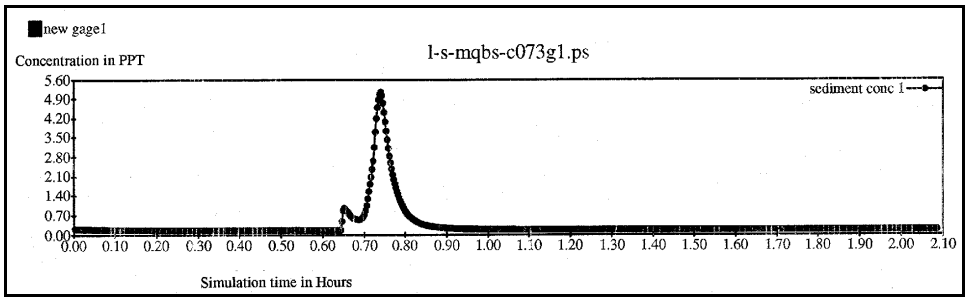

Figure 35. Sediment concentration time history at new Gauge 1, LaGrange Pool, sand, medium flow, boat-shear stresses

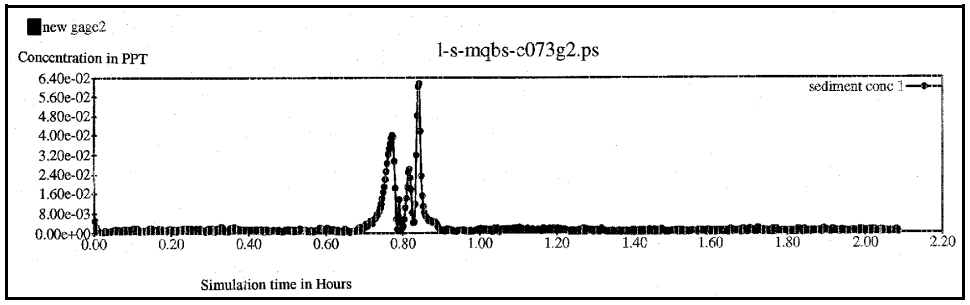

Figure 36. Sediment concentration time history at new Gauge 2, LaGrange Pool, sand, medium flow, boat-shear stresses

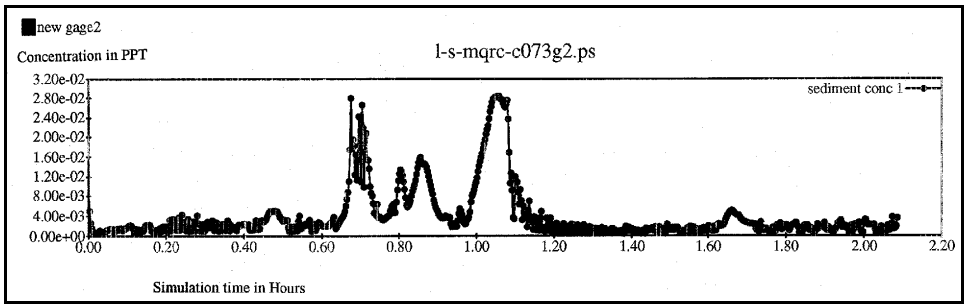

Figure 37. Sediment concentration time history at new Gauge 2, LaGrange Pool, sand, medium flow, shear stress from return current

much longer, being about 20 min. This shows that the boat shear entrains more sediment for these conditions than the long-period waves produced by the return currents, but that the overall turbulence produced by the interaction of ambient and return currents keeps the entrained sand in suspension longer than the boat shear. In either case, the maximum amount of entrained sediment at the backwater entrance does not exceed 28 mg/ℓ.

Ambient sand concentrations varied between 2,000 mg/ℓ, near the banks of the river, and 5,000 mg/ℓ, in the channel, for the high-flow case. The LaGrange high-flow simulation used a boat speed of 1.64 m/sec relative to the ground and a prop-thrust of 191,000 N. Results of the boat-shear run showed slightly lower localized sand entrainment in the channel than the medium- flow case, with the highest concentrations being in the channel directly beneath the tow as it passed (Figure 38). The peak concentration was about 5,300 mg/ℓ and is shown in Figure 39. This value is 300 mg/ℓ higher than ambient conditions and stayed in suspension for about 18 min. Very little of this channel-entrained sand is transported to the backwater entrance. This is shown in Figure 40 where a slight increase of 50 mg/ℓ shows up at the backwater entrance at about hr 0.84. The sediment plume was not noticeable since the ambient concentrations were so high.

A return-current run for the high-flow sand case showed a maximum sand concentration of 2,800 mg/ℓ, which is about 800 mg/ℓ higher than the ambient concentration (Figure 41). In this case more sand was entrained due to the return currents than due to boat shear. The duration of sand suspension was also longer, being about 28 min at the backwater entrance. As in previous cases, the overall turbulence produced by the interaction of ambient and return currents keeps the entrained sediment in suspension longer than the passing boat shear.

General conclusions for the three flow conditions in the LaGrange Pool show that the highest values of entrained 0.1-mm sand above the ambient concentrations and due to the tow passage was 950 mg/ℓ and occurred in the high-flow return-current run. In all the runs, very high concentrations occurred in the channel. But other than in the run indicated above, these caused 55 mg/ℓ or less net change in concentration at the backwater entrance.

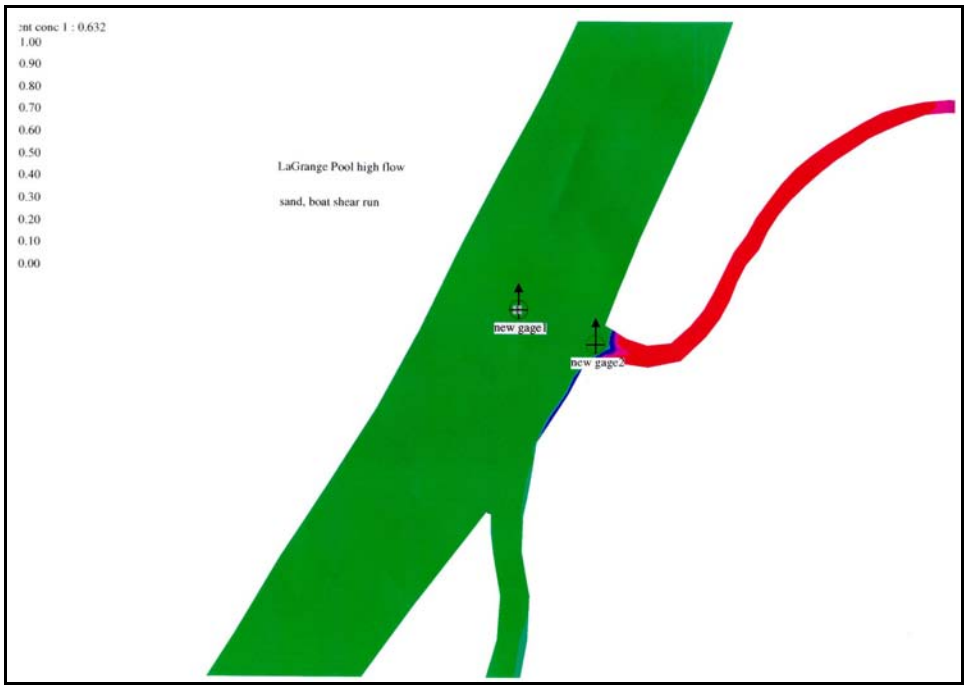

Figure 38. Sediment concentration contours, LaGrange Pool, sand, high flow, boat-shear stresses

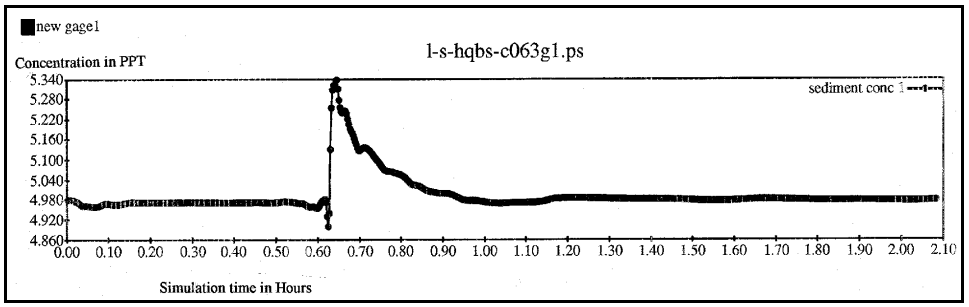

Figure 39. Sediment concentration time history at new Gauge 1, LaGrange Pool, sand, high flow, boat-shear stresses

Cohesive bed

The modified version of SED2D, as described in Chapter 2, was also used for the fine-sediment modeling of the LaGrange Pool. The input requirements for running the model for steady-state conditions consisted of the same hydrodynamic output from RMA2 used in the sand simulations and a run control file for SED2D. There was no d_{50} sediment size classified as with the sand runs. Instead, specific cohesive sediment characteristics are specified. In the channel, the input data were manipulated to simulate a sediment-free bed. This is representative of the portion of the bed consisting of sand. The bed in the remaining parts of the grid was assigned a critical bed shear stress of 0.3 N/m^2, and an

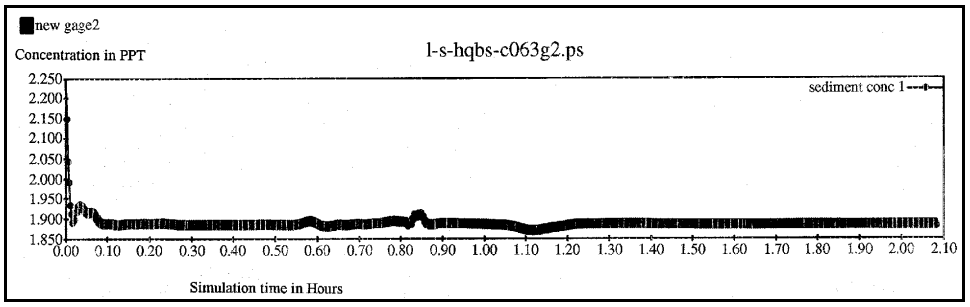

Figure 40. Sediment concentration time history at new Gauge 2, LaGrange Pool, sand, high flow, boat-shear stresses

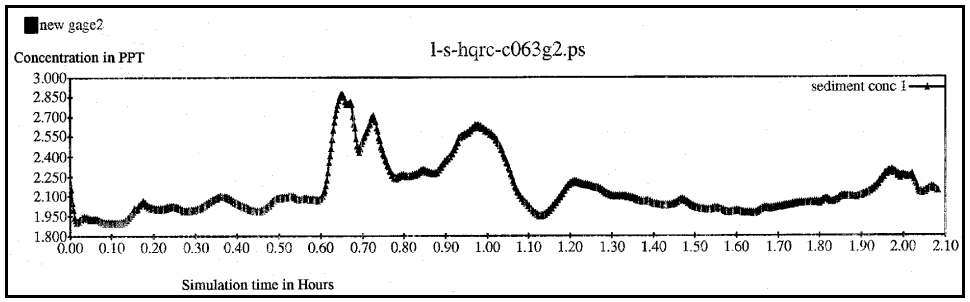

Figure 41. Sediment concentration time history at new Gauge 2, LaGrange Pool, sand, high flow, shear stress from return current

erosion rate constant of 0.0025 kg/m^2/sec. The cohesive sediment fall velocity was assigned a value of 0.0025 m/sec. The sediment diffusion coefficient was assigned a value of 0.33 m^2/sec, and the water temperature a value of 12.8 °C (55 °F). A Manning roughness coefficient of 0.025 was assigned for the determination of bed shear stresses in the channel, 0.030 in the nearshore areas and 0.040 in the backwater areas. Field data were used to estimate inflowing concentration at the upstream boundary.

The above sediment parameters were used for the low-, medium-, and high-flow steady-state initial runs. The only exception was that the initial inflowing concentrations at the inflow boundary lines were adjusted for the differing flow rates. The results of the three simulations all showed that when an equilibrium fine concentration was obtained, deposition and scour patterns were consistent with the river's bathymetric features and hydraulic conditions.

For the dynamic simulations, the same tow characteristics as used in the sand runs were used in the fine-sediment runs. Observations of the simulation results for the three flows are discussed separately in the following paragraphs.

Ambient cohesive sediment concentrations were about 0 mg/ℓ for the low-flow case. A spatial distribution of sediment concentrations for the low-flow boat-shear run (Figure 42) shows an increase to only 24 mg/ℓ of fine-sediment

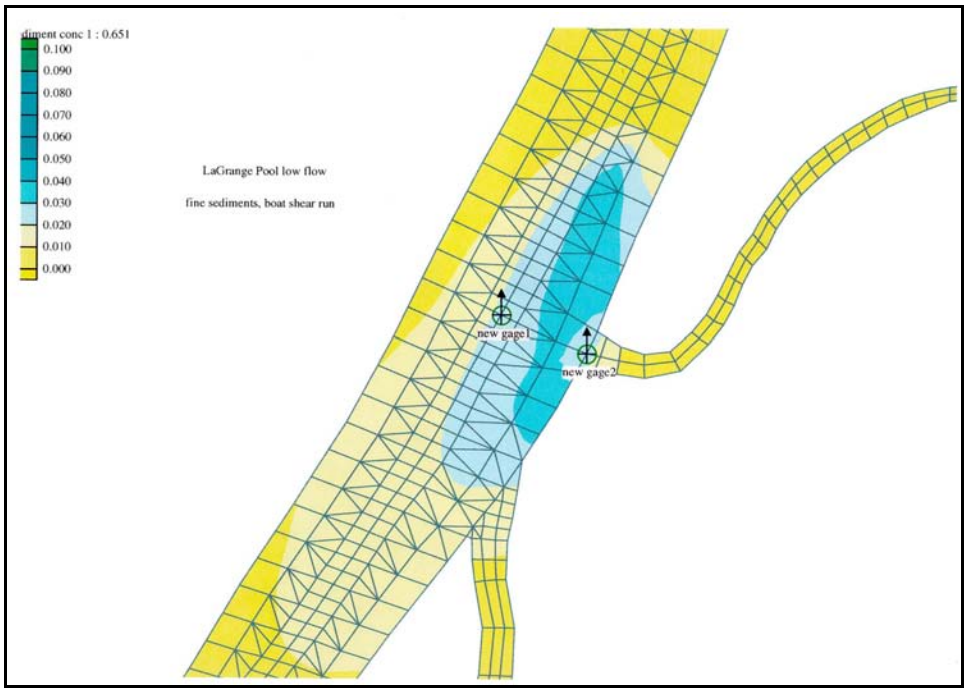

Figure 42. Sediment concentration contours, LaGrange Pool, fines, low flow, boat-shear stresses

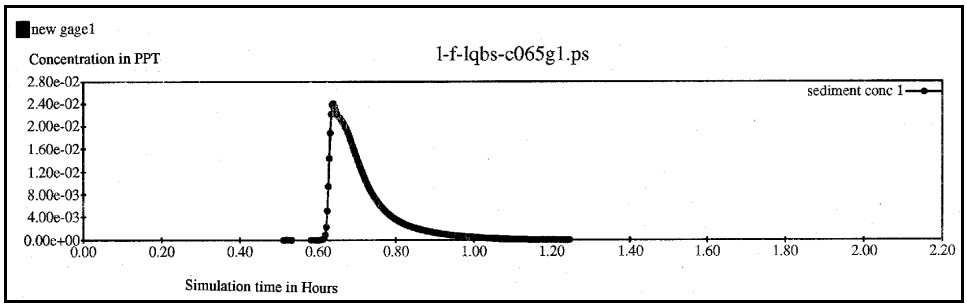

Figure 43. Sediment concentration time history at new Gauge 1, LaGrange Pool, fines, low flow, boat-shear stresses

concentration in the channel (Figure 43) and at the entrance to a backwater area (Figure 44).

A spatial distribution of sediment concentrations for the low-flow return-current simulation (Figure 45) showed localized fine sediment entrainment in the channel (Figure 46) and in the backwater entrance (Figure 47) of 68 mg/ℓ and 40 mg/ℓ, respectively.

Ambient cohesive sediment concentrations were about 35 mg/ℓ in the channel and 2 mg/ℓ at the nearshore for the medium-flow case. Results of the medium-flow boat-shear run (Figure 48) showed somewhat higher localized fine sediment entrainment at both locations than the low-flow case, as seen in Figures 49 and

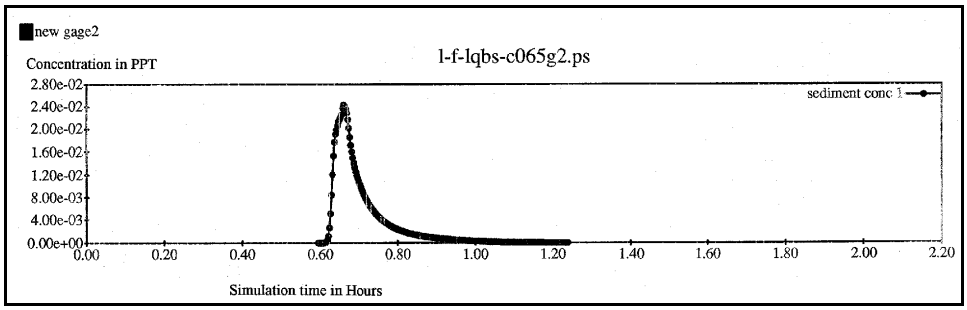

Figure 44. Sediment concentration time history at new Gauge 2, LaGrange Pool, fines, low flow, boat-shear stresses

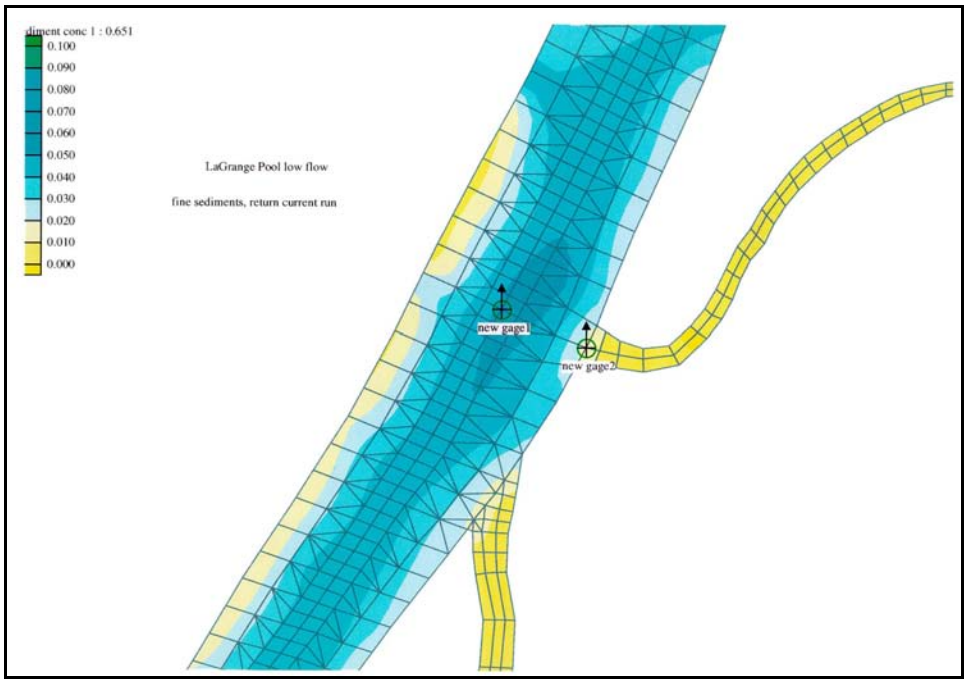

Figure 45. Sediment concentration contours, LaGrange Pool, fines, low flow, shear stress from return current

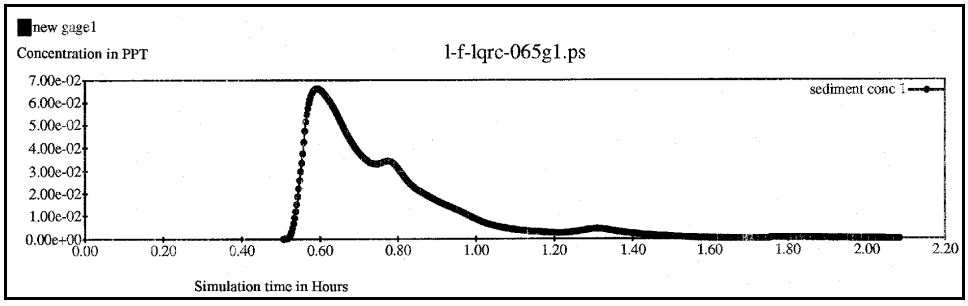

Figure 46. Sediment concentration time history at new Gauge 1, LaGrange Pool, fines, low flow, shear stress from return current

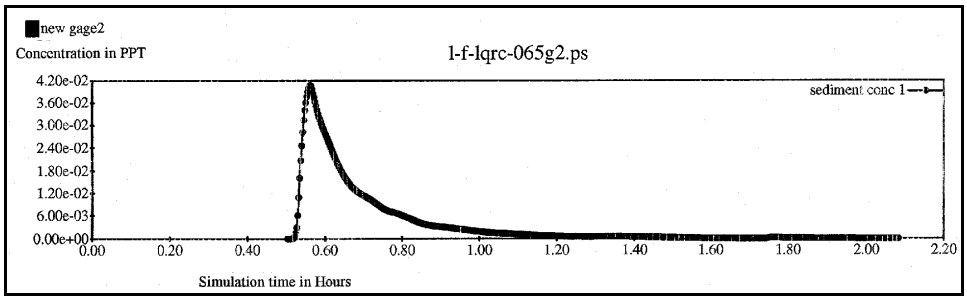

Figure 47. Sediment concentration time history at new Gauge 2, LaGrange Pool, fines, low flow, shear stress from return current

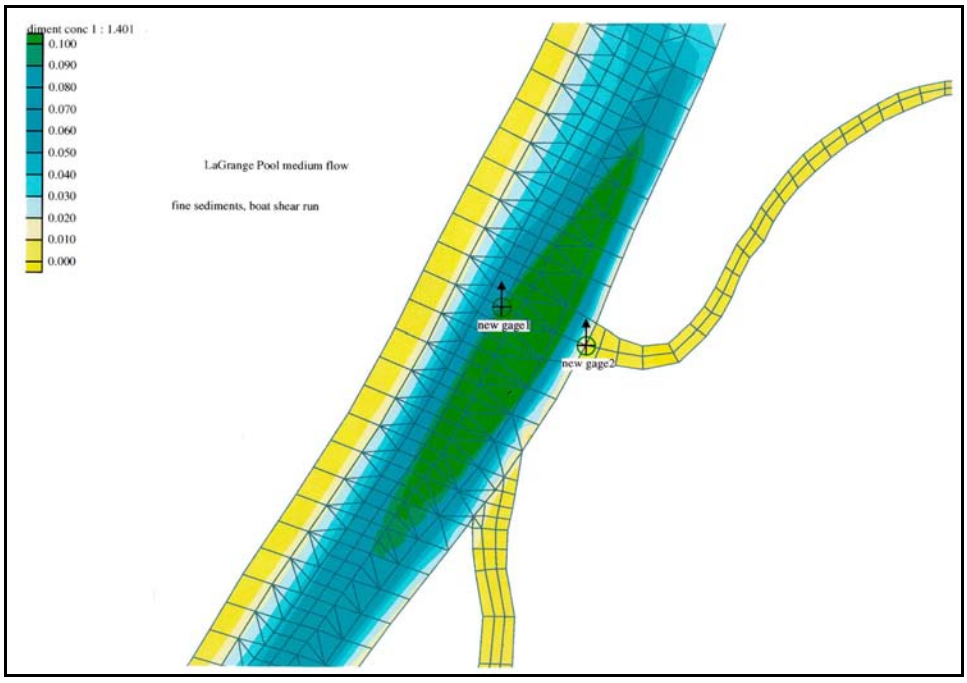

Figure 48. Sediment concentration contours, LaGrange Pool, fines, medium flow, boat-shear stresses

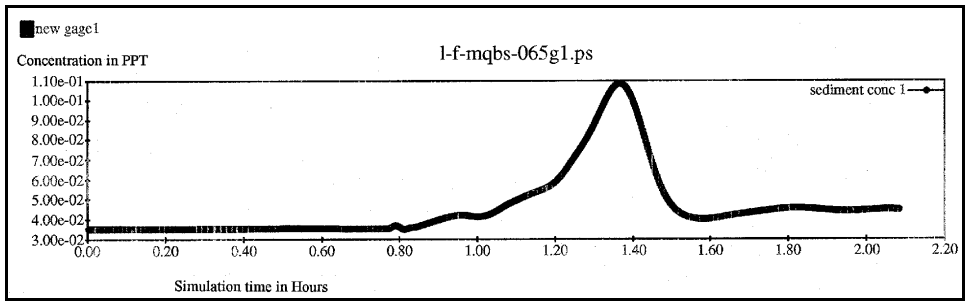

Figure 49. Sediment concentration time history at new Gauge 1, LaGrange Pool, fines, medium flow, boat-shear stresses

50. The net change due to tow passage was 75 mg/ℓ in the channel and 20 mg/ℓ at the backwater entrance.

The medium-flow return-current runs (Figure 51) showed higher values than the boat-shear runs. A net change of about 145 mg/ℓ in the main channel, Figure 52, and 65 mg/ℓ net change in the backwater entrance, Figure 53, was observed.

Ambient cohesive sediment concentrations were about 507 mg/ℓ both in the channel and at the nearshore for the high-flow case. The high-flow runs for both boat-shear and return-current runs showed the highest overall cohesive sediment concentrations as expected. The spatial distributions of sediment concentrations are displayed in Figures 54 and 57 and show uniformly high concentrations throughout the channel. However, the net change due to the tow was less than in the medium-flow runs. Figures 55, 56, 58, and 59 (gage plots) show a maximum change due to the tow of about 41 mg/ℓ at the backwater entrance for the return-current run.

General conclusions for the three flow conditions in the LaGrange Pool for the cohesive sediments show that, for the backwater entrance, the highest value of entrainment above the ambient amount and due to the tow passage was 65 mg/ℓ and occurred in the medium-flow return current run. Once cohesive sediments were entrained, they tended to remain in suspension much longer than sand.

Postprocessing of the SED2D Simulations

The results of the SED2D simulations in the three trend reaches were generalized to determine approximate tow-induced sediment concentrations in other reaches of the Upper Mississippi study area. The SED2D results were used to generate a time series of sediment concentrations at grid points surrounding a moving tow. These are called “design curves”. A program was written (NAVSED) which utilizes these design curves to generate specific concentration time history plots at specific locations as a function of local hydraulic and tow characteristics.

Design curves

The design curves consist of plots of sediment concentration versus time, with the ambient concentration subtracted out (the justification for subtracting out the ambient concentration is given in the discussion of NAVSED). A series of 12 design curves were developed, one from each of the SED2D simulations. Sand curves were developed for high, medium, and low flow in the trend reaches of Pools 8, 26, and LaGrange. Fine curves were developed for high, medium, and low flow for the trend reach in LaGrange Pool. For a given simulation, each curve represents the sediment response at a different lateral distance from

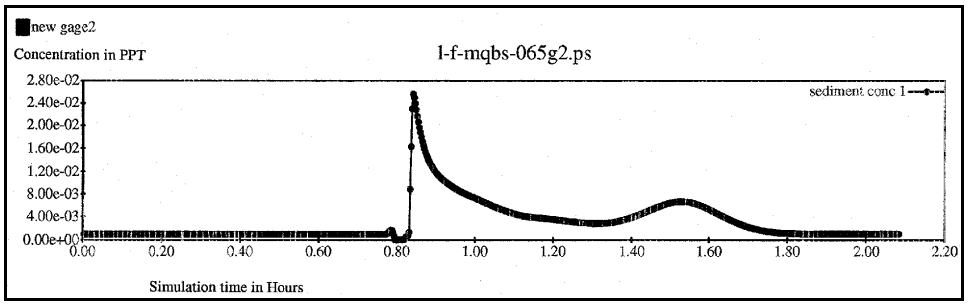

Figure 50. Sediment concentration time history at new Gauge 2, LaGrange Pool, fines, medium flow, boat-shear stresses

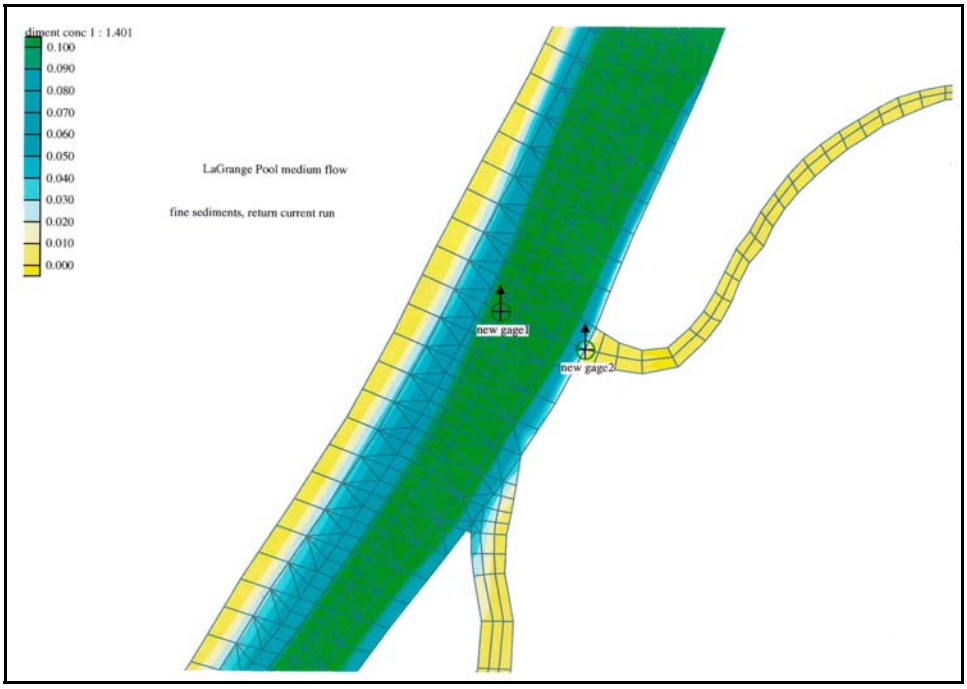

Figure 51. Sediment concentration contours, LaGrange Pool, fines, medium flow, shear stress from return current

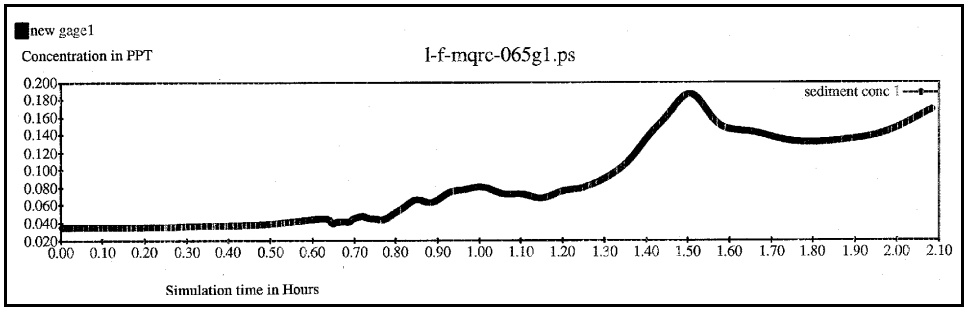

Figure 52. Sediment concentration time history at new Gauge 1, LaGrange Pool, fines, medium flow, shear stress from return current

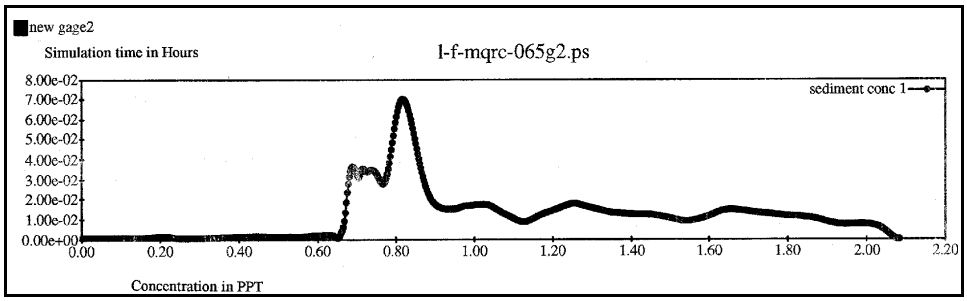

Figure 53. Sediment concentration time history at new Gauge 2, LaGrange Pool, fines, medium flow, shear stress from return current

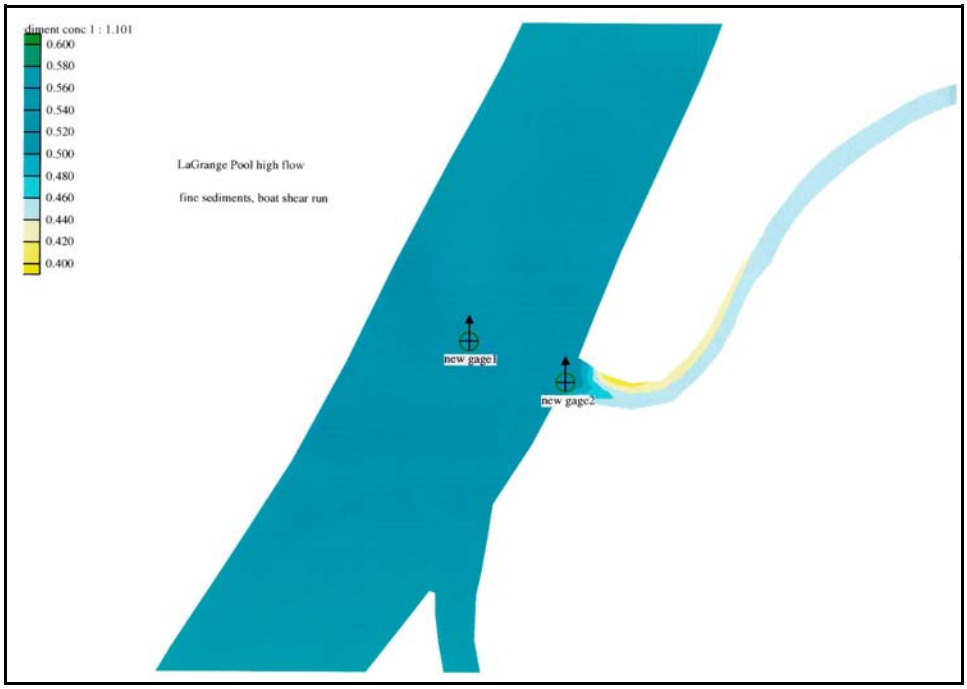

Figure 54. Sediment concentration contours, LaGrange Pool, fines, high flow, boat-shear stresses

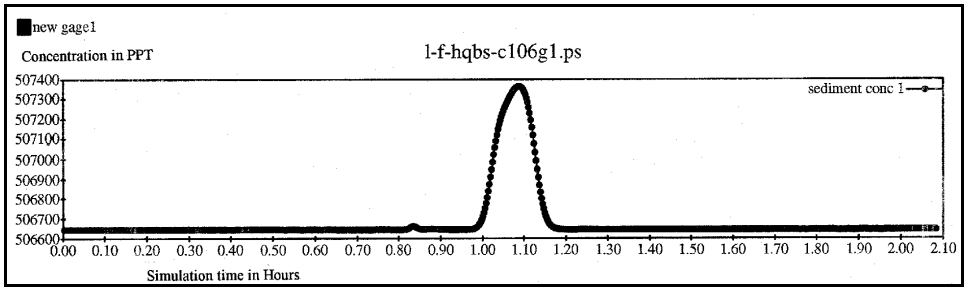

Figure 55. Sediment concentration time history at new Gauge 1, LaGrange Pool, fines, high flow, boat-shear stresses

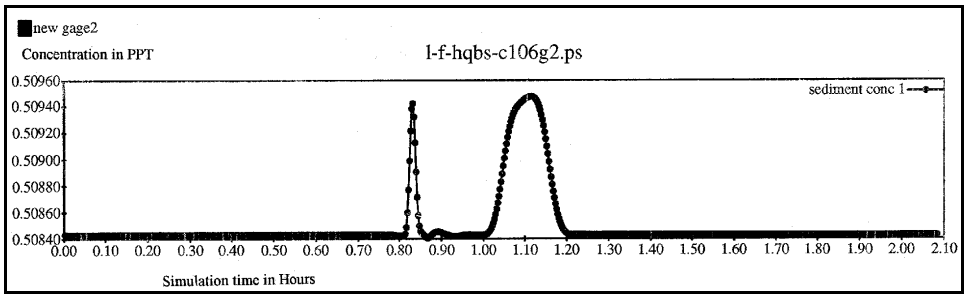

Figure 56. Sediment concentration time history at new Gauge 2, LaGrange Pool, fines, high flow, boat-shear stresses

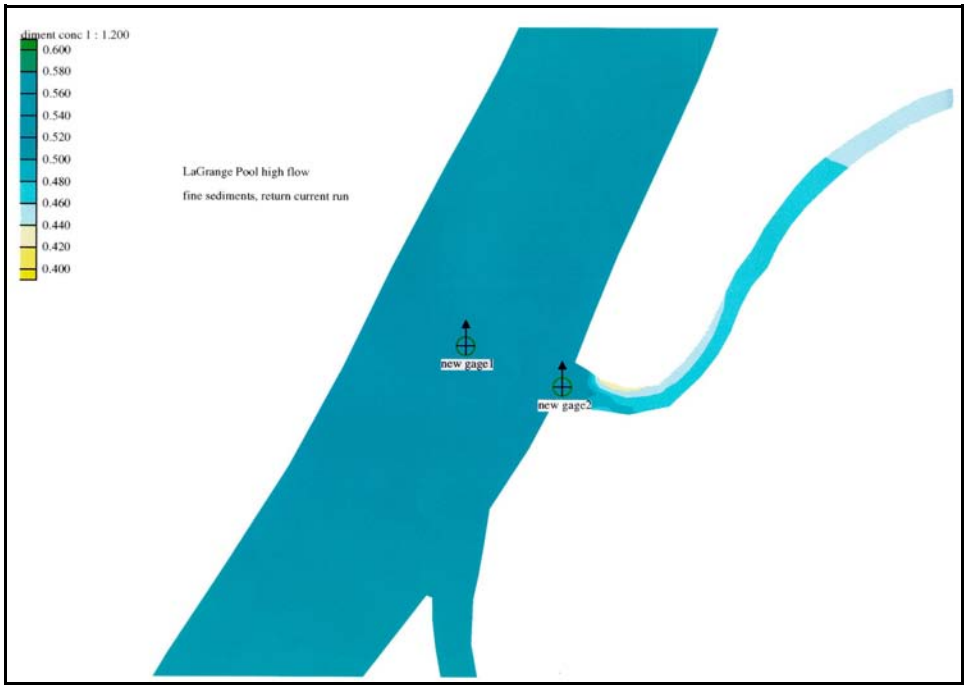

Figure 57. Sediment concentration contours, LaGrange Pool, fines, high flow, shear stress from return current

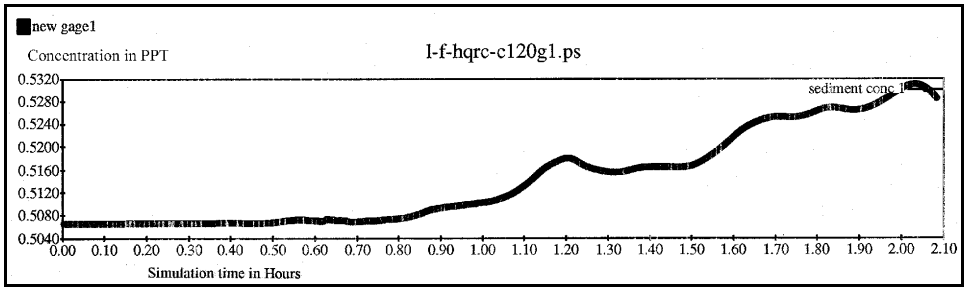

Figure 58. Sediment concentration time history at new Gauge 1, LaGrange Pool, fines, high flow, shear stress from return current

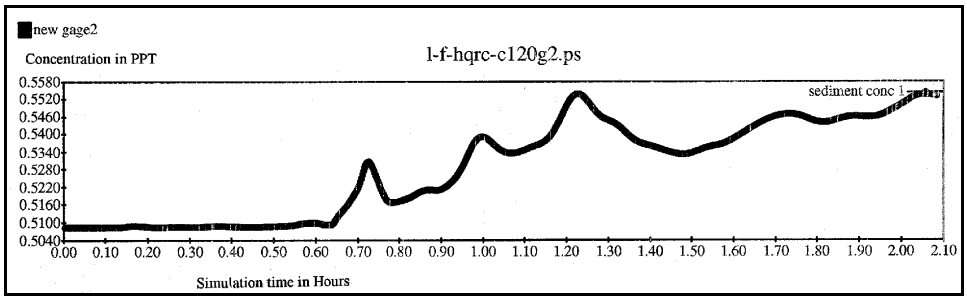

Figure 59. Sediment concentration time history at new Gauge 2, LaGrange Pool, fines, high flow, shear stress from return current

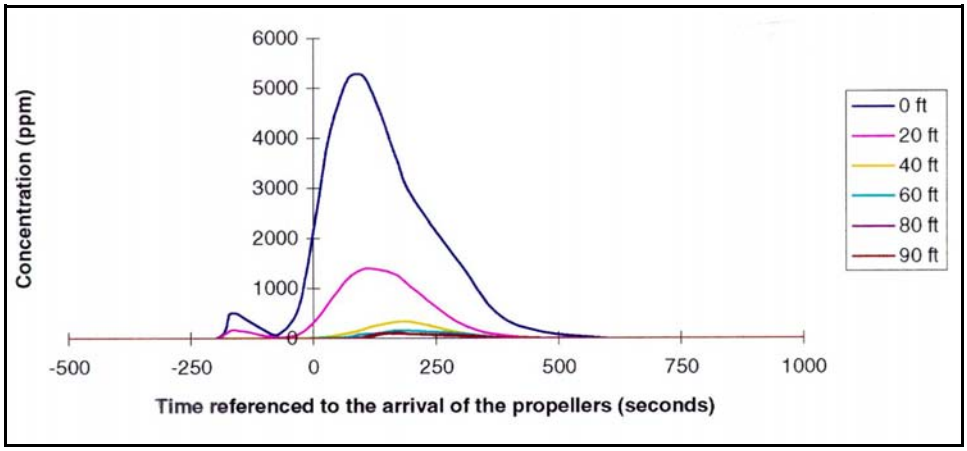

Figure 60. Typical set of design curves (individual curves represent the concentration time history at a given lateral distance from the sailing line)

the center line of the boat. Time is given in seconds, with time 0 representing the arrival time of the propellers (in NAVSED, time 0 is shifted to the arrival time of the bow, corresponding to the convention used in NAVEFF). Figure 60 presents an example of a series of design curves. The design curves are contained in the data file UMMOD.DAT. This data file is comprised of the series of design curves (expressed in tabular form) for each SED2D simulation. It also contains the values of both the peak shear and the ambient concentration given at each specified lateral distance from the boat. UMMOD.DAT is used as standard input to NAVSED.

In order to explain how these design curves are generated, it is useful to shift the frame of reference from the Earth (a Eulerian reference frame) to the boat (a Lagrangian reference frame). In the Lagrangian frame of reference, the boat remains stationary, and the river moves along at a fixed speed, S. Now, a grid can be established of sediment sampling locations around the boat that remain fixed with respect to the boat. The coordinates of each sampling location are specified with respect to a coordinate system with the origin fixed along the center line of the boat, at the propellers. Hence, the x-coordinate of a given sampling location is given by the lateral distance of the location either to port or to starboard, and the y-coordinate is given by the longitudinal distance either

ahead of or behind the boat propellers. (Note that speed can be expressed as the distance traveled divided by the time of travel (i.e., S = d/t). Using this relation, the y-coordinate of each sampling location can be converted from units of distance to units of time. This conversion is useful in the development of the design curves).

Allowing the simulation to proceed from beginning to end and recording only the time average of the concentration at each sampling point (that is, the average value obtained over the course of the simulation) result in a table consisting of one time-averaged concentration associated with each sampling location (see Table 8). This table can be plotted as a series of curves. Each curve is plotted as concentration versus time, with one curve for each lateral sampling distance from the boat (the values found to port and to starboard are averaged to give one value for each lateral distance). Figure 60 represents the curves which result from plotting Table 8 in this way.

NAVSED

NAVSED reads NAVEFF input and output files and generates plots of sediment concentration versus time due to a boat passage for each cell and scenario given in the NAVEFF output. The concentration given is the combined concentration of both fines and sand. The concentrations result from the combined influences of prop/bow shear under the boat, shear due to the return currents, and shear due to the short period waves propagating from the boat to the shore.

NAVSED executes as follows. First, the user is prompted to enter the relevant NAVEFF input/output files together with input specifying which reach is to be used as the "trend" reach for the simulation (i.e., the reach selected from among the three reaches represented in the SED2D simulations deemed most similar to the reach to be analyzed in the NAVSED run. The user can choose from Pool 26, Pool 8, or the LaGrange Pool.) NAVEFF provides NAVSED with values for the cell identification, boat speed, boat dimensions, river mile, river traffic conditions, river stage, local depth, sailing line, distance from the cell to the sailing line, peak shear induced by the vessel in the cell, ambient shear in the cell, sediment grain size, sediment fall velocity, nearshore bed sediment type, nearshore bed sediment strength, and maximum nearshore wave height induced by the vessel.

Information gathered from this input is used to select the relevant design curves from the trend reach (that is, the relevant flow condition; high, medium, or low flow). These are used as the basis for developing a plot of concentration versus time for each of the entries given in the NAVEFF output file.

The procedure for generating a concentration versus time plot at a given cell and for a given scenario is as follows. First, the ambient concentration is found. For sands, this value is calculated using the ambient shear as given in the NAVEFF output file. The expression used to estimate ambient sand

Table 8
Typical Design Curve Tabulation

Time (s)	Distance from Sailing Line					
	0 ft	20 ft	40 ft	60 ft	80 ft	90 ft
-600.00	0.00	0.01	0.00	0.00	0.00	0.00
-400.00	0.00	0.02	0.01	0.00	0.00	0.00
-200.00	2.24	1.08	0.39	0.28	0.07	0.04
-170.00	502.25	166.00	8.29	1.58	0.47	0.31
-130.00	341.66	121.63	8.00	1.80	0.51	0.31
-100.00	161.44	56.25	3.96	0.84	0.25	0.14
-70.00	93.20	29.73	2.31	0.54	0.15	0.08
-30.00	614.95	91.07	5.35	2.61	0.52	0.30
4.00	2372.19	352.00	20.89	8.76	1.76	0.87
30.00	3946.24	692.75	38.85	15.83	2.73	1.38
70.00	5180.64	1192.03	108.24	32.43	4.81	2.64
100.00	5257.50	1387.82	169.81	83.74	22.44	12.87
130.00	4664.26	1390.20	259.81	110.40	93.70	72.13
170.00	3568.20	1268.65	324.49	167.96	95.02	116.14
200.00	2845.11	1016.90	324.37	153.59	84.14	82.31
300.00	1489.08	301.52	115.23	93.18	64.60	45.24
400.00	327.70	52.68	10.35	5.21	6.69	8.64
600.00	3.79	1.43	0.21	0.06	0.03	0.02
800.00	0.17	0.09	0.04	0.02	0.01	0.01
1000.00	0.09	0.04	0.02	0.01	0.01	0.01

concentration as a function of shear stress is the Garcia-Parker equation (Equation 4 in Chapter 2)

For fines, the ambient concentration cannot be accurately estimated with a simple equation. Therefore, it is assumed to be on the order of that found in the trend reach and is estimated by interpolating from the values of ambient concentration given for the trend reach (interpolation here implies the estimation of the concentration at a given lateral distance d from the cell to the center line of the boat, given concentration values at the locations specified in the trend reach data).

Next, the peak shear and the design curve at a specified lateral distance from the cell to the center line of the boat are interpolated (as above) from the peak shear and design curve data for the trend reach. The peak shear values are used

to calculate a concentration ratio to be used later in the estimation of the concentration at the cell. For sands, this ratio (r_s) is found by solving the Garcia-Parker equation for concentration as a function of the peak shear in the cell and dividing this by the concentration calculated using the same equation as a function of the peak shear in the trend reach at the same location.

$$r_s = \frac{C(\tau_p)}{C(\tau_{pt})} \tag{11}$$

where

C = concentration calculated using Garcia-Parker equation

τ_p = the peak shear in the cell from NAVEFF

τ_{pt} = the peak shear in the cell for the trend reach from design curve

For fines, this ratio (r_f) is found in a similar way, except that the Parthenaides equation (Equation 8 in Chapter 2) is used instead of the Garcia-Parker equation.

$$r_f = \frac{\tau_p - \tau_c}{\tau_{pt} - \tau_c} \tag{12}$$

where

τ_c = the critical shear stress for erosion of fines

If the depth at the cell is less than 1.5 m and the appropriate data are present in the NAVEFF output file, the values of sediment concentration versus time due to small waves propagating into the shoreline are calculated according to an algorithm developed by Parchure, McAnally, and Teeter (in preparation).

Finally, the final concentration versus time plot is found as follows:

$$C(t) = C_{fa}(t) + C_{sa}(t) + r_{fb}C_{fbtp}(t) + r_{fr}C_{frtp}(t) + r_{sb}C_{sbtp}(t) + r_{sr}C_{srtp}(t) + C_w(t) \tag{13}$$

where

C(t) = the total concentration at time t

$C_{fa}(t)$ = the ambient concentration of fines at time t

$C_{sa}(t)$ = the ambient concentration of sand at time t

r_{fb} = the concentration ratio (Equation 12) for fines induced by the boat

$C_{fbtp}(t)$ = the peak concentration of fines induced by the boat in the trend reach at time t

r_{fr} = the concentration ratio (Equation 12) for fines induced by the return current

$C_{frtp}(t)$ = the peak concentration of fines induced by the return current in the trend reach at time t

r_{sb} = the concentration ratio (Equation 11) for sand induced by the boat

$C_{sbtp}(t)$ = the peak concentration of sand induced by the boat in the trend reach at time t

r_{sr} = the concentration ratio (Equation 11) for sand induced by the return current

$C_{srtp}(t)$ = the peak concentration of sand induced by the return current in the trend reach at time t

$C_w(t)$ = the concentration of fines due to wave action at the shoreline at time t

The time values used in this calculation are given in the NAVSED code and are written to the NAVSED output file. Time 0 represents the arrival time of the bow.

There are two significant approximations implicit in Equation 13. The first approximation is that the concentration at the cell can be expressed as the product of the concentration at the same location in the trend reach and the concentration ratio. In effect, this assumes that the shape of a given curve will be the same for all values of the peak concentration. The second approximation is that the bulk concentration can be found by summing the contributions of sediment resulting from each source of shear. For sands, this approximation is adequate only if there is little or no temporal overlap of the application of the shear stresses in the cell. This is because Equation 11 is highly nonlinear with respect to shear stress. Therefore, the sand concentration due to two separate sources of shear applied at a given time cannot be estimated adequately by simply summing the concentrations resulting from each shear source applied in isolation.

Note that, unlike Equation 11, Equation 12 is linear with respect to shear stress. Therefore, for fines, the approximation appears to be satisfactory regardless of the degree of temporal overlap of the applied shear.

5 Conclusions and Recommendations

Conclusions

Two-dimensional numerical models were used to calculate the entrainment, transport, and deposition of sediments due to towboat passage. The models were applied to portions of Pool 8 and Pool 26 in the Mississippi River and to the LaGrange Pool in the Illinois River. Calculations were made for tow loadings and speeds that were reasonable for the pool and that would create relatively high shear stresses on the riverbed. Time histories of sediment concentration were calculated at every node in the numerical grid. The ensemble of these data can be used to evaluate the effects of towboat passage on channel and nearshore increases in sediment concentrations, and, thus, possibly also on aquatic organisms. Examples of calculated sediment concentration time histories at two locations in each pool, one in the navigation channel and another at the entrance to a backwater area, were provided in this report for illustrative purposes.

A bed sampling program was conducted in conjunction with the numerical modeling. In general, it was determined that the bed of the Mississippi River, in the study reaches, was composed primarily of sand-size material. There are some locations where cohesive sediments were found on the riverbed, especially along the shoreline and in backwater areas, but for generalized computations of entrainment due to tow passage in the navigation channel, the entire bed of the river can be assumed to be sand. The bed of the Illinois River in the LaGrange Pool was found to be less uniform than the bed of the Mississippi River pools. The sampling program indicated that the navigation channel in the LaGrange Pool is composed primarily of fine sand. Patches of cohesive bed sediment were found in the navigation channel, and cohesive material dominated the bed of the channel adjacent to the navigation channel. For purposes of making generalized computations of entrainment due to tow passage in the navigation channel, it is appropriate to model the navigation channel using a sand bed and the adjacent channel area using a cohesive bed. The SED2D model cannot run both sediment types together.

The entrainment of sands by tow passage in the three trend reaches was significant in some cases, but, in all cases, the duration was relatively short. For example, a maximum instantaneous sand concentration of 28,000 mg/ℓ was calculated under the tow for one flow condition in Pool 8, but most of the resuspended sediment returned to the bed in 18 sec. The numerical sedimentation model indicated that sand entrainment by passing tows was most significant at low flow in the Mississippi River. There was no apparent correlation between sand entrainment and flow intensity in the LaGrange Pool. The Garcia-Parker equation, which was used to calculate sand entrainment, predicted concentrations that are considered to be on the high end of the uncertainty range. This equation was used in the numerical model for two reasons: (a) it produced sediment concentrations that can be considered representative of the maximum reasonable effect due to tow passage, and (b) because of its formulation (entrainment is a function of only shear velocity and depth), it is well suited for application as a generalized relationship to determine sediment entrainment for a variety of hydrodynamic and tow passage conditions defined by the existing NAVEFF computer program.

Cohesive sediment entrainment by towboat passage was calculated only in the LaGrange Pool. It was determined that, once cohesive sediment was entrained, it stayed in suspension much longer than sand. There is a high degree of uncertainty associated with the calculated cohesive sediment concentrations due to the high degree of uncertainty associated with the critical cohesive bed properties. Calculated cohesive concentrations should be used in a qualitative rather than a quantitative sense (i.e. primarily used to make comparisons between the effects of different hydrodynamic or tow passage conditions).

Recommendations

A more detailed bed sampling program, focusing more on geomorphological features rather than arbitrary distances along a sailing line, would provide a more complete description of the spatial variability of the riverbed, especially in the LaGrange Pool. In addition, a better definition of the characteristics of the cohesive bed deposits is needed. The five cohesive samples collected and analyzed in the LaGrange Pool suggested considerable spatial variability in the critical cohesive bed material parameters. With this additional bed material data, a more accurate definition of sediment entrainment for a variety of bed materials could be calculated with the numerical sedimentation model.

It is recommended that additional suspended sediment sampling be conducted in order to develop a complete description of characteristics of the measured suspended sediment load. Samples need to be collected in sufficient quantities so that size class distributions can be determined in the laboratory. This is especially important in the LaGrange Pool where significant fine sediment is suspended.

The calculated sand entrainment, using the Garcia-Parker equation, is greater than that calculated using most other sediment transport equations. If the calculated magnitudes and durations of sand concentration are determined to be

critical for the survival of aquatic organisms, then a more detailed investigation into the sediment transport equation is recommended. It may be that the equation itself can be modified for the extremely high shear velocities imposed by the tow passage, or another sediment transport equation may provide more realistic entrainment values.

References

Ackers, P. (1993). "Sediment transport in open channels: Ackers and White update." Proceedings, The Institution of Civil Engineers Water Maritime and Energy 101(4) December 1993, 247-9.

Ackers, P., and White, W. R. (1973). "Sediment transport: New approach and analysis," *Journal of the Hydraulics Division,* ASCE, Vol. 99, No.HY11, 2041-60.

Edwards, T. K., and Glysson, G. D. (1988). "Field methods for measurement of fluvial sediment," Open-File Report 86-531, U.S. Geological Survey.

Fagerburg, T. L., and Pratt, T. C. (1998). "Interim report for the upper Mississippi River-Illinois River system navigation study, upper Mississippi River navigation and sedimentation field data collection summary report," ENV Report 6, Rock Island District, U.S. Army Corps of Engineers, Rock Island, IL.

Garcia, M. H., Admiraal, D. M., and Rodriguez, J. F. (1999). "Sediment entrainment functions for navigation - induced resuspension," Civil Engineering Studies, Hydraulic Engineering Studies No. 61, University of Illinois, Urbana.

Garcia, M. H., and Parker, G. (1991). "Entrainment of bed sediment into suspension," *Journal of Hydraulic Engineering* 117(4), 414-35.

Knight, S. K., and Parchure, T. M. "Interim report for the upper Mississippi River-Illinois River system navigation study, hydraulic analysis of recreational boat waves on the upper Mississippi River-Illinois River system," In preparation, ENV Report. Rock Island District, U.S. Army Corps of Engineers, Rock Island, IL.

Krone, R. B. (1962). "Flume studies of the transport of sediment in estuarial shoaling processes," Hydraulic Engineering Laboratory, University of California, Berkeley.

Maynord, S. T. (1996). "Return velocity and drawdown in navigable waterways," Technical Report HL-96-7, U.S. Army Engineer Waterways Experiment Station, Vicksburg, MS.

_____ . (2000). "Physical forces near commercial tows," ENV Report 19, U.S. Army Engineer Research and Development Center, Vicksburg, MS.

_____ . "Power vs. speed for shallow-draft navigation," In preparation, Technical Report, U.S. Army Engineer Research and Development Center, Vicksburg, MS.

Parchure, T. M., McAnally, W. H., Jr., and Teeter, A. M. "Wave-induced sediment resuspension near the shorelines of the upper Mississippi River," In preparation, U.S. Army Engineer Research and Development Center, Vicksburg, MS.

Parthenaides, E. (1965). "Erosion and deposition of cohesive soils," *Journal of the Hydraulics Division*, ASCE March, 755-71.

Pokrefke, T. J., Maynord, S. T., Berger, R. C., and Rhee, G. P. "Tow-induced backwater and secondary channel sedimentation," In preparation, U.S. Army Engineer Research and Development Center, Vicksburg, MS.

Rouse, H. (1938). "Experiments on the mechanics of sediment suspension." Proceedings, Fifth International Congress for Applied Mechanics 55, John Wiley and Sons, New York.

Stockstill, R. L., and Berger, R. C. (1999). "A two-dimensional flow model for vessel-generated currents," ENV Report 10, U.S. Army Engineer Waterways Experiment Station, Vicksburg, MS.

Thomas, W. A., and McAnally, W. H. (1991). "User's manual for the generalized computer program system, open-channel flow and sedimentation, TABS-MD," IR HL-85-1, U.S. Army Engineer Waterways Experiment Station, Vicksburg MS.

U.S. Army Corps of Engineers. (1994). *Upper Mississippi River hydro-dynamics: Discharge distribution in Pool 8, 1987-1993*. U.S. Army Engineer District, St. Paul.

REPORT DOCUMENTATION PAGE

Form Approved
OMB No. 0704-0188

1. REPORT DATE *(DD-MM-YYYY)*	2. REPORT TYPE	3. DATES COVERED *(From - To)*
January 2001	Interim report	

4. TITLE AND SUBTITLE
Entrainment and Transport of Sediments by Towboats in the Upper Mississippi River and Illinois Waterway, Numerical Model Study

5a. CONTRACT NUMBER

5b. GRANT NUMBER

5c. PROGRAM ELEMENT NUMBER

6. AUTHOR(S)
Ronald R. Copeland, David D. Abraham, Gregory H. Nail, Rebecca Seal, Gary L. Brown

5d. PROJECT NUMBER

5e. TASK NUMBER

5f. WORK UNIT NUMBER

7. PERFORMING ORGANIZATION NAME(S) AND ADDRESS(ES)

U.S. Army Engineer Research and Development Center
Coastal and Hydraulics Laboratory
3909 Halls Ferry Road
Vicksburg, MS 39180-6199

8. PERFORMING ORGANIZATION REPORT NUMBER

9. SPONSORING / MONITORING AGENCY NAME(S) AND ADDRESS(ES)

See reverse.

10. SPONSOR/MONITOR'S ACRONYM(S)
ENV Report 37

11. SPONSOR/MONITOR'S REPORT NUMBER(S)

12. DISTRIBUTION / AVAILABILITY STATEMENT

Approved for public release; distribution is unlimited.

13. SUPPLEMENTARY NOTES

14. ABSTRACT

A numerical model study was conducted to determine the magnitude and duration of increased sediment concentration due to towboat passage. The quantity of bed material transport into backwater areas was also predicted. This was accomplished using two 2-dimensional numerical models for hydrodynamics (RMA2 and HIVEL) and a sediment transport model (SED2D). Amibent hydrodynamic bed shear stresses were calculated using RMA2. Bed shear stresses created by drawdown and return currents were calculated using HIVEL. Bed shear stresses induced by the bow pressure waves and the tow's propeller jet as a function of depth and ambient velocity were determined external to the numerical models using an algorithm developed from experimental techniques. The combined bed shear stresses from these three sources were imported into the SED2D sediment model to calculate entrainment and transport. The currently available SED2D model was modified to simulate towboat passage and to entrain bed sediments from rapidly changing bed shear stresses. The two-dimensional depth-averaged unsteady-flow sediment transport model was then used to simulate the advection and diffusion of suspended sediment. Portions of Pools 8 and 26 on the Mississippi River and the LaGrange Pool on the Illinois River were modeled. The study

(Continued)

15. SUBJECT TERMS
Illinois Waterway, Numerical modeling, Sediment entrainment by towboats, Sedimentation, Upper Mississippi River

16. SECURITY CLASSIFICATION OF:			17. LIMITATION OF ABSTRACT	18. NUMBER OF PAGES	19a. NAME OF RESPONSIBLE PERSON
a. REPORT	b. ABSTRACT	c. THIS PAGE			19b. TELEPHONE NUMBER *(include area code)*
UNCLASSIFIED	UNCLASSIFIED	UNCLASSIFIED		91	

9. (Concluded)

U.S. Army Engineer District, Rock Island, Clock Tower Building, P.O. Box 2004, Rock Island, IL 61204-2004
U.S. Army Engineer District, St. Louis, 1222 Spruce Street, St. Louis, MO 63103-2833
U.S. Army Engineer District, St. Paul, Army Corps of Engineers, Centre, 190 5th Street East, St. Paul, MN 55101-1638

14. ABSTRACT (Concluded)

included collection of bed-material and suspended sediment data. Model results showed very little impact on ambient sediment concentrations on the Mississippi River where the predominate bed sediment was medium sand. Likewise, on the Illinois River where the predominant bed material in the center of the navigation channel was fine sand, sediment entrained by towboats was quickly redeposited. However, cohesive sediment, which is located in patches on the bed and all along the edge of the navigation channel, remained in suspension much longer than the sand.